

NUMERICAL INVESTIGATION OF ENTRANCE
REGION FLOW HEAT TRANSFER OF
VISCOPLASTIC FLUIDS IN ROTATING
CONCENTRIC ANNULI

Thesis

Submitted in partial fulfillment of the requirements for the degree of
DOCTOR OF PHILOSOPHY

by

SRINIVASA RAO NADIMINTI



DEPARTMENT OF MATHEMATICAL AND COMPUTATIONAL SCIENCES

NATIONAL INSTITUTE OF TECHNOLOGY KARNATAKA,

SURATHKAL, MANGALORE - 575025

AUGUST 2017

Dedicated to the lotus feet of my dearest goddess

Yellamma Devi

and
my beloved parents

Mr. N. Simhachalam Naidu
Mrs. N. Dhalamma

and
my beloved sisters

Mrs. Sridevi and Ms. Mangamma

DECLARATION

By the Ph.D. Research Scholar

I hereby declare that the Research Thesis entitled “**NUMERICAL INVESTIGATION OF ENTRANCE REGION FLOW HEAT TRANSFER OF VISCOPLASTIC FLUIDS IN ROTATING CONCENTRIC ANNULI**” which is being submitted to the **National Institute of Technology Karnataka, Surathkal** in partial fulfillment of the requirements for the award of the Degree of **Doctor of Philosophy in Mathematical and Computational Sciences** is a *bonafide report of the research work carried out by me*. The material contained in this Research Thesis has not been submitted to any University or Institution for the award of any degree.

121183MA12F02, SRINIVASA RAO NADIMINTI

Department of Mathematical and Computational Sciences

Place: NITK, Surathkal.

Date:

CERTIFICATE

This is to *certify* that the Research Thesis entitled “**NUMERICAL INVESTIGATION OF ENTRANCE REGION FLOW HEAT TRANSFER OF VISCOPLASTIC FLUIDS IN ROTATING CONCENTRIC ANNULI**” submitted by **SRINIVASA RAO NADIMINTI**, (Register Number: 121183MA12F02) as the record of the research work carried out by him, is *accepted as the Research Thesis submission* in partial fulfillment of the requirements for the award of degree of **Doctor of Philosophy**.

Dr. A. KANDASAMY

Research Guide

Chairman - DRPC

ACKNOWLEDGMENT

I whole heartedly thank my dearest goddess *Yellamma Devi* for enriching me with knowledge, strength and confidence to complete this research work. I owe a deep sense of gratitude to my master *Prof. A. Kandasamy*, Department of MACS, National Institute of Technology Karnataka, Surathkal for consenting to be my guide, providing valuable suggestions, tirelessly going through my work, suggesting improvement at every step and offering rare insights and scholarly counselling. It is indeed a wonderful experience and bliss to work with him.

I would like to extend my sincere gratitude to *Dr.B. Ashraf Ali*, Department of Chemical Engineering and *Dr. Chandhini G*, Department of MACS, National Institute of Technology Karnataka, for their scholarly advices, continuous support and consistent encouragement as my RPAC members.

I wish to thank profusely the National Institute of Technology Karnataka, for giving me the opportunity and all the needed facilities to carry out my research work. In particular, I express my warm and sincere thanks to *Prof. Santhosh George*, Head of the department. Also, express my sincere thanks to all the faculty members, research scholars of department of MACS, National Institute of Technology Karnataka, for their kind co-operation, continuous support and constant encouragement.

Place: NITK, Surathkal

SRINIVASA RAO NADIMINTI

Date:

ABSTRACT

The study of the entrance region flow, sometimes called entry length problem, is of considerable technical importance due to its immediate application in various designs of those chemical, biomedical and food processes in which the flows of Newtonian and non-Newtonian fluids are encountered. Furthermore, such an entrance flow is encountered in almost every industrial process involving non-Newtonian suspensions, emulsion or solutions. In recent times, experimental researches have shown clear evidence that the use of non-Newtonian fluids with variable viscosity can improve the fluid properties relative to that of fluids with constant viscosity. Particularly, Rheologists intend to use non-Newtonian fluids characterized by an yield value called viscoplastic fluids. Some of the important fluids which belong to this class are Bingham plastic, Casson fluid and Hershel-Bulkley fluids. The present work is on the study of the entrance region flow heat transfer of viscoplastic fluids in rotating concentric annuli. The analysis has been carried out over the wide range of non-Newtonian fluid flow parameters and geometrical considerations. The development of boundary layer is visualized when the fluid enters an annulus and the fully developed velocity profile is observed in the region starting from the point down-stream where the boundary layers meet asymptotically with the outer edge of the plug flow zone. The effects of non-Newtonian flow characteristics and geometrical characteristics on the velocity profiles, pressure variation and temperature distribution along the radial direction have been discussed.

Keywords: Entrance Region Flow, Concentric Annuli, Heat Transfer, Bingham Fluid, Casson Fluid, Herschel-Bulkley Fluids, Yield Stress.

Contents

Abstract	i
List of Figures	v
1 INTRODUCTION	1
1.1 FUNDAMENTAL EQUATIONS OF FLUID MECHANICS	1
1.2 CLASSIFICATION BASED ON SHEAR STRESS	3
1.2.1 Newtonian Fluids and Non-Newtonian Fluids	4
1.3 TIME-INDEPENDENT NON-NEWTONIAN FLUIDS	5
1.4 ENTRANCE REGION AND FULLY DEVELOPED FLOW	8
1.4.1 Steps Involved in the Analysis of Entrance Region Flow	10
1.5 LITERATURE SURVEY	11
1.6 ORGANIZATION OF THE THESIS	13
2 ENTRANCE REGION FLOW HEAT TRANSFER IN CON- CENTRIC ANNULI WITH ROTATING INNER WALL FOR BINGHAM FLUID	17
2.1 INTRODUCTION	17
2.2 MATHEMATICAL FORMULATION OF THE PROBLEM	18
2.3 SOLUTION OF THE PROBLEM	22

2.4	RESULTS AND DISCUSSION	25
2.5	CONCLUSION	28
3	ENTRANCE REGION FLOW HEAT TRANSFER IN CON- CENTRIC ANNULI WITH ROTATING INNER WALL FOR CASSON FLUID	49
3.1	INTRODUCTION	49
3.2	MATHEMATICAL FORMULATION OF THE PROBLEM .	50
3.3	SOLUTION OF THE PROBLEM	54
3.4	RESULTS AND DISCUSSION	57
3.5	CONCLUSION	59
4	ENTRANCE REGION FLOW HEAT TRANSFER IN CON- CENTRIC ANNULI WITH ROTATING INNER WALL FOR HERSCHEL-BULKLEY FLUIDS	71
4.1	INTRODUCTION	71
4.2	MATHEMATICAL FORMULATION OF THE PROBLEM .	72
4.3	SOLUTION OF THE PROBLEM	75
4.4	RESULTS AND DISCUSSION	77
4.5	CONCLUSION	80
5	CONCLUSION AND FUTURE SCOPE	95
5.1	CONCLUSION	95
5.2	FUTURE SCOPE	96
	REFERENCES	97
	PUBLICATIONS	103

List of Figures

1.1	Shear Rate in Newtonian Fluid	4
1.2	Rheogram	8
1.3	Entrance and Fully Developed Flow in a Pipe	9
2.1	Geometry of the Problem	19
2.2	Grid Formation for Finite-Difference Representations	22
2.3	Tangential Velocity Profile for $N=0.3$ at $Z=0.02$	29
2.4	Tangential Velocity Profile for $N=0.5$ at $Z=0.02$	29
2.5	Tangential Velocity Profile for $N=0.8$ at $Z=0.02$	30
2.6	Tangential Velocity Profile for $N=0.3$ at $Z=0.03$	30
2.7	Tangential Velocity Profile for $N=0.5$ at $Z=0.03$	31
2.8	Tangential Velocity Profile for $N=0.8$ at $Z=0.03$	31
2.9	Axial Velocity Profile for $N=0.3$ at $Z=0.02$	32
2.10	Axial Velocity Profile for $N=0.5$ at $Z=0.02$	32
2.11	Axial Velocity Profile for $N=0.8$ at $Z=0.02$	33
2.12	Axial Velocity Profile for $N=0.3$ at $Z=0.03$	33
2.13	Axial Velocity Profile for $N=0.5$ at $Z=0.03$	34
2.14	Axial Velocity Profile for $N=0.8$ at $Z=0.03$	34
2.15	Radial Velocity Profile for $N=0.3$ at $Z=0.02$	35

2.16	Radial Velocity Profile for $N=0.5$ at $Z=0.02$	35
2.17	Radial Velocity Profile for $N=0.8$ at $Z=0.02$	36
2.18	Radial Velocity Profile for $N=0.3$ at $Z=0.03$	36
2.19	Radial Velocity Profile for $N=0.5$ at $Z=0.03$	37
2.20	Radial Velocity Profile for $N=0.8$ at $Z=0.03$	37
2.21	Pressure Variation for $N=0.3$ at $Z=0.02$	38
2.22	Pressure Variation for $N=0.5$ at $Z=0.02$	38
2.23	Pressure Variation for $N=0.8$ at $Z=0.02$	39
2.24	Pressure Variation for $N=0.3$ at $Z=0.03$	39
2.25	Pressure Variation for $N=0.5$ at $Z=0.03$	40
2.26	Pressure Variation for $N=0.8$ at $Z=0.03$	40
2.27	Temperature Distribution for $N=0.3$, $Pr=7$ and $B=0$	41
2.28	Temperature Distribution for $N=0.8$, $Pr=7$ and $B=0$	41
2.29	Temperature Distribution for $N=0.3$, $Pr=7$ and $B=10$	42
2.30	Temperature Distribution for $N=0.8$, $Pr=7$ and $B=10$	42
2.31	Temperature Distribution for $N=0.3$, $Pr=7$ and $B=20$	43
2.32	Temperature Distribution for $N=0.8$, $Pr=7$ and $B=20$	43
2.33	Temperature Distribution for $N=0.3$, $Pr=7$ and $B=30$	44
2.34	Temperature Distribution for $N=0.8$, $Pr=7$ and $B=30$	44
2.35	Temperature Distribution for $N=0.3$, $Pr=15$ and $B=0$	45
2.36	Temperature Distribution for $N=0.8$, $Pr=15$ and $B=0$	45
2.37	Temperature Distribution for $N=0.3$, $Pr=15$ and $B=10$	46
2.38	Temperature Distribution for $N=0.8$, $Pr=15$ and $B=10$	46

2.39	Temperature Distribution for $N=0.3$, $Pr=15$ and $B=20$. . .	47
2.40	Temperature Distribution for $N=0.8$, $Pr=15$ and $B=20$. . .	47
2.41	Temperature Distribution for $N=0.3$, $Pr=15$ and $B=30$. . .	48
2.42	Temperature Distribution for $N=0.8$, $Pr=15$ and $B=30$. . .	48
3.1	Geometry of the Problem	51
3.2	Grid Formation for Finite-Difference Representations	54
3.3	Tangential Velocity Profile for $N=0.3$, $R = 0.1$ at $Z = 0.01$. .	60
3.4	Tangential Velocity Profile for $N=0.5$, $R = 0.1$ at $Z = 0.02$. .	60
3.5	Tangential Velocity Profile for $N=0.8$, $R = 0.05$ at $Z = 0.03$. .	61
3.6	Axial Velocity Profile for $N=0.3$, $R = 0.1$ at $Z = 0.01$	61
3.7	Axial Velocity Profile for $N=0.5$, $R = 0.1$ at $Z = 0.02$	62
3.8	Axial Velocity Profile for $N=0.8$, $R = 0.05$ at $Z = 0.03$	62
3.9	Radial Velocity Profile for $N=0.3$, $R = 0.1$ at $Z = 0.01$	63
3.10	Radial Velocity Profile for $N=0.5$, $R = 0.1$ at $Z = 0.02$	63
3.11	Radial Velocity Profile for $N=0.8$, $R = 0.05$ at $Z = 0.03$	64
3.12	Pressure Variation for $N=0.3$, $R = 0.1$ at $Z = 0.01$	64
3.13	Pressure Variation for $N=0.5$, $R = 0.1$ at $Z = 0.02$	65
3.14	Pressure Variation for $N=0.8$, $R = 0.05$ at $Z = 0.03$	65
3.15	Temperature Distribution for $N=0.3$, $Pr=15$ and $Y_c=0$	66
3.16	Temperature Distribution for $N=0.8$, $Pr=15$ and $Y_c=0$	66
3.17	Temperature Distribution for $N=0.3$, $Pr=15$ and $Y_c=10$	67
3.18	Temperature Distribution for $N=0.8$, $Pr=15$ and $Y_c=10$	67
3.19	Temperature Distribution for $N=0.3$, $Pr=15$ and $Y_c=20$	68

3.20	Temperature Distribution for $N=0.8$, $Pr=15$ and $Y_c=20$. . .	68
3.21	Temperature Distribution for $N=0.3$, $Pr=15$ and $Y_c=30$. . .	69
3.22	Temperature Distribution for $N=0.8$, $Pr=15$ and $Y_c=30$. . .	69
4.1	Tangential Velocity Profile for $N=0.3$, $n=0.5$, $R = 0.1$, $Z = 0.02$	81
4.2	Tangential Velocity Profile for $N=0.3$, $n=1$, $R = 0.1$ at $Z = 0.02$	81
4.3	Tangential Velocity Profile for $N=0.3$, $n=1.5$, $R = 0.1$, $Z = 0.02$	82
4.4	Tangential Velocity Profile for $N=0.8$, $n=0.5$, $R = 0.05$, $Z = 0.03$	82
4.5	Tangential Velocity Profile for $N=0.8$, $n=1$, $R = 0.05$ at $Z = 0.03$	83
4.6	Tangential Velocity Profile for $N=0.8$, $n=1.5$, $R = 0.05$, $Z = 0.03$	83
4.7	Axial Velocity Profile for $N=0.3$, $n=0.5$, $R = 0.1$ at $Z = 0.02$.	84
4.8	Axial Velocity Profile for $N=0.3$, $n=1$, $R = 0.1$ at $Z = 0.02$. .	84
4.9	Axial Velocity Profile for $N=0.3$, $n=1.5$, $R = 0.1$ at $Z = 0.02$.	85
4.10	Axial Velocity Profile for $N=0.8$, $n=0.5$, $R = 0.05$ at $Z = 0.03$	85
4.11	Axial Velocity Profile for $N=0.8$, $n=1$, $R = 0.05$ at $Z = 0.03$.	86
4.12	Axial Velocity Profile for $N=0.8$, $n=1.5$, $R = 0.05$ at $Z = 0.03$	86
4.13	Radial Velocity Profile for $N=0.3$, $n=1$, $R = 0.1$ at $Z = 0.02$.	87
4.14	Radial Velocity Profile for $N=0.8$, $n=1$, $R = 0.05$ at $Z = 0.03$	87
4.15	Pressure Variation for $N=0.3$, $n=0.5$, $R = 0.1$ at $Z = 0.02$. .	88
4.16	Pressure Variation for $N=0.3$, $n=1$, $R = 0.1$ at $Z = 0.02$. . .	88
4.17	Pressure Variation for $N=0.3$, $n=1.5$, $R = 0.1$ at $Z = 0.02$. .	89
4.18	Pressure Variation for $N=0.8$, $n=0.5$, $R = 0.05$ at $Z = 0.03$. .	89
4.19	Pressure Variation for $N=0.8$, $n=1$, $R = 0.05$ at $Z = 0.03$. . .	90
4.20	Pressure Variation for $N=0.8$, $n=1.5$, $R = 0.05$ at $Z = 0.03$. .	90

4.21	Temperature Distribution for $N=0.3$, $n=0.5$, $Pr=7$ and $Y_h=0$	91
4.22	Temperature Distribution for $N=0.8$, $n=0.5$, $Pr=7$ and $Y_h=10$	91
4.23	Temperature Distribution for $N=0.3$, $n=1$, $Pr=7$ and $Y_h=0$.	92
4.24	Temperature Distribution for $N=0.8$, $n=1$, $Pr=7$ and $Y_h=10$.	92
4.25	Temperature Distribution for $N=0.3$, $n=1.5$, $Pr=7$ and $Y_h=0$	93
4.26	Temperature Distribution for $N=0.8$, $n=1.5$, $Pr=7$ and $Y_h=10$	93

Nomenclature

m the number of radial increments in the numerical mesh network
 p the pressure
 n the flow behaviour index
 t the fluid temperature at any point
 t_0 the Fluid temperature at annulus entry
 t_w the Isothermal wall temperature
 p_0 the initial pressure
 u_0 the uniform inlet velocity
 $u, v,$ and w the velocity components in z, r, θ directions, respectively
 r, θ and z the cylindrical coordinates
 ρ the density of the fluid
 μ the viscosity of the model
 μ_r the reference viscosity
 α the thermal diffusivity
 τ_0 the yield stress
 ω the regular angular velocity
 P the dimensionless pressure
 R, Z the dimensionless coordinates in the radial and axial directions
 R_1, R_2 the radius of the inner and outer cylinders, respectively
 B, Y_c the Bingham number and Casson number respectively
 Y_h, Pr the Herschel-Bulkley number and Prandtl's number respectively
 Re, T_a the modified Reynolds number and Taylor number respectively
 N the aspect ratio of the annulus
 U, V, W the dimensionless velocity components
 K the thermal conductivity
 C_p the specific heat at constant pressure
 $\Delta R, \Delta Z$ the mesh sizes in the radial and axial directions, respectively.

Chapter 1

INTRODUCTION

1.1 FUNDAMENTAL EQUATIONS OF FLUID MECHANICS

A fluid, one of the basic constituents of life, is a combined notion of liquids and gases and the subject that deals with the investigation of motion and equilibrium of fluids is called Fluid Mechanics. The application of fluid mechanics falls into diversified branches of science and engineering like astrophysics, biomechanics, plasma physics, biomedicine, hydraulics, lubrication, Aeronautical engineering, Chemical engineering, Mechanical engineering, etc. Fluid behavioural aspects can be studied under three different categories as given below.

1. **Statics** - Fluid elements are at rest with respect to each other and thus free from shearing stresses.
2. **Kinematics** - Study of translation, rotation and rate of deformation of fluid particles.
3. **Dynamics** - Consideration of forces acting on the fluid particles in motion with respect to one another.

This work mainly focuses on the aspects of dynamics of fluids. Since relative motion of particles exists, shearing forces are important in the analysis of flow of fluids. The phenomena considered in fluid dynamics are macroscopic and hence a fluid is regarded as a continuous medium (or Continuum). This means that any small volume element in the fluid is always supposed so large that it still contains a very great number of molecules. This is called the “Continuum Hypothesis”.

Fluids can be broadly classified into two types based on the density:

1. Constant Density Solution (Incompressible fluids)
2. Variable Density Solution (Compressible fluids) (Yuan 1970)

The investigation of any fluid motion finally ends in solving a set of non-linear partial differential equations called the Fundamental Equations of Fluid Mechanics. The fundamental equations governing any flow phenomena are stated below:

1. **Equation of Continuity:** Mass can neither be created nor destroyed (Law of Conservation of Mass)

$$\frac{\partial \rho}{\partial t} + \nabla \cdot (\vec{q} \rho) = 0 \quad (1.1.1)$$

Where density is denoted by ρ and \vec{q} is the velocity of the fluid at time t .

2. **Equation of Motion:** The total force acting on a fluid mass enclosed in an arbitrary volume fixed in space is equal to the time rate of change of linear momentum (Law of Conservation of Momentum)

$$\rho \frac{D\vec{q}}{Dt} = \vec{X}\rho - \nabla p + \nabla \cdot \tau \quad (1.1.2)$$

Where τ and p represent viscous stress tensor (contains only deviator stresses) and pressure of the fluid, \vec{X} is the body force. The Momentum equation when written in component form gives rise to **Navier-Stokes Equations**.

3. **Equation of Energy:** The energy added to a closed system increases the internal energy per unit mass of the fluid (Law of conservation of Energy)

$$\rho \frac{DU}{Dt} = -(\nabla \cdot \vec{Q}) - P(\nabla \cdot \vec{q}) + \phi \quad (1.1.3)$$

Where U is called internal energy, \vec{Q} is Heat flux vector, $\phi = \nabla \cdot (\vec{q} \tau) - \vec{q} \nabla \cdot \tau$ is the Dissipation function.

4. **Equation of State:** Perfect gas equation:

$$\frac{P}{\rho} = RT \quad (1.1.4)$$

Real gas equation (Van der Waals equation):

$$P = \rho RT \left(\frac{1}{1 - \rho\beta} + \frac{\alpha\rho}{RT} \right)$$

Where R is the perfect gas constant, α and β are constants for a given gas. The above four equations form the backbone of Fluid Mechanics (Schlichting and Gersten 2000).

1.2 CLASSIFICATION BASED ON SHEAR STRESS

Further, based on the application of stress in the fluid, we can classify fluids into two types:-

1. Newtonian Fluids
2. Non-Newtonian Fluids

1.2.1 Newtonian Fluids and Non-Newtonian Fluids

Newtonian fluids are those fluids, which obey the Newton's law, which states "Shear stress is proportional to the velocity gradient". Hence, if we plot a graph of shear stress vs. rate of strain we get a straight line passing through the origin. This is called the flow curve or *Rheogram* of the fluid. The Figure (1.1) shows the shear rate in Newtonian fluid. The constitutive equation for a Newtonian fluid is given by,

$$\tau_{ij} = \left(\frac{2}{3}\mu v_{k,k}\right)\delta_{ij} + \mu(v_{i,j} + v_{j,i}) \quad (1.2.1)$$

where τ_{ij} , v_{ij} , μ and δ_{ij} represent shear stress components, velocity components, viscosity and *Kronecker's delta* function respectively.

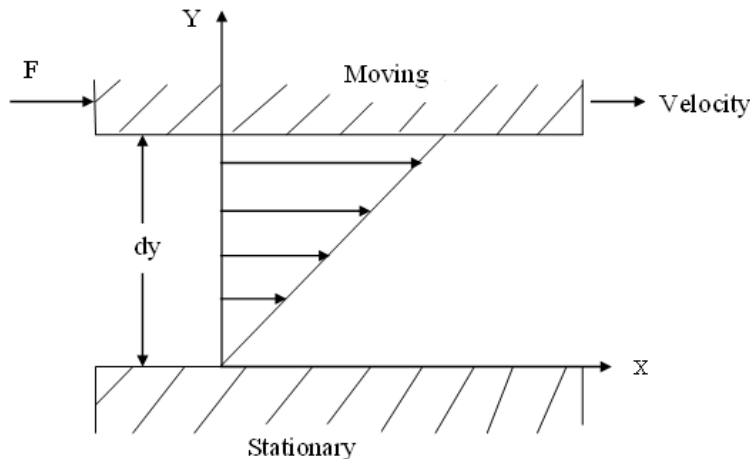


Figure 1.1 Shear Rate in Newtonian Fluid

Any fluid which does not obey Newton's law or any fluid whose flow curve is not linear is called non-Newtonian fluid i.e., the viscosity of a non-Newtonian fluid is not a constant at a given temperature and pressure but depends on various other factors such as the rate of shear in the fluid, apparatus in which the fluid is contained or even the previous history of the fluid. The subject that deals with the non-Newtonian fluids is called *Rheology*. Based on the

non-linearity of the flow curve and time in which the fluid has been sheared, we can classify non-Newtonian fluids as follows:-

1. Time-Independent Non-Newtonian fluids:- Fluids in which the rate of shear at any point is a function of shearing stress only.
2. Time-Dependent Non-Newtonian fluids:- Fluids in which the rate of shear rate and shear stress depends on the time the fluid has been sheared or on its previous history.
3. Viscoelastic fluids:- Fluids which have characteristics of both solids and fluids and exhibit partial elastic recovery after deformation (Wilkinson 1960).

1.3 TIME-INDEPENDENT NON-NEWTONIAN FLUIDS

These types of fluids are governed by the rheological equation of the form

$$e_{ij} = f(\tau_{ij}) \quad (1.3.1)$$

We also name them as non-Newtonian viscous fluids. These fluids can be subdivided into four categories (Skelland 1967) depending upon the nature of the function ' f ' which are given below:

1. Bingham Plastic
 2. Power-law fluids
 3. Casson fluid
 4. Herschel-Bulkley fluids
1. **Bingham plastic (or Bingham fluid):** The flow curve is a straight line with intercept on the shear stress axis. Bingham solid is a material

which supports finite stress elastically without flow and which flows with constant mobility (or plastic fluidity) when the stresses are sufficiently great. The flow of an isotropic incompressible Bingham material is given by (Bird et al. 1983)

$$\begin{aligned} e_{ij} &= 0 && \text{if } \tau < \tau_0 \\ \tau_{ij} &= 2 \left[\mu + \frac{\tau_0}{(2e_{ij}e_{ij})^{\frac{1}{2}}} \right] e_{ij} && \text{if } \tau \geq \tau_0 \end{aligned} \quad (1.3.2)$$

Where μ is the plastic viscosity, τ_0 is the yield stress, τ_{ij} is shear stress and $e_{ij} = (\frac{\partial v_i}{\partial x_j} + \frac{\partial v_j}{\partial x_i})$ is called rate of strain tensor. Practical examples of Bingham materials are greases, pastes and suspensions of polymers.

2. **Power-law fluids:** These fluids are characterized by the equation called “Power-law” given by

$$\tau_{ij} = m \left| \sum_c \sum_d e_{cd} e_{cd} \right|^{\frac{n-1}{2}} e_{ij} \quad (1.3.3)$$

Where m and n are called the consistency index and flow behaviour index of a particular fluid. These fluids show no yield value. The flow curve for these types of fluids becomes linear only at very high rates of shear.

If $n < 1$, then the apparent viscosity (ratio of shear stress to the shear rate) falls progressively with shear rate and these types of fluids are called Pseudo-plastic fluids.

If $n > 1$, then the apparent viscosity for these materials increases with increasing rates of shear and these types of fluids are called Dilatant fluids.

$n = 1$ exhibits Newtonian fluid behaviour. Certain types of high polymers, starch pastes and biological fluids have been characterized as Power-law fluids.

3. **Casson fluid:** These fluids are characterized by an yield stress. A Casson fluid is a shear thinning liquid which has an infinite viscosity at

zero rate of shear, yield stress below which no flow occurs, and a zero viscosity at infinite rate of shear. The constitutive equation governing these types of fluids is given by (Fung 1981).

$$\begin{aligned} e_{ij} &= 0 && \text{if } \tau < \tau_0 \\ \tau_{ij} &= 2 \left[k_c^2 + \tau_0 + \frac{2k_c\tau_0^{\frac{1}{2}}}{(\sum_c \sum_d e_{cd}e_{cd})^{\frac{1}{4}}} \right] e_{ij} && \text{if } \tau \geq \tau_0 \end{aligned} \quad (1.3.4)$$

Where k_c^2 is a constant for a particular fluid and called the Cassons viscosity and τ_0 is the yield stress. This equation has been found to be accurately applicable to silicone suspensions, blood, lithographic varnishes used for preparation of printing inks and synovial fluid present in the knee, ankle of man and cattle.

4. **Herschel-Bulkley fluids:** Herschel-Bulkley fluids are materials possessing a yield value and in flow, they exhibit the characteristics of shear thinning or shear thickening materials. Shear thinning materials are those which decreases in viscosity as the rate of shear increases and shear thickening materials are the one which increases in viscosity as the rate of shear increases. Herschel-Bulkley fluid is the empirical combination of Bingham plastic material and Power law fluids. These materials are also called yield–Power law fluids. The constitutive equation of the Herschel-Bulkley model is given by (Alexandrou et al. 2001)

$$\begin{aligned} e_{ij} &= 0 && \text{if } \tau < \tau_0 \\ \tau_{ij} &= \left(\tau_0 + \eta_1 \left(\frac{e_{ij}e_{ij}}{2} \right)^{\frac{n}{2}} \right) \frac{e_{ij}}{\left(\frac{e_{ij}e_{ij}}{2} \right)^{\frac{1}{2}}} && \text{if } \tau \geq \tau_0 \end{aligned} \quad (1.3.5)$$

Colloidal suspensions, starch pastes, and blood flow through narrow tubes are characterized by Herschel-Bulkey model.

In the present research work, we are confining our studies to Incompressible, Time-independent Non–Newtonian fluids with yield stress and in particular Bingham, Casson and Herschel-Bulkley fluids. The rheogram of these fluids is depicted in Figure (1.2). The physical importance of the yield stress fluids are that the material/fluid behaves like a plastic until a certain amount of stress called the yield stress τ_0 is applied. When the stress exceeds the yield

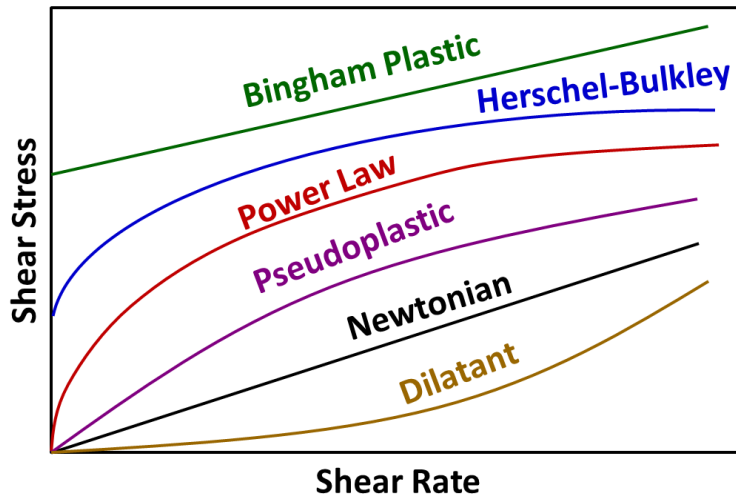


Figure 1.2 Rheogram

stress it behaves like a fluid. Since these fluids have both viscous and plastic properties, they are also called *Viscoplastic fluids*.

1.4 ENTRANCE REGION AND FULLY DEVELOPED FLOW

Any fluid flowing through a pipe will have to enter it at some location. The region is called the entrance region. Flow in the entrance region of the pipe is quite complex. As shown in the Figure (1.3), the fluid typically enters the pipe with a nearly uniform velocity profile at section 1. As the fluid moves through the pipe, viscous effects cause it to stick to the pipe wall (the no-slip boundary condition). This is true whether the fluid is relatively inviscid air or very viscous oil (William 2010).

Thus a boundary layer in which the viscous effects are important is produced along the pipe wall such that the initial velocity profile changes with the distance along the pipe, x , until the fluid reaches the end of the entrance length, section 2, beyond which the velocity profile does not develop with x . The boundary layer has grown in thickness and completely fills the pipe. For the fluid outside the boundary layer, viscous effects are negligible (it is contained in the inviscid core surrounding the centre line from section 1 to section

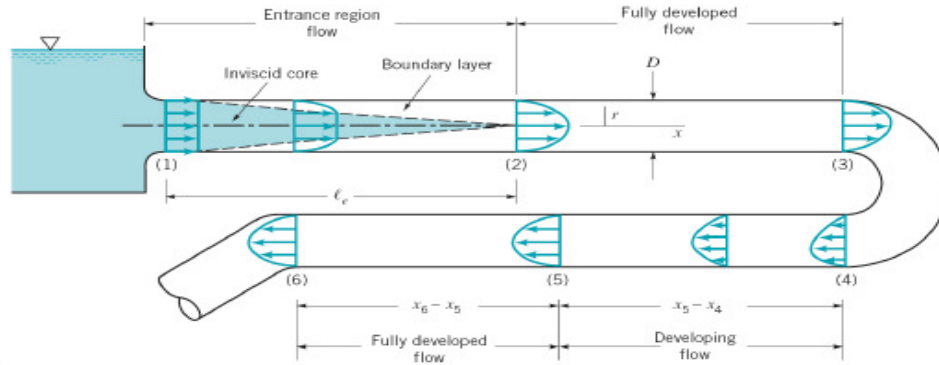


Figure 1.3 Entrance and Fully Developed Flow in a Pipe

2), however for the fluid in the boundary layer viscous effects are important. The shape of the velocity profile in the pipe depends on whether the flow is laminar or turbulent as does the length of the entrance region. Calculating the velocity profile and pressure distribution at the entrance region is quite complex, however as the flow steadies out, the flow becomes simpler to describe since the flow is only a function of the distance from the pipe centre line, and r is independent of x . This is true until there is an abrupt change in the shape of the pipe at section 3.

The flow between sections 2 and 3 is termed as fully developed. Once the abrupt change in shape has occurred, beyond point 4, the flow gradually returns to being fully developed at section 5 and continues on till another abrupt change occurs in the pipe design at point 6. Fully developed in a constant diameter pipe may be driven by gravity and/or pressure forces. For horizontal pipe flow, gravity is neglected. Only the pressure difference is a factor.

We are interested in investigating the laminar flow of non-Newtonian fluids in the entrance region of annular channel. In particular, we are analyzing these problems with the assumption that the inner cylinder is rotating and the outer cylinder is at rest. The entrance region flow in channels constitutes a problem of fundamental interest in engineering applications such as nuclear reactors, polymer processing industries, haemodialyzers and capillary membrane oxygenators. In such installations, the behaviour of the fluid in the entrance region may play a significant part in the total length of the channel

and the pressure drop may be markedly greater than for the case where the flow is regarded as fully developed throughout the channel. Fluid enters a horizontal inlet channel from a large chamber with an uniform velocity along the axial direction. The analysis has been carried out over the wide range of non-Newtonian fluid characteristics and for different values of aspect ratios, (the ratio of the radius of the inner cylinder to that of the outer cylinder) in the case of annuli. The development of boundary layer is visualized when the fluid enters an annulus and the fully developed velocity profile is observed in the region starting from the point down-stream where the boundary layers meet asymptotically with the outer edge of the plug flow zone.

1.4.1 Steps Involved in the Analysis of Entrance Region Flow

The importance of entrance region problem is in analyzing the velocity profiles, pressure variation and temperature distribution in the entrance region of a fluid flow in the rotating concentric annuli. The following are the steps involved in investigating the entrance region flow of non-Newtonian fluid in rotating concentric annuli:

1. The governing equations are deduced from the Navier-Stokes equations by using the Prandtl's boundary layer assumptions.
2. Tangential velocity components W in different regions are derived from the governing equations by using boundary conditions of the problem.
3. Using the tangential velocity components W in different regions, the axial velocity components U and pressure variation P are computed at a time along the radial direction R . Using W , U , P the radial velocity component V is computed.
4. Again using the velocity profiles U and V , the temperature distribution T are thus, obtained numerically for various values of non-Newtonian fluid characteristics and different values of geometrical parameters, wherever applicable.

1.5 LITERATURE SURVEY

Many authors have analyzed the entrance region flow in different channels, like, tubes, pipes, cylinder, between two parallel plates, straight channels, through concentric annulus, between two rotating cylinders, etc. for different non-Newtonian fluids like Casson, Bingham, Hershel-Bulkley, Power-law, etc. The problems are investigated using numerical methods to find the variation of velocity profile, pressure variation, temperature distribution for various flow parameters and geometrical considerations. Some of the relevant studies are briefed here.

The problem of entrance region flow heat transfer in a concentric annuli with rotating inner walls for a Newtonian fluid was studied by many authors. A contribution to the numerical solution of developing laminar flow in the entrance region of concentric annuli with rotating inner walls studied by Coney and El-Shaarawi (1974a). Also, laminar heat transfer in the entrance region of concentric annuli with rotating inner walls was reported by the same authors (1974b). Further, finite difference analysis for laminar flow heat transfer in concentric annuli with simultaneously developing hydrodynamic and thermal boundary layers was also studied by Coney and El-Shaarawi (1975).

Narang (1983) analyzed the entrance region flow of Bingham fluid between parallel plates and could get the exact solution for the problem. Nowak and Gajdeczko (1983) solved numerically the laminar entrance region flow of the Bingham fluid in circular tube. Mishra et al. (1985) studied the flow of the Bingham plastic in the concentric annulus and obtained the results for boundary layer thickness, centre core velocity, pressure drop. Representing blood as Bingham fluid model, Tandon et al. (1994) analyzed the flow in the arteries. Kandasamy (1996) investigated the entrance region flow heat transfer in concentric annuli for a Bingham fluid and presented the velocity distributions, temperature and pressure in the entrance region. Poole and Chhabra (2010) reported the results of a systematic numerical investigation of developing laminar pipe flow of yield stress fluids.

Gupta (1987, 1990) analyzed the entrance flow of Power-law fluids through a

straight channel by studying a hydro dynamically equivalent model of an appropriate Newtonian fluid. Laminar flow heat transfer in the entrance region of concentric annuli for power law fluid was studied by Batra and Sudarsan (1992). Rachid (2002) studied the laminar flow of a Power-law fluid in a circular tube and flow was analyzed in both the inlet and filled regions using an integral boundary layer method. Maia and Gasparetto (2003) applied finite difference method for the Power-law fluid in the annuli and found difference in the entrance geometries. Sayed-Ahmed and Sharaf-El-Din (2006) applied finite difference method to study the laminar flow of a Power-Law fluid in the concentric annulus.

The flow of a Casson fluid in the entrance of annular tubes was investigated numerically by Liu and Shah (1975). Analytical solution for the entrance region blood flow in a concentric annuli obtained by Batra and Jena (1990) by assuming the blood to obey Casson model. Batra and Das (1992) developed the stress-strain relation for the Casson fluid in the annular space between two coaxial rotating cylinders where the inner cylinder was at rest and outer cylinder rotating. Batra and Kandasamy (1992) studied the entrance region flow of Casson fluid in a straight channel numerically without making assumptions on the form of velocity profile within the boundary layer region by a cross sectional integration of the momentum differential equation. Pham (1994) analyzed entry and exit flows of Casson fluids. Flow of Casson fluid in a pipe filled with a homogeneous porous medium was considered by Dash et al. (1996). Cheng and Deville (1996) studied the pulsatile flow of non-Newtonian fluids through arterial stenosis by the Casson model. Ahmed and Attia (1998) investigated Magneto hydrodynamic flow and heat transfer of a non-Newtonian fluid in an eccentric annulus. Flow of Casson fluid in a narrow tube with a side branch was investigated by Misra and Ghosh (2000). A non-Newton fluid flow model for blood flow through a catheterized artery-steady flow was analyzed by Sankar and Hemalatha (2007). The Casson fluid over an unsteady stretching surface was investigated by Swati et al. (2013)

Batra and Kandasamy (1990) numerically investigated the flow of Hershel-Bulkley Fluids in a duct without pre-assuming the form of velocity profile within the boundary layer region. Das (1992) studied the flow of Herschel-

Bulkley fluid in a circular tube by using the momentum integral and momentum energy integral techniques, and found that in the case of the momentum energy method the values of entrance length and loss coefficient are appreciably higher than those obtained by using the momentum integral method. Round and Yu (1993) analyzed the developing flows of Herschel-Bulkley fluids through concentric annuli. Nouar et al. (1995) reported the results of numerical analysis of the thermal convection for Herschel-Bulkley fluids. Soares et al. (1999) analyzed the heat transfer in the entrance region flow of viscoplastic material inside the tubes. Numerical modeling of helical flow of viscoplastic fluid in eccentric annuli was done by Hussain and Sharif (2000). The problem of laminar heat transfer convection for Herschel-Bulkley within concentric annular ducts was studied by Viana et al. (2001) with the help of integral transform method considering the plug flow region. Hammad et al. (2001) analyzed the laminar flow of a Herschel-Bulkley fluid over an axisymmetric sudden expansion. Manglik and Fang (2002) numerically investigated the flow of non-Newtonian fluids through annuli. The study of heat transfer to viscoplastic materials flowing axially through concentric annuli was investigated by Soares et al. (2003). Kandasamy et al. (2007b) investigated the entrance region flow of heat transfer in concentric annuli for Herschel-Bulkley fluids and presented the velocity distributions, temperature and pressure in the entrance region. Recently, Pai and Kandasamy (2014) have investigated the entrance region flow of Herschel-Bulkley fluid in an annular cylinder without making prior assumptions on the form of velocity profile within the boundary layer region.

1.6 ORGANIZATION OF THE THESIS

The present work focuses on the analysis of entrance region flow of time independent non-Newtonian fluid with yield stress categories, namely, Bingham, Casson, Herschel-Bulkley fluids in concentric annuli with heat transfer. The analysis has been carried out under the assumption that the inner cylinder is rotating and the outer cylinder is at rest. With the Prandtl's boundary layer assumptions, the equations of conservation of mass, momentum and en-

ergy are discretized and solved using linearized implicit finite difference technique. The system of linear and non-linear algebraic equations thus obtained has been solved by the Gauss-Jordan method and Newton-Raphson iterative method respectively. The development of axial velocity profile, radial velocity profile, tangential velocity profile, pressure variation and temperature distribution along the radial direction in the entrance region have been determined for different values of non-Newtonian flow characteristics and geometrical parameters. The effects of these on the flow properties have been discussed.

In Chapter 1, a brief introduction to the fundamental equations fluid mechanics is given and further the fluids are classified based on the stress-strain relations or the fluid constitutive equations. A short insight is provided so as to recall the constitutive theory of non-Newtonian fluid, the assumptions of boundary layer and brief history of entrance region flow. Further, a review of some of the important literature related to the present work has been given in this chapter.

In chapter 2, the entrance region flow heat transfer in concentric annuli with rotating inner wall for Bingham non-Newtonian fluid has been studied numerically. The inner cylinder is assumed to be rotating with a constant angular velocity and the outer cylinder is stationary. A finite difference analysis is used to obtain the velocity components, pressure variation and temperature distribution along the radial direction. With the Prandtl's boundary layer assumptions, the continuity, momentum and energy equations are solved iteratively using a finite difference method. Computational results are obtained for various non-Newtonian flow parameters and geometrical considerations. The development of the axial velocity profile, radial velocity profile, tangential velocity profile, pressure variation and temperature distribution in the entrance region have been analyzed. From this study, it is found that the tangential velocity decreases from the inner wall to outer wall of the annulus. Also, it is observed that the value of pressure increases from a minimum at the inner wall to a maximum at the outer wall and the pressure does not vary so much with respect to the radial coordinate in the region near the outer wall. The effect of the inner wall rotation on all these flow characteristics seem to be

less significant. Further it is found that by increasing the Bingham number, the temperature decreases. Comparison of the present results with the results available in literature for various particular cases has been done and found to be in agreement.

The chapter 3 deals with the problem of entrance region flow heat transfer of Casson fluid in concentric annuli with rotating inner wall. The Casson fluid enters the horizontal concentric annuli from a large chamber with a uniform flat velocity along the axial direction and with some initial pressure and temperature. The inner cylinder rotates with constant angular velocity and the outer cylinder is at rest. We consider the flow as steady, laminar, incompressible, axisymmetric with constant physical properties, having negligible viscous dissipation and no internal heat generation. Moreover, it is assumed that the axial heat diffusion is negligible as compared to the radial diffusion. Using finite difference technique with Prandtl's boundary layer assumptions, the equations of conservation of mass, momentum and energy are solved iteratively. The development of axial velocity profile, radial velocity profile, tangential velocity profile, pressure variation and temperature distribution in the entrance region have been determined for different values of aspect ratio, Casson number, Prandtl's number and axial position. The axial velocity component increases when the annular gap is becoming small for all values of Casson numbers. It is observed that the temperature keeps decreasing for the fluids with high Casson number. Moreover, it is found that the temperature is high when the flow is taking place in a small annular gap. Comparisons are done with the results of other recent works for various particular cases and good agreement is observed.

A finite difference analysis of the entrance region flow heat transfer of Herschel-Bulkley fluids in concentric annuli with rotating inner wall has been carried out and presented in the next chapter. The analysis is made for simultaneously developing hydrodynamic boundary layer in concentric annuli with the inner cylinder assumed to be rotating with a constant angular velocity and the outer cylinder being stationary. A finite difference analysis is used to obtain the velocity profiles, pressure variation and temperature distribution

along the radial direction. With the Prandtl's boundary layer assumptions, the continuity, momentum and energy equations are solved iteratively using a finite difference method. Computational results are obtained for various non-Newtonian flow parameters and geometrical considerations. A significant asymmetry is found in the entrance region which is gradually reduced as the flow develops. For smaller values of aspect ratio and higher values of Herschel-Bulkley number the flow is found to stabilize more gradually. Also, it is found that increasing the flow behaviour index, the axial velocity component increases at all values of Herschel-Bulkley numbers and the velocity profile develops faster as flow behaviour index increases. It indicates that the axial velocity is more for shear thinning fluids and for shear thickening fluids the axial velocity component is less. Further, it is observed that the velocity profile takes the parabolic form as n tends to 1 with Herschel-Bulkley number being zero (Newtonian fluid). The values of radial velocity are negative in the region near the outer wall since it is in the opposite direction to the radial coordinate R and it has positive values near the inner wall because it has the same direction of the radial coordinate. This phenomena is due to the rotation of the inner cylinder of the annulus. Also, it is observed that the the temperature decreases from the rotating inner wall to the stationary outer wall of the annulus. Moreover, for the fluids with high Herschel Bulkley numbers, i.e., for high viscous fluids the temperature is found to decreasing. The present results are compared with results of particular cases of non-rotating cylinders, the Bingham and Power-law fluids and are found to be matching.

The present work is mainly about the investigation of velocity profiles, pressure variation and temperature distribution of viscoplastic fluids along the radial direction in the entrance region of concentric annuli with rotating inner wall. The last chapter concludes the entire research work presented and describes possible future research work in this area.

Chapter 2

ENTRANCE REGION FLOW HEAT TRANSFER IN CONCENTRIC ANNULI WITH ROTATING INNER WALL FOR BINGHAM FLUID

2.1 INTRODUCTION

The study of non-Newtonian laminar flow heat transfer in the entrance region of an annuli is of practical importance in engineering applications such as design of compact heat exchangers, axial-flow turbo machinery and polymer processing industries. Very often, optimum conditions are provided by laminar flow operations for keeping low pumping power in proportion to the heat transfer rate. In the nuclear reactor field, this happens when coolant flow rates are reduced. In case of turbulent flow, when heating starts at the duct entrance, the hydrodynamic boundary layers normally are linear near the duct entrance and the transitions to turbulence occurs at some distance downstream from the entrance. Hence, it is necessary to take into consideration the presence of such laminar entrance flow in calculating the heat transfer parameters for a duct in which the fully developed flow is turbulent. Many important industrial fluids are non-Newtonian in their flow characteristics and are referred to as rheological fluids. These include blood; various suspensions such as coalwater or coal-oil slurries, glues, inks, foods; polymer solutions; paints and many others. The fluid considered here is the Bingham model, which is of 'time-independent yield stress' fluid category.

In this chapter, the problem of entrance region flow heat transfer of Bingham fluid in concentric annuli with rotating inner wall has been investigated. The analysis has been carried out under the assumption that the inner cylinder is rotating and the outer cylinder is at rest. With Prandtl's boundary layer assumptions, the equation of conservation of mass, momentum and energy are discretized and solved using linearized implicit finite difference technique. The system of linear algebraic equations thus obtained, has been solved by the Gauss-Jordan method. The development of axial velocity profile, radial velocity profile, tangential velocity profile, pressure variation and temperature distribution in the entrance region have been determined for different values of non-Newtonian flow characteristics and geometrical parameters along the radial direction. The effects of these on the flow properties have been discussed.

2.2 MATHEMATICAL FORMULATION OF THE PROBLEM

The geometry of the problem is shown in Figure (2.1). The Bingham fluid enters the horizontal concentric annuli with inner and outer radius R_1 and R_2 , respectively, from a large chamber with a uniform flat velocity profile u_0 along the axial direction z and with an initial pressure p_0 and temperature t_0 . The inner cylinder rotates with an angular velocity ω and the outer cylinder is at rest. The flow is steady, laminar, incompressible, axisymmetric with constant physical properties, having negligible viscous dissipation and no internal heat generation. Moreover, it is assumed that the axial heat diffusion is negligible as compared to the radial diffusion. We consider a cylindrical polar coordinate system with the origin at the inlet section on the central axis of the annulus, the z -axis along the axial direction and the radial direction r perpendicular to the z -axis.

Under the above assumptions with the usual Prandtl's boundary layer assumptions Schlichting and Gersten (2000), the governing equations in polar coordinate system (r, θ, z) for a Bingham fluid in the entrance region are:

$$\text{Continuity equation : } \frac{\partial(rv)}{\partial r} + \frac{\partial(ru)}{\partial z} = 0 \quad (2.2.1)$$

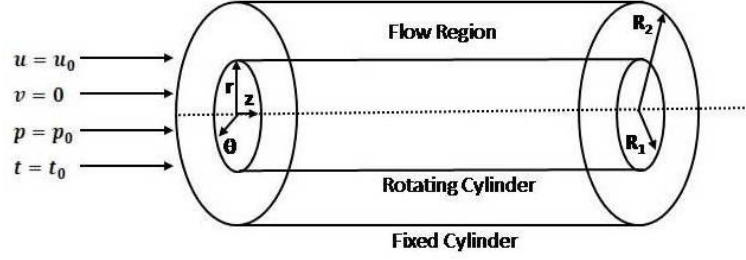


Figure 2.1 Geometry of the Problem

$$r - \text{momentum equation} : \frac{w^2}{r} = \frac{1}{\rho} \frac{\partial p}{\partial r} \quad (2.2.2)$$

$$\theta - \text{momentum equation} : v \frac{\partial w}{\partial r} + u \frac{\partial w}{\partial z} + \frac{vw}{r} = \frac{1}{\rho r^2} \frac{\partial}{\partial r} \left(r^2 \left[\tau_0 + \mu r \frac{\partial}{\partial r} \left(\frac{w}{r} \right) \right] \right) \quad (2.2.3)$$

$$z - \text{momentum equation} : v \frac{\partial u}{\partial r} + u \frac{\partial u}{\partial z} = -\frac{1}{\rho} \frac{\partial p}{\partial z} + \frac{1}{\rho r} \frac{\partial}{\partial r} \left(r \left[\tau_0 + \mu \frac{\partial u}{\partial r} \right] \right) \quad (2.2.4)$$

$$\text{Energy equation} : v \frac{\partial t}{\partial r} + u \frac{\partial t}{\partial z} = \alpha \left[\frac{\partial^2 t}{\partial r^2} + \frac{1}{r} \frac{\partial t}{\partial r} \right] \quad (2.2.5)$$

where u , v , w are the velocity components in z , r , θ directions respectively, t is the fluid temperature at any point, ρ is the density of the fluid, α is the thermal diffusivity, τ_0 is the yield stress, μ is the viscosity and p is the pressure.

The boundary conditions associated with the hydrodynamic part of the problem are given by

$$\begin{aligned} &\text{for } z \geq 0 \text{ and } r = R_1, v = u = 0 \text{ and } w = \omega R_1 \\ &\text{for } z \geq 0 \text{ and } r = R_2, v = u = w = 0 \\ &\text{for } z = 0 \text{ and } R_1 < r < R_2, u = u_0 \\ &\text{at } z = 0, p = p_0 \end{aligned} \quad (2.2.6)$$

Using the boundary conditions (2.2.6), the continuity Equation (2.2.1) can be expressed in the following integral form:

$$2 \int_{R_1}^{R_2} r u dr = (R_2^2 - R_1^2) u_0 \quad (2.2.7)$$

Introducing the following dimensionless variables and parameters,

$$R = \frac{r}{R_2}, U = \frac{u}{u_0}, V = \frac{\rho v R_2}{\mu_r}, W = \frac{w}{\omega R_1}, N = \frac{R_1}{R_2}, P = \frac{p - p_0}{\rho u_0^2}$$

$$Z = \frac{2z(1 - N)}{R_2 Re}, B = \frac{\tau_0 R_2}{\mu u_0}, T_a = \frac{2\omega^2 \rho^2 R_1^2 (R_2 - R_1)^3}{\mu_r^2 (R_1 + R_2)}, \text{ here } \mu_r = \mu \left(\frac{\omega R_1}{R_2} \right)$$

$$T = \frac{t - t_0}{t_w - t_0}, Re = \frac{2\rho(R_2 - R_1)u_0}{k}, Pr = \frac{\mu C_p}{K}$$

Here B is the Bingham number, Re is the Reynolds number, T_a is the Taylor number, μ_r is know as reference viscosity, Pr is the Prandtl's number, C_p is the specific heat at constant pressure, K is the thermal conductivity, t_0 is the fluid temperature at annulus entry, t_w is the isothermal wall temperature and N is known as aspect ratio of the annulus.

Equations (2.2.1) to (2.2.5) and (2.2.7) in the dimensionless form are given by

$$\frac{\partial V}{\partial R} + \frac{V}{R} + \frac{\partial U}{\partial Z} = 0 \quad (2.2.8)$$

$$\frac{W^2}{R} = \frac{Re^2(1 - N)}{2(1 + N)T_a} \frac{\partial P}{\partial R} \quad (2.2.9)$$

$$V \frac{\partial W}{\partial R} + U \frac{\partial W}{\partial Z} + \frac{VW}{R} = \frac{\partial^2 W}{\partial R^2} + \frac{1}{R} \frac{\partial W}{\partial R} - \frac{W}{R^2} + \frac{2B}{R} \quad (2.2.10)$$

$$V \frac{\partial U}{\partial R} + U \frac{\partial U}{\partial Z} = -\frac{\partial P}{\partial Z} + \frac{1}{R} \frac{\partial U}{\partial R} + \frac{\partial^2 U}{\partial R^2} + \frac{B}{R} \quad (2.2.11)$$

$$V \frac{\partial T}{\partial R} + U \frac{\partial T}{\partial Z} = \frac{1}{Pr} \left[\frac{\partial^2 T}{\partial R^2} + \frac{1}{R} \frac{\partial T}{\partial R} \right] \quad (2.2.12)$$

and

$$2 \int_N^1 RU dR = (1 - N^2) \quad (2.2.13)$$

The boundary conditions (2.2.6) associated with the hydrodynamic part of the problem in the dimensionless form are given by

$$\begin{aligned} &\text{for } Z \geq 0 \text{ and } R = N, V = U = 0 \text{ and } W = 1 \\ &\text{for } Z \geq 0 \text{ and } R = 1, V = U = W = 0 \\ &\text{for } Z = 0 \text{ and } N < R < 1, U = 1 \\ &\text{at } Z = 0, P = 0 \end{aligned} \quad (2.2.14)$$

For the thermal part, considering the outer cylinder to be adiabatic and the inner cylinder to be isothermal, the problem has been solved under the following boundary conditions:

$$\begin{aligned} &\text{for } Z \geq 0, T = 1 \text{ at } R = N \\ &\text{for } Z \geq 0, \frac{\partial T}{\partial R} = 0 \text{ at } R = 1 \\ &\text{for } Z = 0 \text{ and } N < R < 1, T = 0 \end{aligned} \quad (2.2.15)$$

The problem can be similarly analyzed for the case when the inner cylinder is adiabatic and the outer cylinder is isothermal. The boundary conditions for

this case will be

$$\begin{aligned}
 &\text{for } Z \geq 0, T = 1 \text{ at } R = 1 \\
 &\text{for } Z \geq 0, \frac{\partial T}{\partial R} = 0 \text{ at } R = N \\
 &\text{for } Z = 0 \text{ and } N < R < 1, T = 0
 \end{aligned} \tag{2.2.16}$$

2.3 SOLUTION OF THE PROBLEM

The numerical analysis and the method of solution adopted here can be considered as an indirect extension of the work of Coney and El-Shaarawi (1974a). Considering the mesh network of Figure (2.2), the following difference representations are made. Here ΔR and ΔZ represent the grid size along the radial and axial directions respectively.

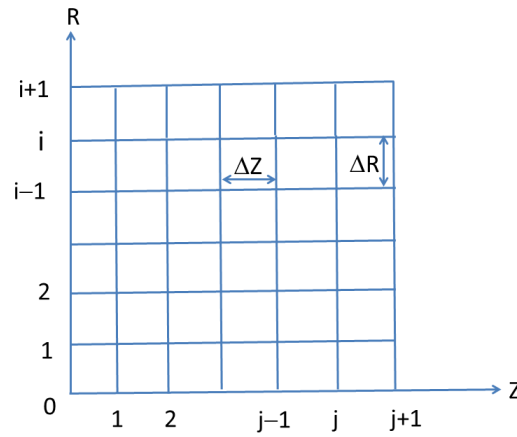


Figure 2.2 Grid Formation for Finite-Difference Representations

$$\begin{aligned}
 V_{i+1,j+1} &= V_{i,j+1} \left(\frac{N + i\Delta R}{N + (i+1)\Delta R} \right) - \frac{\Delta R}{4\Delta Z} \left(\frac{2N + (2i+1)\Delta R}{N + (i+1)\Delta R} \right) * \\
 &(U_{i+1,j+1} + U_{i,j+1} - U_{i+1,j} - U_{i,j})
 \end{aligned} \tag{2.3.1}$$

$$\frac{W_{i,j+1}^2}{N + i\Delta R} = \frac{(1 - N)Re^2}{2T_a(1 + N)} \frac{P_{i,j+1} - P_{i-1,j+1}}{\Delta R} \quad (2.3.2)$$

$$\begin{aligned} Vi,j & \left(\frac{W_{i+1,j+1} + W_{i+1,j} - W_{i-1,j} - W_{i-1,j+1}}{4\Delta R} \right) + Ui,j \left(\frac{W_{i,j+1} - W_{i,j}}{\Delta Z} \right) + \\ \frac{V_{i,j}W_{i,j}}{N + i\Delta R} & = \frac{W_{i+1,j+1} + W_{i+1,j} - 2W_{i,j+1} - 2W_{i,j} + W_{i-1,j} + W_{i-1,j+1}}{2(\Delta R)^2} + \\ \frac{W_{i+1,j+1} + W_{i+1,j} - W_{i-1,j} - W_{i-1,j+1}}{(N + i\Delta R)4\Delta R} & - \frac{W_{i,j}}{(N + i\Delta R)^2} + \frac{2B}{N + i\Delta R} \end{aligned} \quad (2.3.3)$$

$$\begin{aligned} Vi,j & \left(\frac{U_{i+1,j+1} - U_{i-1,j+1}}{2\Delta R} \right) + Ui,j \left(\frac{U_{i,j+1} - U_{i,j}}{\Delta Z} \right) = - \left(\frac{P_{i,j+1} - P_{i,j}}{\Delta Z} \right) + \\ \left(\frac{U_{i+1,j+1} - U_{i-1,j+1}}{(N + i\Delta R)2\Delta R} \right) & + \left(\frac{U_{i+1,j+1} - 2U_{i,j+1} + U_{i-1,j+1}}{(\Delta R)^2} \right) + \frac{B}{N + i\Delta R} \end{aligned} \quad (2.3.4)$$

Where $i=0$ at $R=N$ and $i=m$ at $R=1$. Here m is the number of radial increments in the mesh.

The application of trapezoidal rule to Equation (2.2.13) gives

$$\frac{\Delta R}{2}(NU_{0,j} + U_{m,j}) + \Delta R \sum_{i=1}^{m-1} U_{i,j}(N + i\Delta R) = \left(\frac{1 - N^2}{2} \right)$$

The boundary condition (2.2.14) gives $U_{0,j} = U_{m,j} = 0$ and the above equation reduces to

$$\Delta R \sum_{i=1}^{m-1} U_{i,j}(N + i\Delta R) = \left(\frac{1 - N^2}{2} \right) \quad (2.3.5)$$

The set of difference Equations (2.3.1) to (2.3.6) have been solved by the iterative procedure. Starting at the $j=0$ column (annulus entrance) and applying Equation (2.3.3) for $1 \leq i \leq m - 1$, we get a system of linear algebraic equations. This system has been solved by using Gauss-Jordan method to obtain the values of the tangential velocity component W at the second column $j=1$.

Then applying Equations (2.3.2) and (2.3.4) for $1 \leq i \leq m - 1$ and Equation (2.3.5), we get a system of linear equations. Again solving this system by Gauss-Jordan method, we obtain the values of the axial velocity component U and the pressure P at the second column $j=1$. Finally, the values of the radial velocity component V at the second column $j=1$ are obtained from Equation (2.3.1) by Gauss-Jordan method using the known values of U . Repeating this procedure, we can advance, column by column, along the axial direction of the annulus until the flow becomes axially and tangentially fully developed.

With the values of V and U known, the energy Equation (2.2.12) can be considered as a linear equation in T with variable coefficients. By using the implicit finite difference technique, the energy equation can be represented as

$$\begin{aligned}
& T_{i+1,j+1} \left(\frac{V_{i,j+1} + V_{i,j}}{8\Delta R} - \frac{1}{2Pr(\Delta R)^2} - \frac{1}{4(N + i\Delta R)Pr\Delta R} \right) + \\
& T_{i-1,j+1} \left(\frac{1}{4(N + i\Delta R)Pr\Delta R} - \frac{V_{i,j+1} + V_{i,j}}{8\Delta R} - \frac{1}{2Pr(\Delta R)^2} \right) = \\
& T_{i,j} \left(\frac{U_{i,j+1} + U_{i,j}}{2\Delta Z} - \frac{1}{Pr(\Delta R)^2} \right) - T_{i,j+1} \left(\frac{U_{i,j+1} + U_{i,j}}{2\Delta Z} + \frac{1}{Pr(\Delta R)^2} \right) + \\
& T_{i+1,j} \left(\frac{1}{2Pr(\Delta R)^2} + \frac{1}{4(N + i\Delta R)Pr\Delta R} - \frac{V_{i,j+1} + V_{i,j}}{8\Delta R} \right) + \\
& T_{i-1,j} \left(\frac{V_{i,j+1} + V_{i,j}}{8\Delta R} - \frac{1}{2Pr(\Delta R)^2} - \frac{1}{4(N + i\Delta R)Pr\Delta R} \right) \quad (2.3.6)
\end{aligned}$$

Equation (2.3.6), with the boundary conditions (2.2.15), have been solved to obtain the temperature distribution in the annular entrance region. The system of linear equations associated with each column has been solved by Gauss-Jordan elimination method.

2.4 RESULTS AND DISCUSSION

Numerical calculations have been performed for all admissible values of Bingham number B , aspect ratio N and various parameters as shown in Table (2.4.1). The Prandtl's number has been chosen initially as 7 and gradually increased to 15. The velocity profiles and pressure variation along radial direction R have been computed for different values of N and B and shown in Figures (2.3) to (2.26). The temperature distributions during the rotation of the inner wall of the annuli have been shown in Figures (2.27) to (2.42).

Table 2.4.1 List of Various Parameters Used

Various Values of Parameters					
Aspect Ratio N	Radial Position R	Position	Axial Position Z	$Rt=Re^2/Ta$	Bingham Number B
0.3	0.1		0.02, 0.03	0, 20	0, 10, 20, 30
0.5	0.1		0.02, 0.03	0, 20	0, 10, 20, 30
0.8	0.05		0.02, 0.03	0, 20	0, 10, 20, 30

Figures (2.3) to (2.8) show the development of the tangential velocity profile component W for $N=0.3, 0.5, 0.8$ at axial positions of $Z=0.02, 0.03$ and for different values of Bingham numbers B . Here, the parameter Rt which is the ratio of Reynolds number to Taylor number is fixed as 20. The values of tangential velocity decrease from the inner wall to outer wall of the annulus. Also, it is found that with the increase of aspect ratio N , the tangential velocity profile increases. That is, the tangential velocity is more when the gap of the annuli is small. Further, it is found that with the increase of Bingham number, the tangential velocity profile increases. This means, the tangential velocity tends to increase for thick viscous fluids when the inner cylinder is rotating. From the computed results corresponding to various values of Rt , it is observed that the effect of the parameter Rt is negligible for the tangential velocity.

Figures (2.9) to (2.14) show the development of the axial velocity profile component U for same parameter values. The computation has been done for various values of the parameter Rt to study the effect of rotation of inner

cylinder. The values corresponding to $Rt=0$ and 20 are depicted in these figures. It is found that the velocity component U increases with the increase of Bingham number B as well as aspect ratio N . Also for stationary ($Rt=0$) as well as rotating inner cylinder ($Rt=20$), it is observed that the velocity profile takes the parabolic form when Bingham number B reaches zero (Newtonian fluid) for both the cases. But the rotational effect on the axial velocity component is very small as per the observed results. Here, our results corresponding to $B=0$ match with the results of Coney and El-Shaarawi (1974a) and $Rt=0$ with various Bingham numbers match with the results of Kandasamy (1996).

The radial velocity profile component V for $N = 0.3, 0.5$ and 0.8 for different values of Bingham number B and axial positions are depicted in the Figures (2.15) to (2.20). Again, the parameter Rt values are taken as 0 and 20 for computational purpose. The values of radial velocity are negative in the region near the outer wall since it is in the opposite direction to the radial coordinate R and it has positive values near the inner wall because it has the same direction of the radial coordinate. The values of the radial velocity decreases with increase of Rt and Bingham number B at any cross section of the axis. The results of particular cases like $Rt=0$ (without rotation) and $B=0$ (Newtonian fluid) match fully with the earlier research works of the same authors.

Figures (2.21) to (2.26) show the distribution of the pressure P along the radial coordinate R for the same chosen values of the parameters involved. It is found that the value of P increases from a minimum at the inner wall to a maximum at the outer wall. Further, it is found that with increase of Bingham numbers, increases the pressure values P . This is because of the pressure will tend to be higher for thick viscous fluids. Moreover, it is observed that the pressure is slowly becoming independent of the radial coordinate in the region close to the outer wall. The effect of inner wall rotation on the fluid pressure seems to be very low at any cross section. Here also, the results corresponding to $B=0$ and $Rt=0$ are in agreement with the earlier results of same authors.

Figures (2.27) to (2.42) shows the temperature distribution T and it is observed from the results obtained, that the temperature decreases with increase

of Bingham number B for a fixed annular width. Other wise we can say that the temperature distribution is less for a high viscous fluids. The temperature is found to decrease from the rotating inner wall gradually to the stationary outer wall of the annulus. This is for the case of inner wall being isothermal and outer wall being adiabatic in our analysis. The pattern may be in reverse if the outer cylinder is isothermal and inner cylinder is adiabatic. Further, the temperature keeps increasing, if we reduce the annular gap for a fixed Bingham number.

For our computation, the Prandtl's number has been initially set as 7 and the results of the temperature distribution have been obtained by increasing the value of Prandtl's number Pr up to 15. The results corresponding to $Pr=7$ and $Pr=15$ are shown here. The temperature is found to decrease gradually when we increase the Prandtl's number by fixing the other parameters, Bingham number and aspect ratio. Again, for high viscous fluids i.e., for the fluids with high Bingham number, the temperature is found to be decreasing. But the temperature is becoming more along the axial direction for the fixed aspect ratio, Bingham number and Prandtl's number.

The present results are compared with available results in literature for various particular cases and are found to be in agreement. When the Bingham number $B=0$, our results match with the results corresponding to Newtonian fluid of Coney and El-Shaarawi (1974a). In the case of stationary cylinders, the results in our analysis are matching with the results of Kandasamy (1996). Also in the case of non-thermal part these results match with the results of Nadiminti and Kandasamy (2016b).

2.5 CONCLUSION

Numerical results for the entrance region flow heat transfer in concentric annuli with rotating inner wall for Bingham fluid are presented. The effects of the parameters N , Pr and B on the velocity profiles, pressure variation and temperature distribution are studied along radial direction R . The present results are found in agreement with the results corresponding to various particular cases available in literature.

From this study, the following can be concluded.

1. Tangential velocity decrease from the inner wall to outer wall of the annulus and the tangential velocity is high for thick viscous fluids.
2. Increasing the aspect ratio N , the axial velocity component U increases at all values of Bingham numbers B .
3. Radial velocity is found to be dependent only on the axial coordinate.
4. Pressure increases from a minimum at the inner wall to a maximum at the outer wall of the annulus and pressure does not vary so much with respect to the radial coordinate in the region near the outer wall.
5. The temperature decreases from the rotating inner wall to the stationary outer wall of the annulus.
6. When increasing the Bingham numbers B , it is observed that the temperature decreases.
7. With the increase of Prandtl's numbers, the temperature decreases.
8. When aspect ratio N increases, it is found that the temperature increases.
9. With the increase of axial position Z , the temperature also increases.

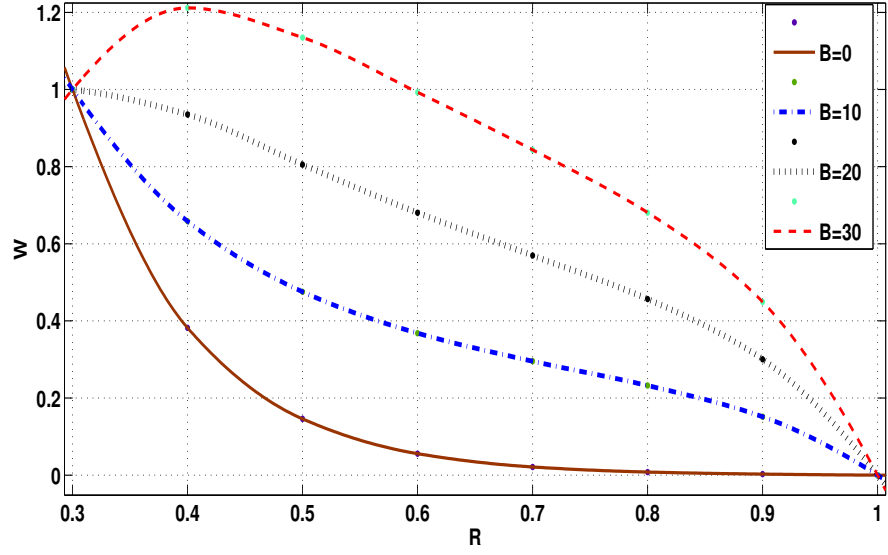


Figure 2.3 Tangential Velocity Profile for $N=0.3$ at $Z=0.02$

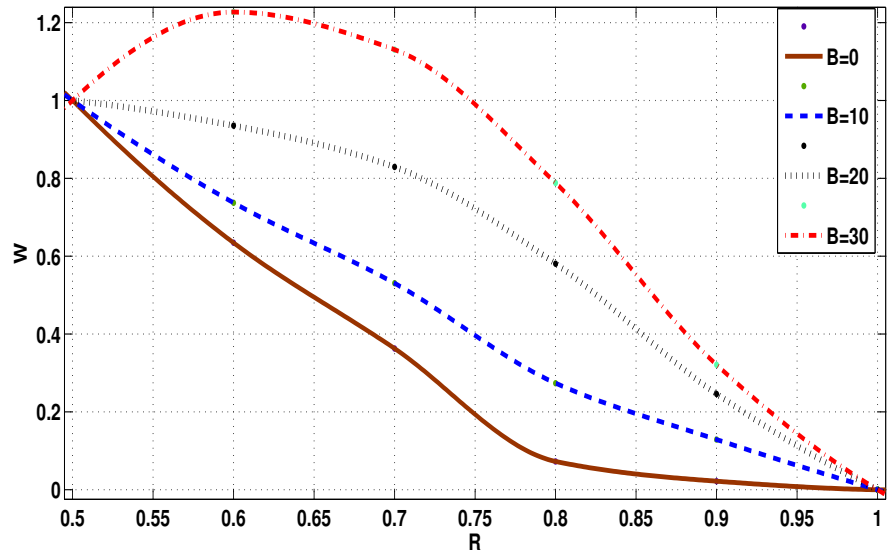


Figure 2.4 Tangential Velocity Profile for $N=0.5$ at $Z=0.02$

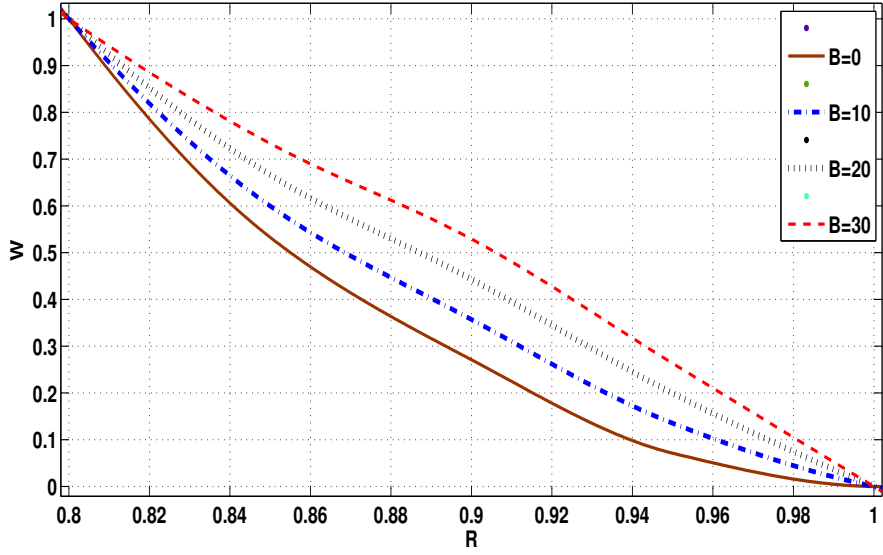


Figure 2.5 Tangential Velocity Profile for $N=0.8$ at $Z=0.02$

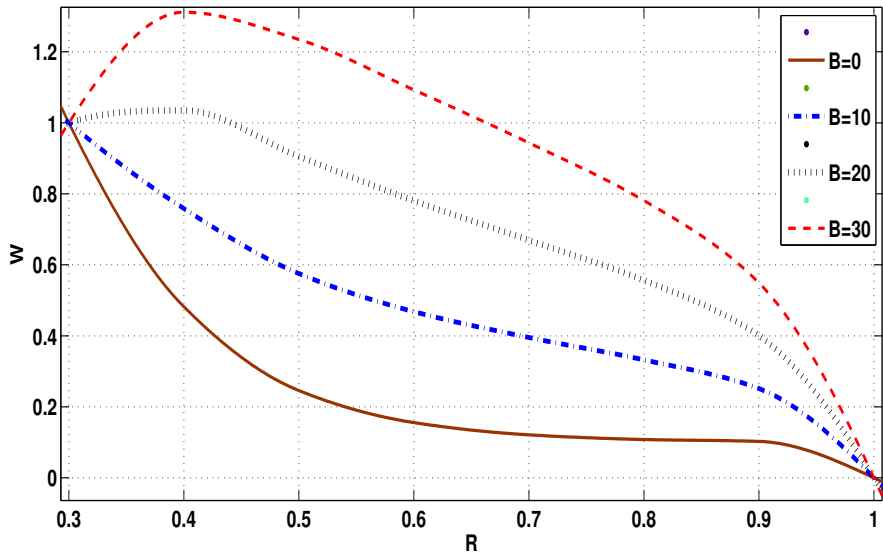


Figure 2.6 Tangential Velocity Profile for $N=0.3$ at $Z=0.03$

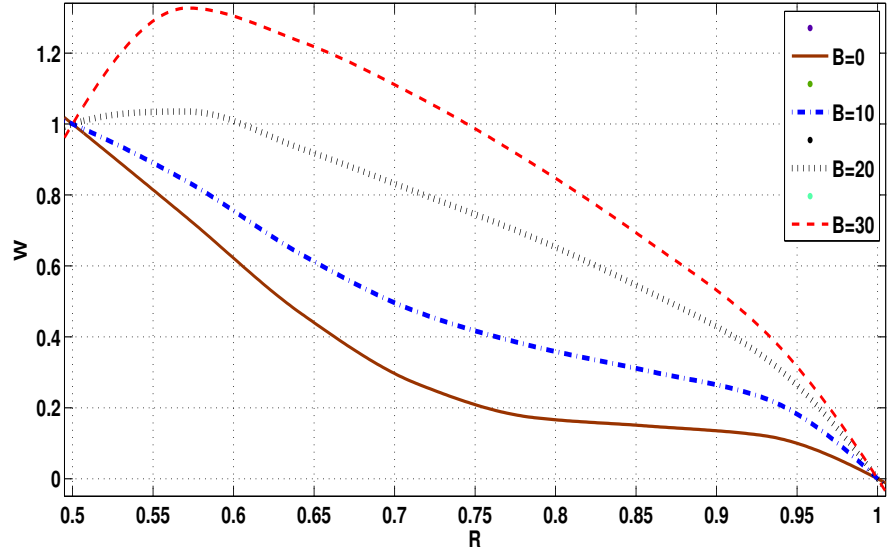


Figure 2.7 Tangential Velocity Profile for $N=0.5$ at $Z=0.03$

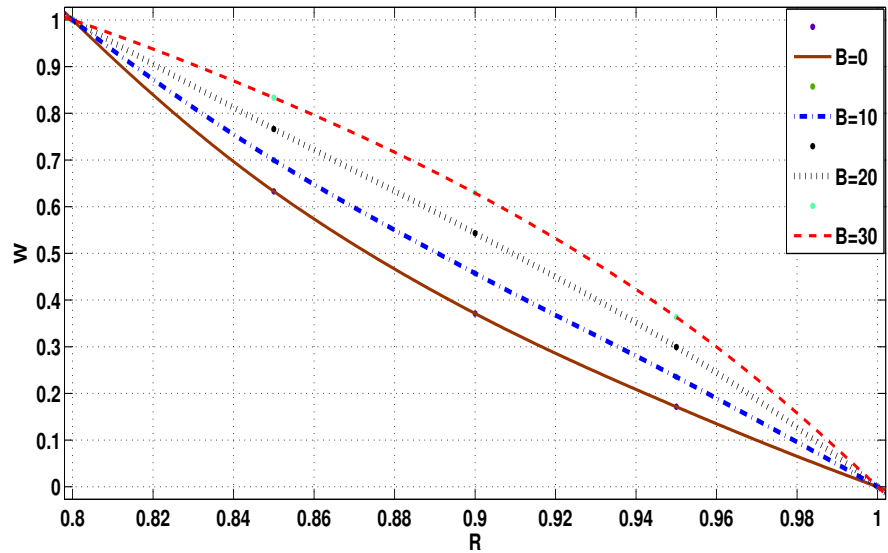


Figure 2.8 Tangential Velocity Profile for $N=0.8$ at $Z=0.03$

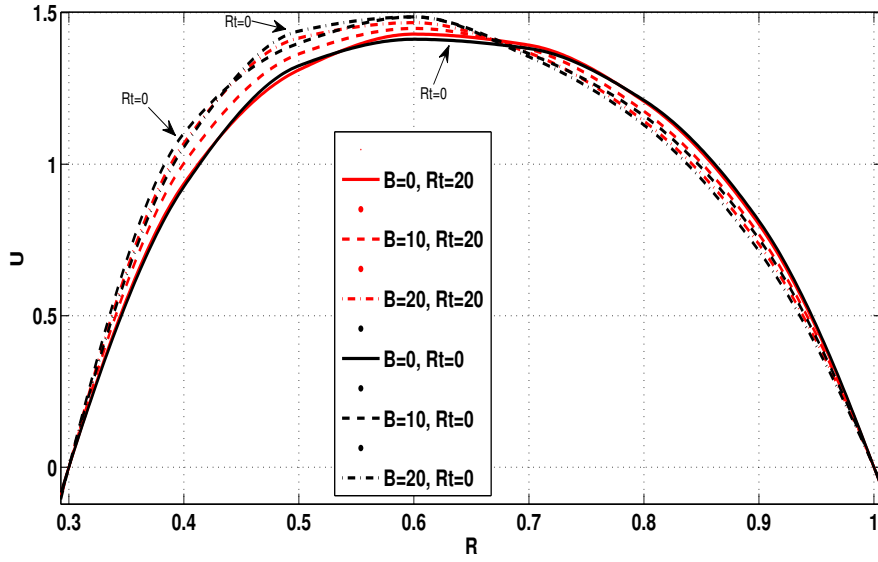


Figure 2.9 Axial Velocity Profile for $N=0.3$ at $Z=0.02$

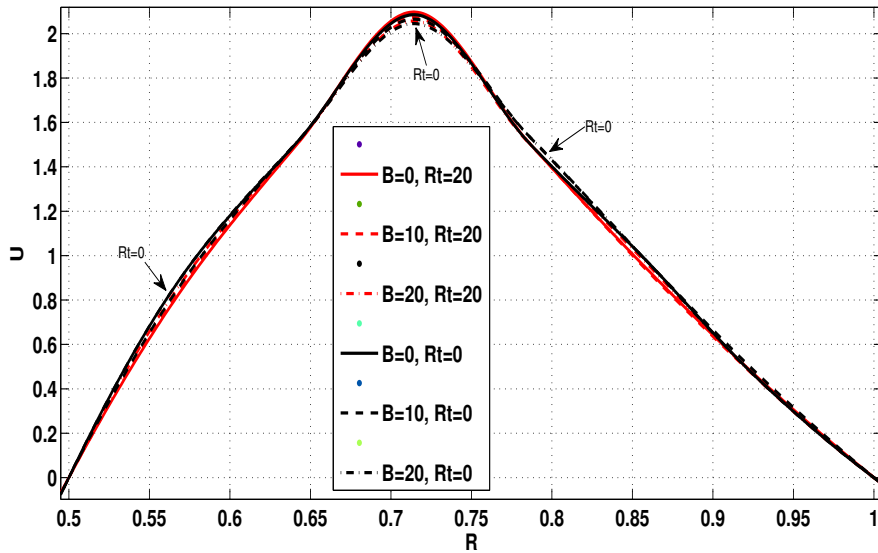


Figure 2.10 Axial Velocity Profile for $N=0.5$ at $Z=0.02$

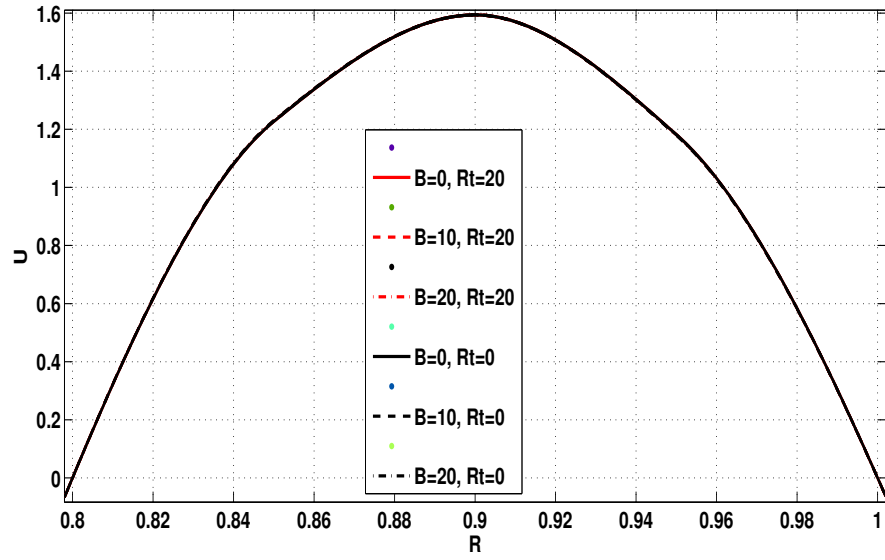


Figure 2.11 Axial Velocity Profile for $N=0.8$ at $Z=0.02$

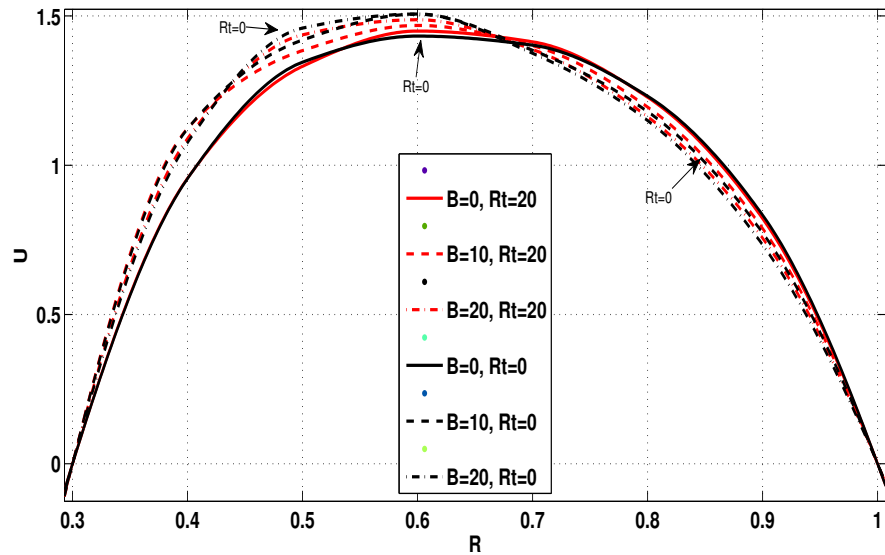


Figure 2.12 Axial Velocity Profile for $N=0.3$ at $Z=0.03$

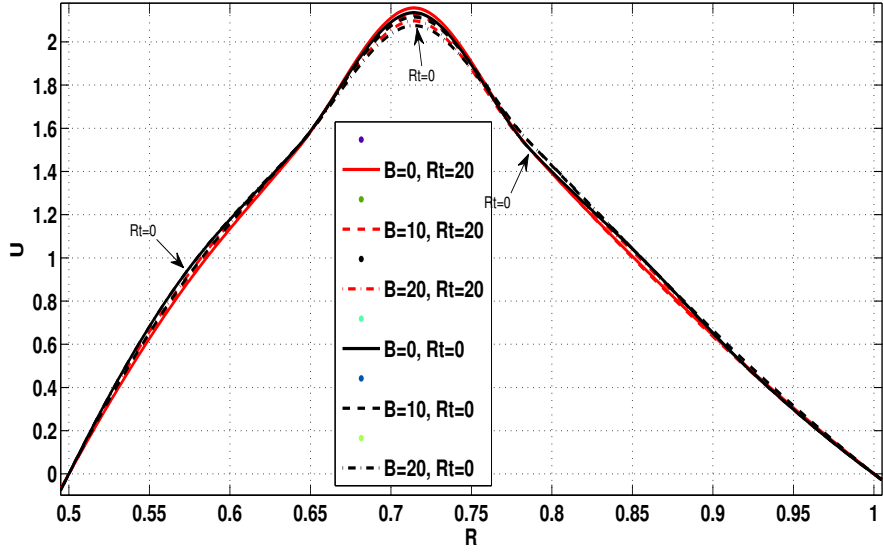


Figure 2.13 Axial Velocity Profile for $N=0.5$ at $Z=0.03$

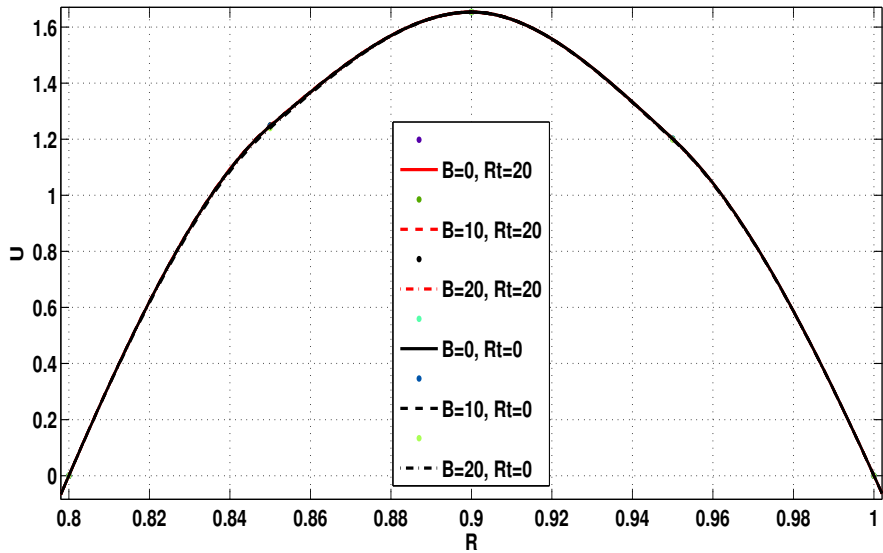


Figure 2.14 Axial Velocity Profile for $N=0.8$ at $Z=0.03$

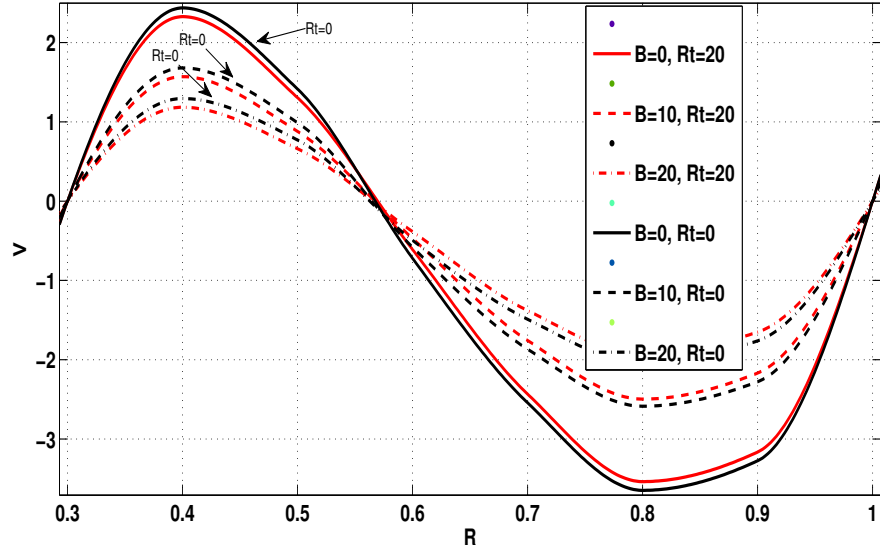


Figure 2.15 Radial Velocity Profile for $N=0.3$ at $Z=0.02$

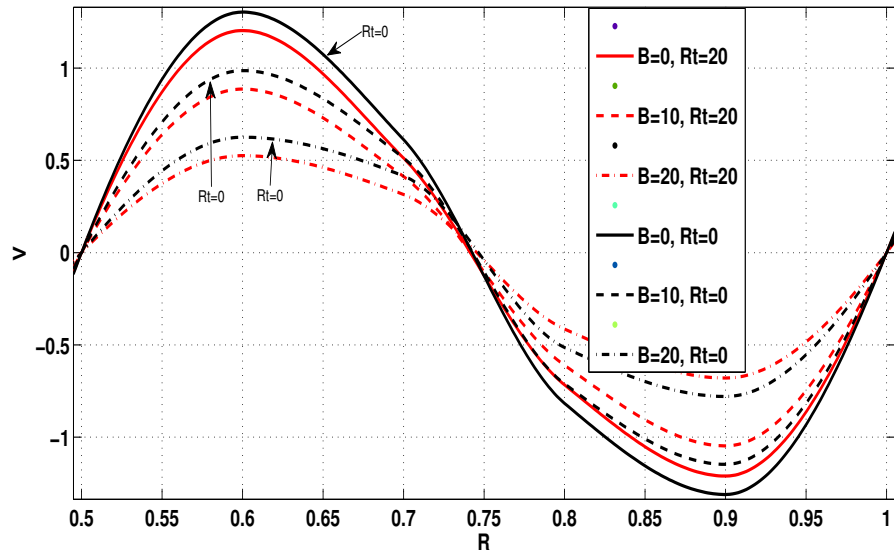


Figure 2.16 Radial Velocity Profile for $N=0.5$ at $Z=0.02$

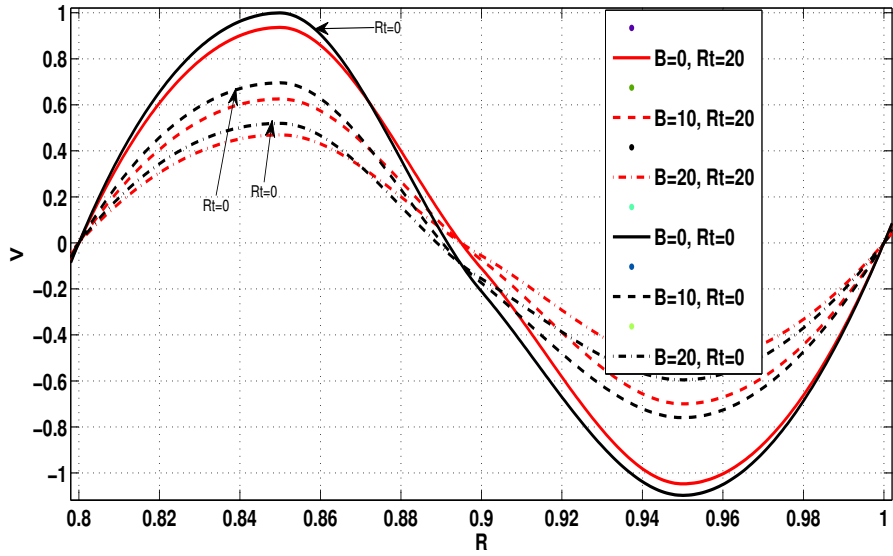


Figure 2.17 Radial Velocity Profile for $N=0.8$ at $Z=0.02$

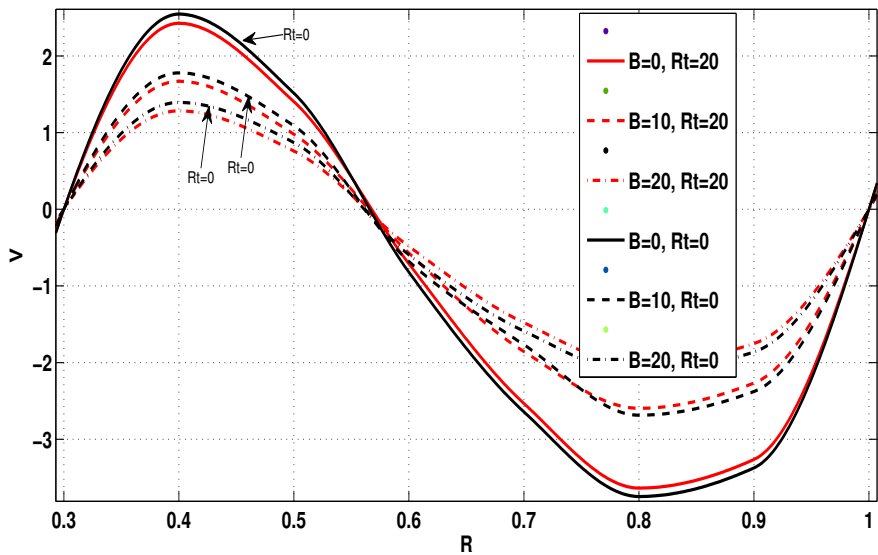


Figure 2.18 Radial Velocity Profile for $N=0.3$ at $Z=0.03$

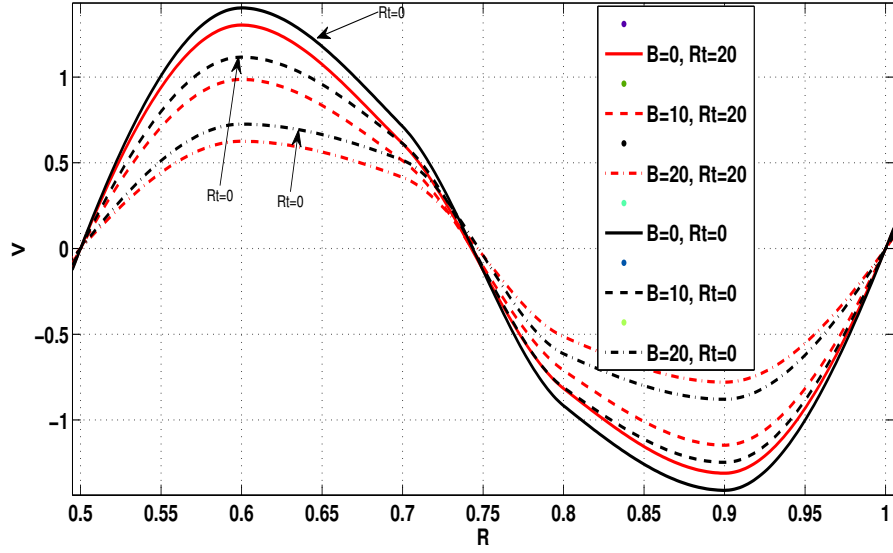


Figure 2.19 Radial Velocity Profile for $N=0.5$ at $Z=0.03$

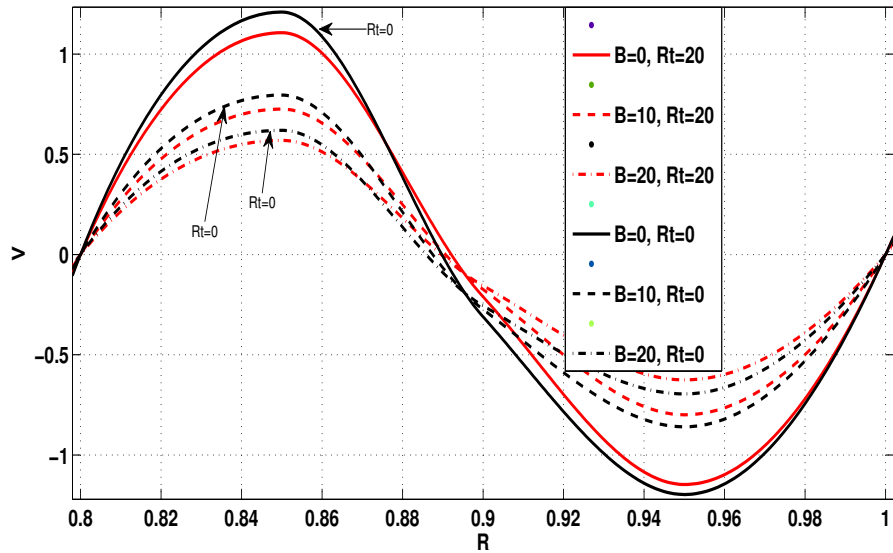


Figure 2.20 Radial Velocity Profile for $N=0.8$ at $Z=0.03$

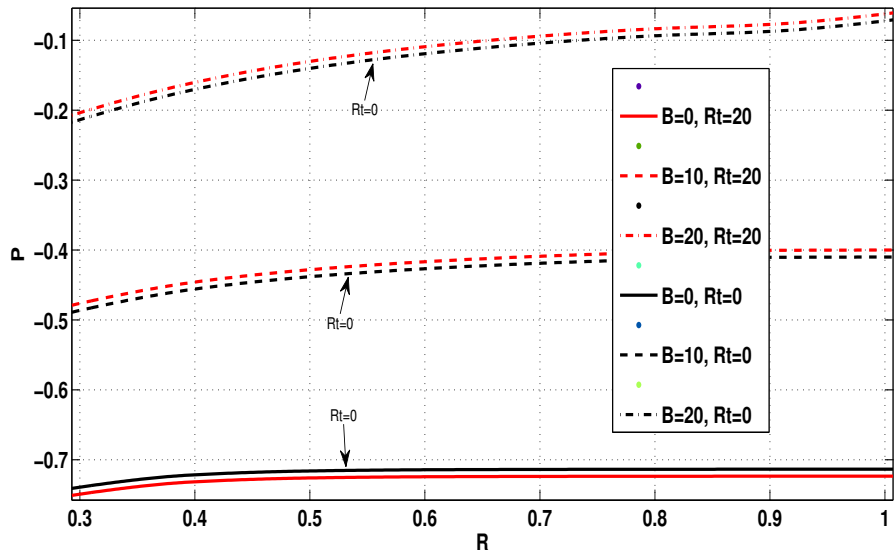


Figure 2.21 Pressure Variation for $N=0.3$ at $Z=0.02$

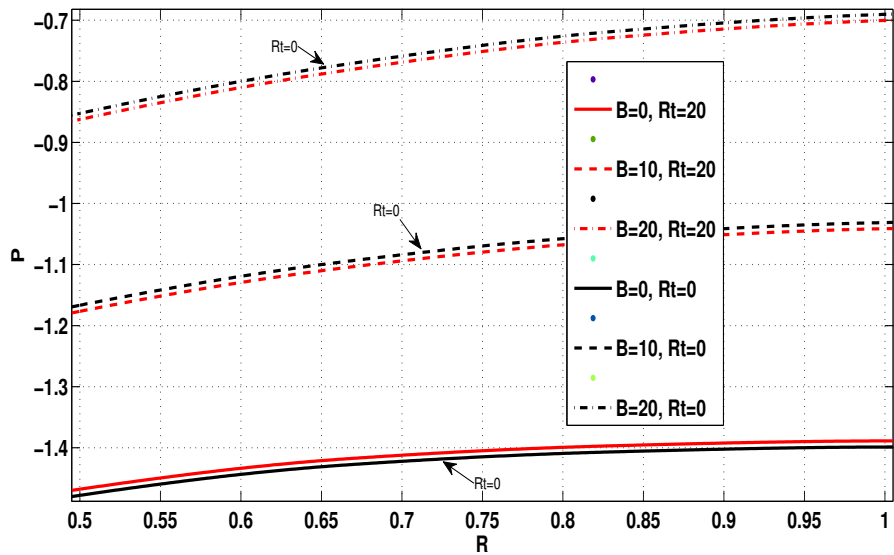


Figure 2.22 Pressure Variation for $N=0.5$ at $Z=0.02$

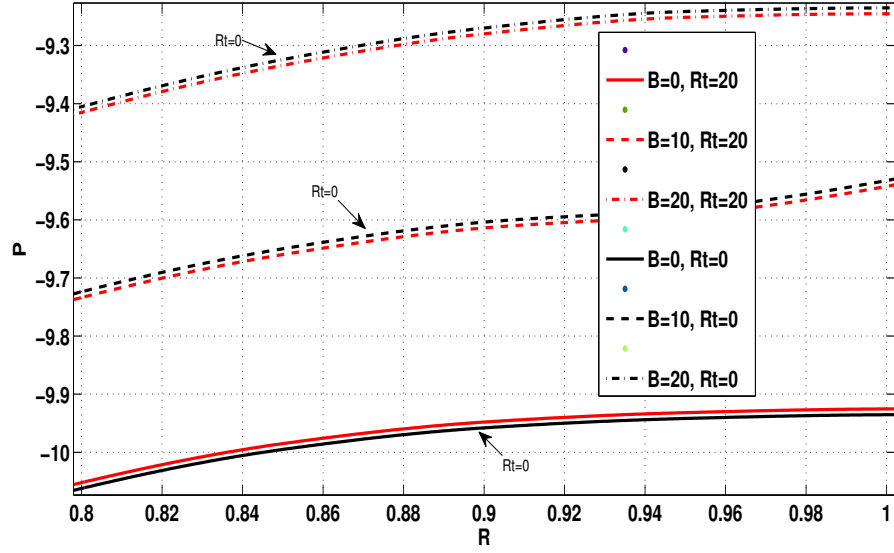


Figure 2.23 Pressure Variation for $N=0.8$ at $Z=0.02$

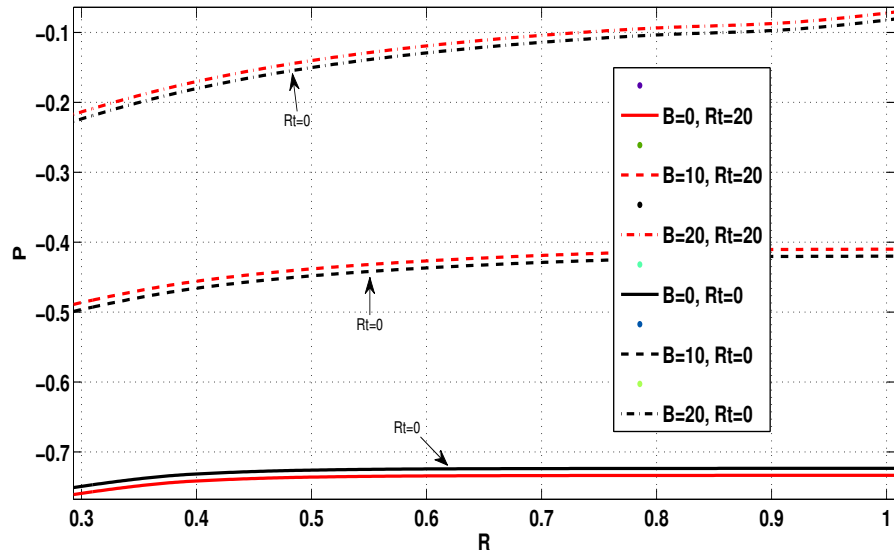


Figure 2.24 Pressure Variation for $N=0.3$ at $Z=0.03$

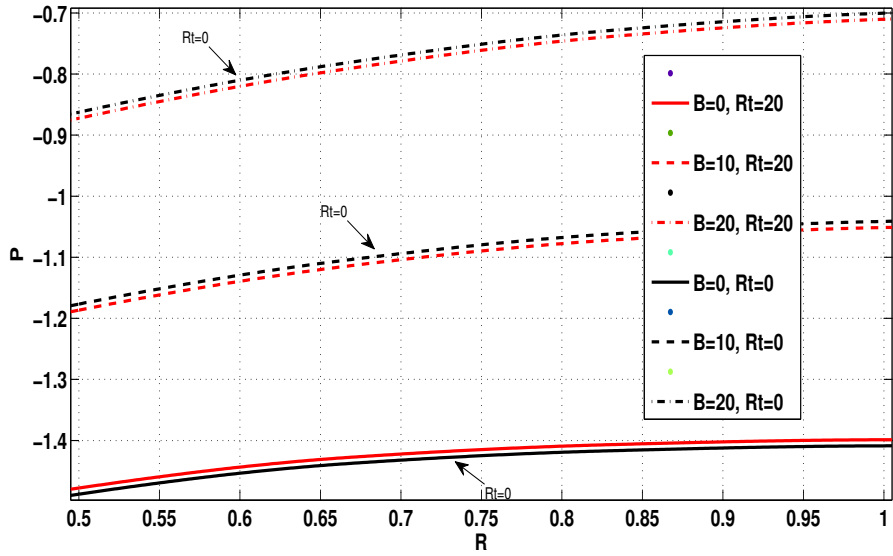


Figure 2.25 Pressure Variation for $N=0.5$ at $Z=0.03$

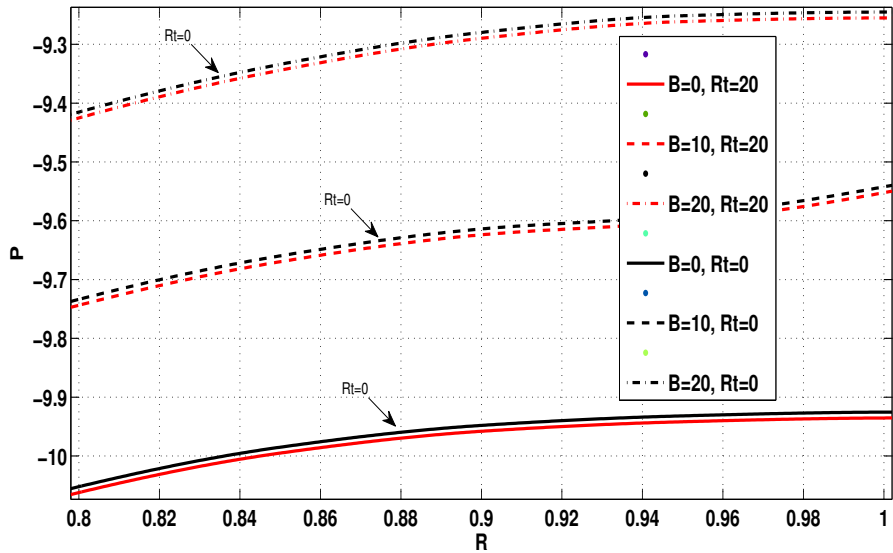


Figure 2.26 Pressure Variation for $N=0.8$ at $Z=0.03$

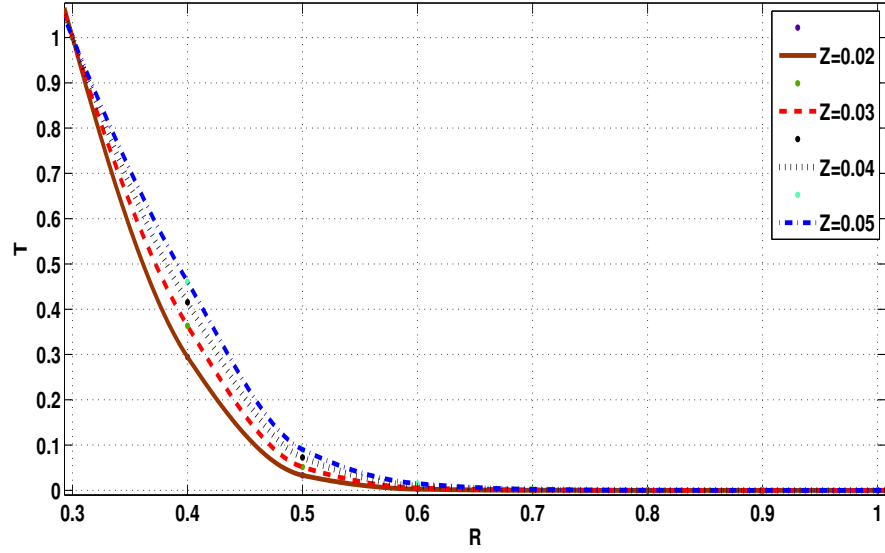


Figure 2.27 Temperature Distribution for $N=0.3$, $Pr=7$ and $B=0$

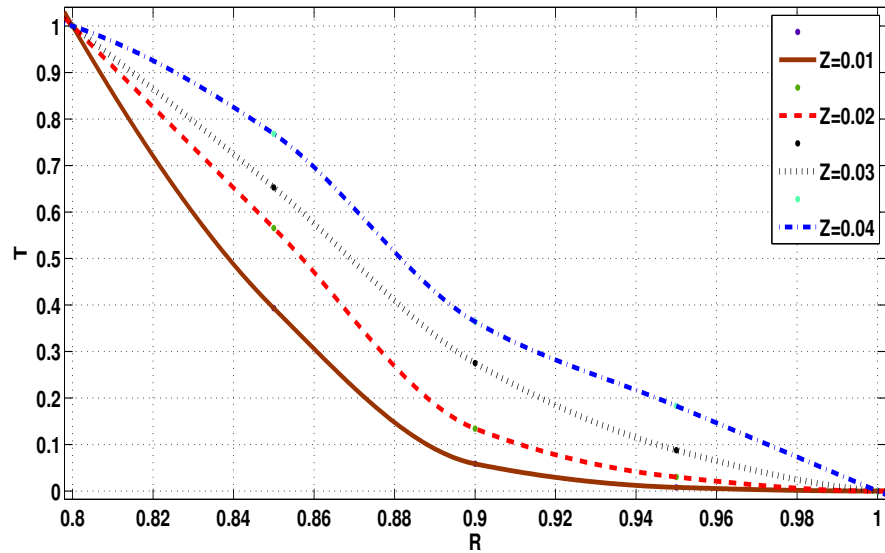


Figure 2.28 Temperature Distribution for $N=0.8$, $Pr=7$ and $B=0$

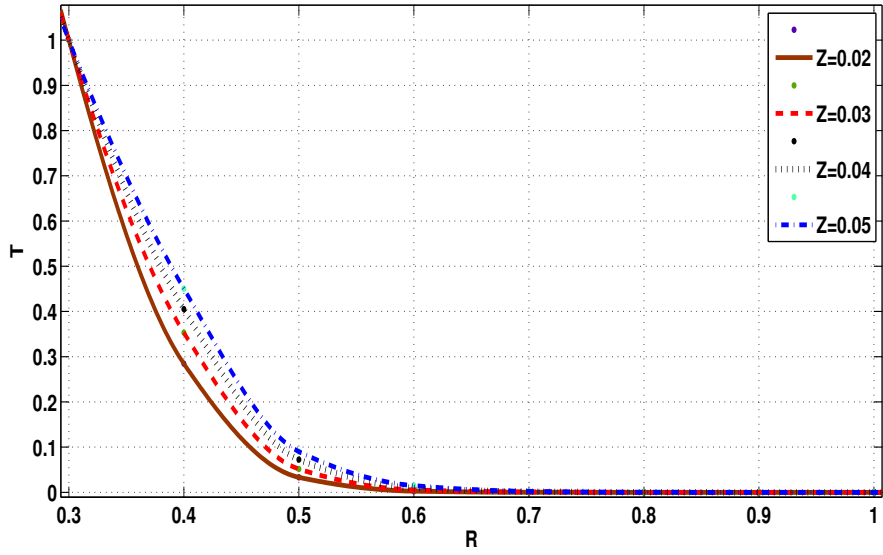


Figure 2.29 Temperature Distribution for $N=0.3$, $Pr=7$ and $B=10$

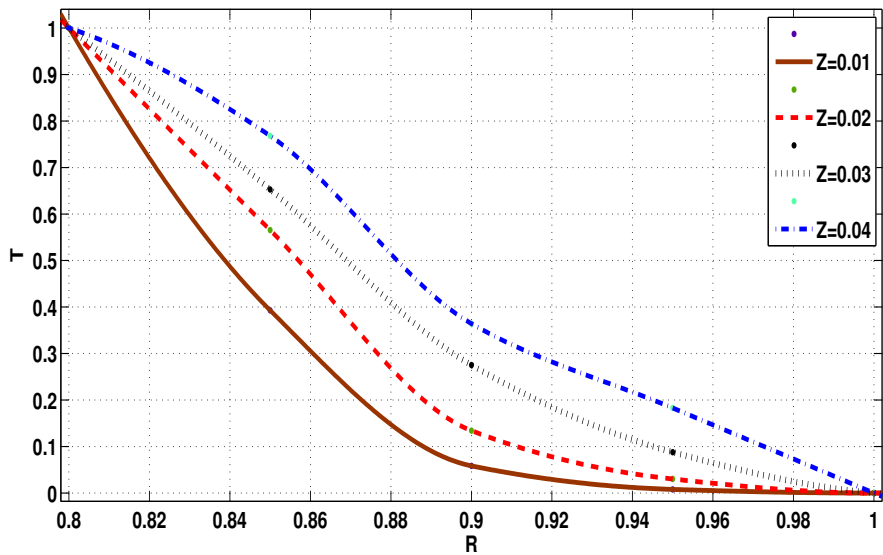


Figure 2.30 Temperature Distribution for $N=0.8$, $Pr=7$ and $B=10$

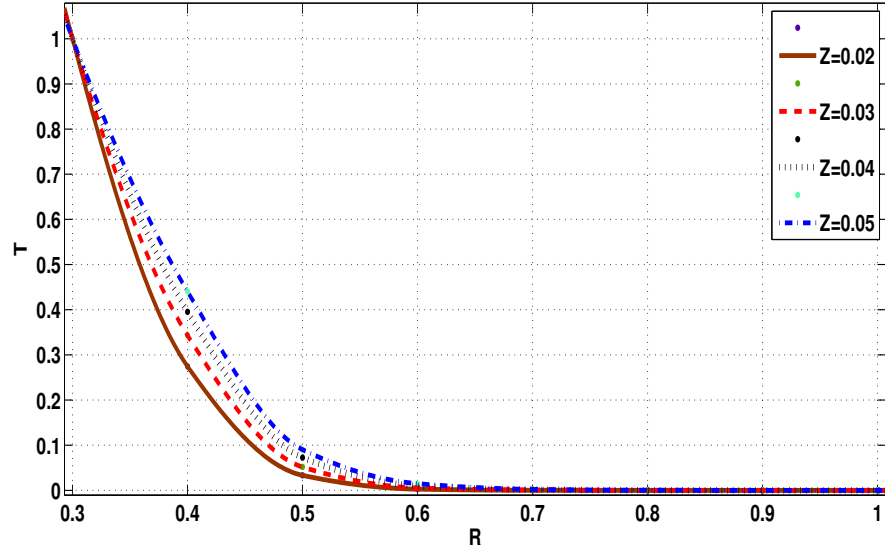


Figure 2.31 Temperature Distribution for $N=0.3$, $Pr=7$ and $B=20$

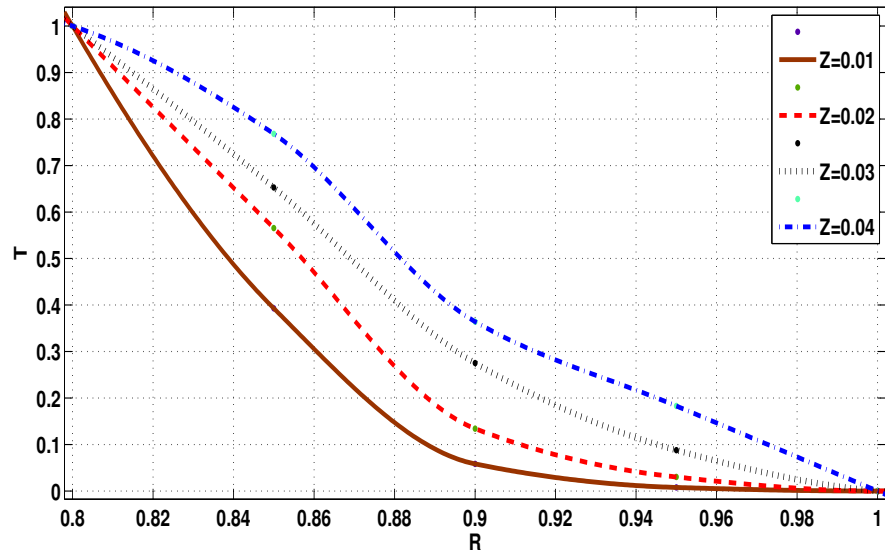


Figure 2.32 Temperature Distribution for $N=0.8$, $Pr=7$ and $B=20$

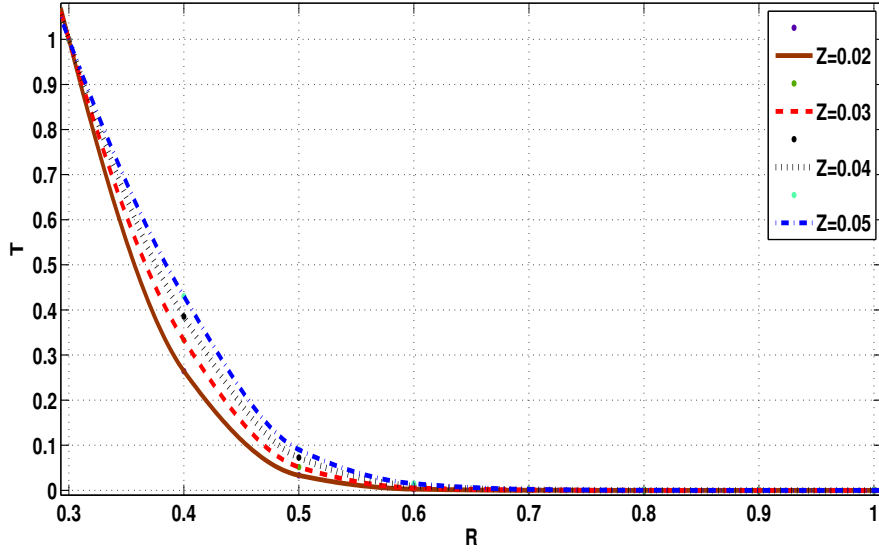


Figure 2.33 Temperature Distribution for $N=0.3$, $Pr=7$ and $B=30$

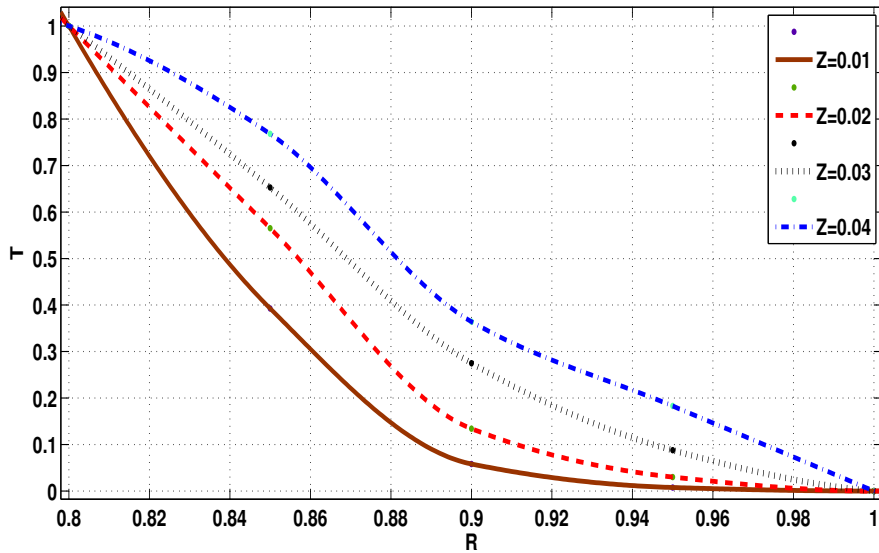


Figure 2.34 Temperature Distribution for $N=0.8$, $Pr=7$ and $B=30$

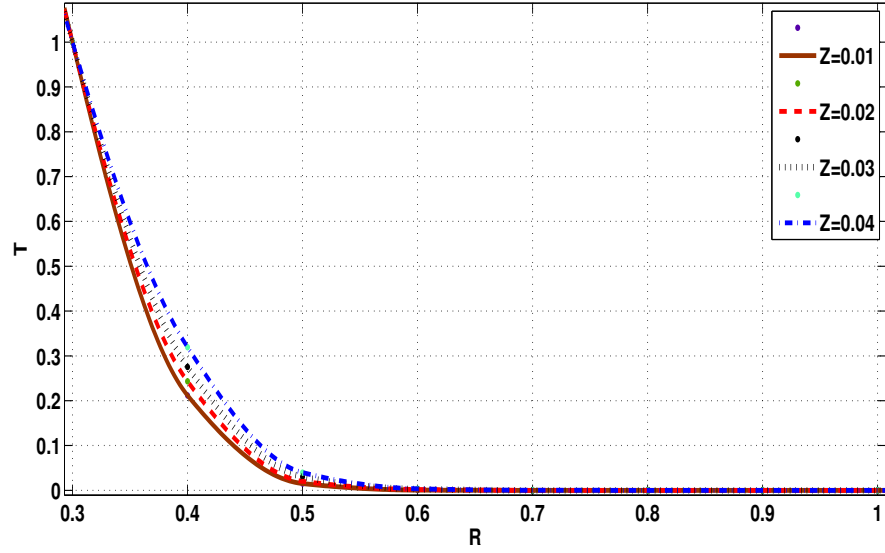


Figure 2.35 Temperature Distribution for $N=0.3$, $Pr=15$ and $B=0$

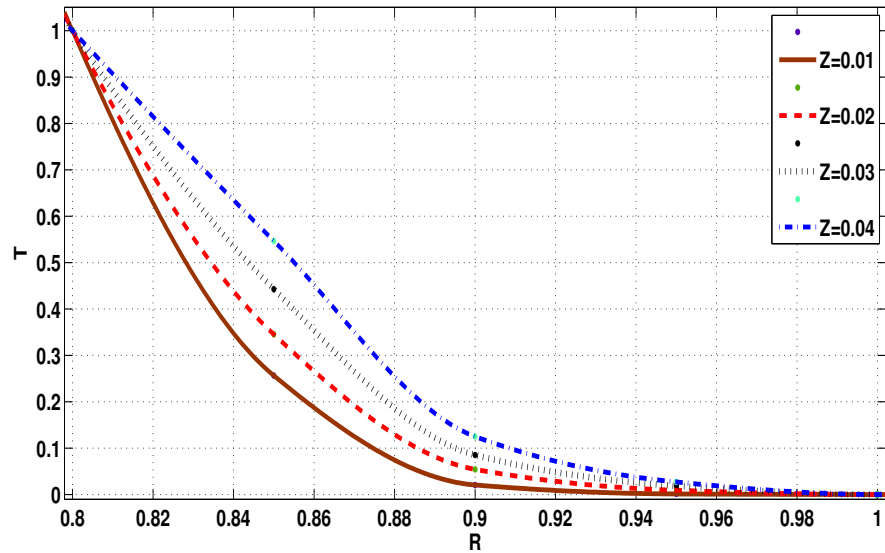


Figure 2.36 Temperature Distribution for $N=0.8$, $Pr=15$ and $B=0$

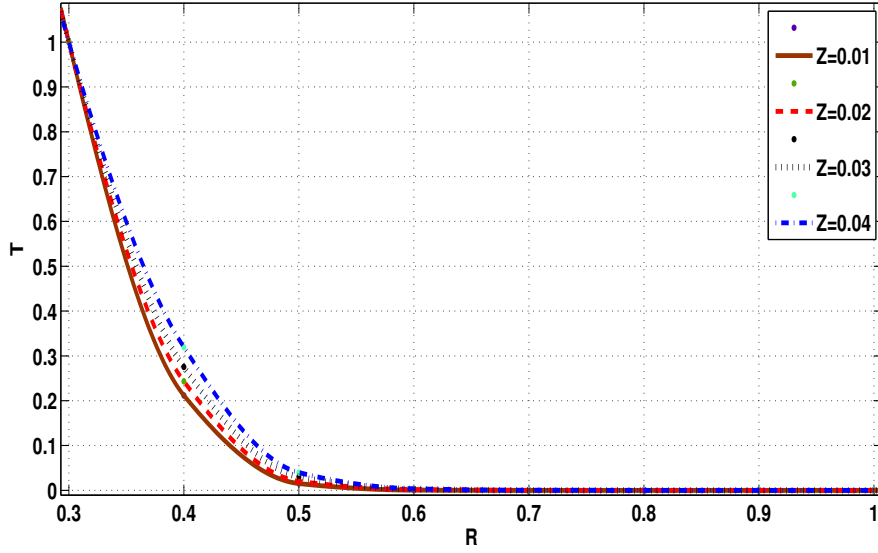


Figure 2.37 Temperature Distribution for $N=0.3$, $Pr=15$ and $B=10$

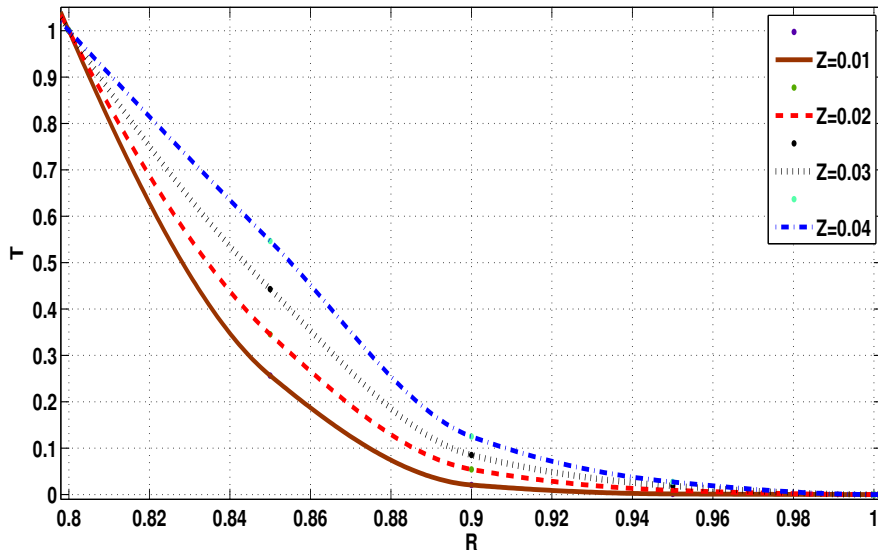


Figure 2.38 Temperature Distribution for $N=0.8$, $Pr=15$ and $B=10$

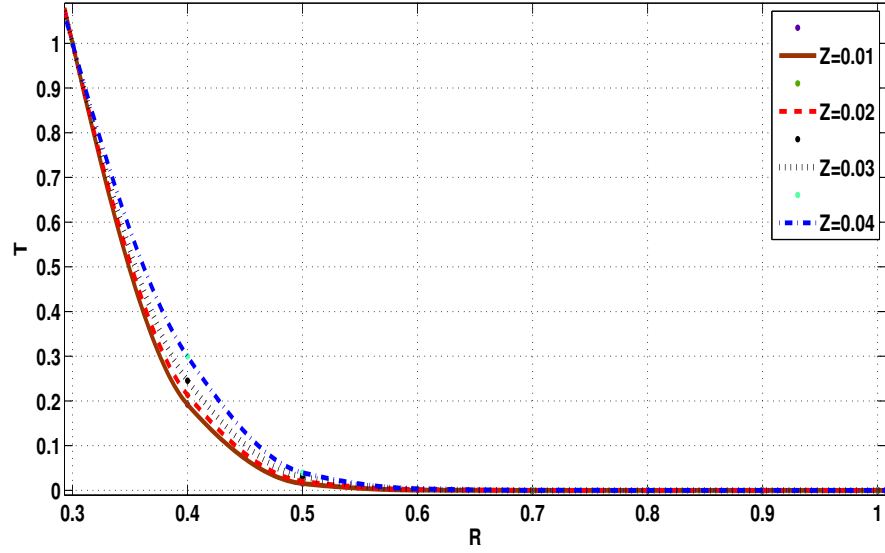


Figure 2.39 Temperature Distribution for $N=0.3$, $Pr=15$ and $B=20$

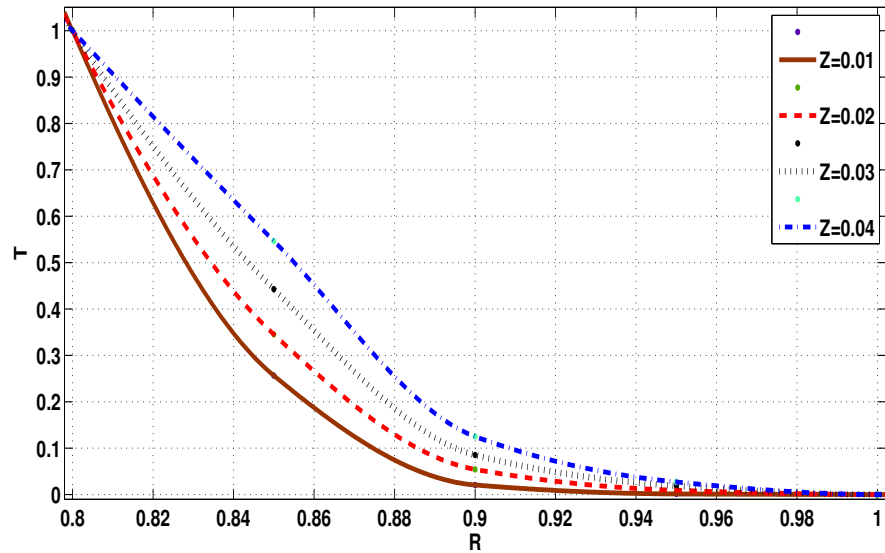


Figure 2.40 Temperature Distribution for $N=0.8$, $Pr=15$ and $B=20$

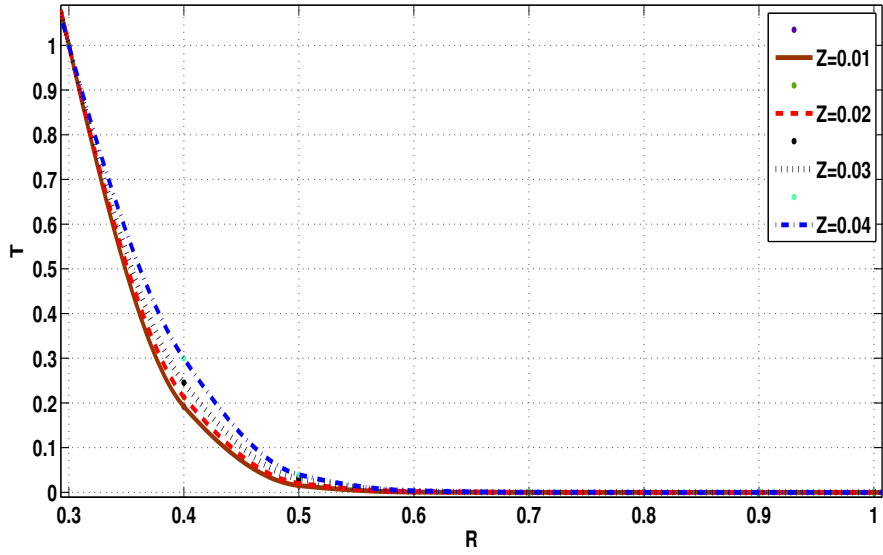


Figure 2.41 Temperature Distribution for $N=0.3$, $Pr=15$ and $B=30$

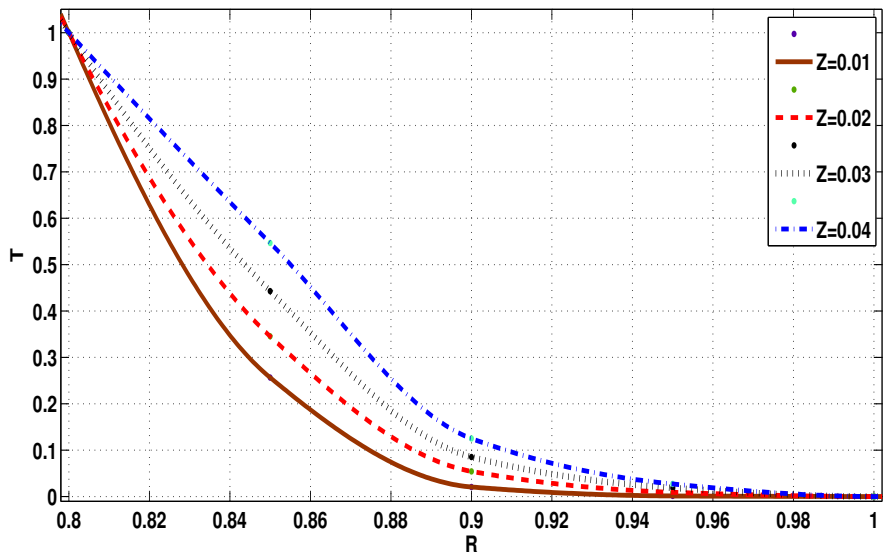


Figure 2.42 Temperature Distribution for $N=0.8$, $Pr=15$ and $B=30$

Chapter 3

ENTRANCE REGION FLOW HEAT TRANSFER IN CONCENTRIC ANNULI WITH ROTATING INNER WALL FOR CASSON FLUID

3.1 INTRODUCTION

The problem of entrance region flow heat transfer in concentric annuli with rotating inner wall for non-Newtonian fluids is of practical importance in engineering applications such as the design of cooling systems for electric machines, compact rotary heat exchangers and combustion chambers, axial-flow turbo machinery and polymer processing industries. In the nuclear reactor field, laminar flow conditions occur when the coolant flow rates are reduced during periods of low power operation. Many important industrial fluids are non-Newtonian in their flow characteristics and are referred to as rheological fluids. These include blood, various suspensions such as coalwater or coal-oil slurries, glues, inks, foods, polymer solutions, paints and many others. The fluid considered here is the Casson model, which is of 'time-independent yield stress' fluid category.

This chapter deals with the problem of entrance region flow heat transfer of Casson fluid in concentric annuli with rotating inner wall. The analysis has been carried out under the assumption that the inner cylinder is rotating and the outer cylinder is at rest. With Prandtl's boundary layer assumptions, the equation of conservation of mass, momentum and energy are dis-

cretized and solved using linearized implicit finite difference technique. The system of non-linear algebraic equations thus obtained, has been solved by the Newton-Raphson iterative method for simultaneous non-linear equations. The development of axial velocity profile, radial velocity profile, tangential velocity profile, pressure variation and temperature distribution in the entrance region have been determined for different values of non-Newtonian flow characteristics and geometrical parameters along the radial direction. The effects of these on flow properties have been discussed.

3.2 MATHEMATICAL FORMULATION OF THE PROBLEM

The Casson fluid enters the horizontal concentric annuli with inner and outer radius R_1 and R_2 , respectively, from a large chamber with a uniform flat velocity profile u_0 along the axial direction z and with some initial pressure p_0 and temperature t_0 . The inner cylinder rotates with an angular velocity ω and the outer cylinder is at rest. The geometry of the problem is shown in Figure (3.1). We consider the flow as steady, laminar, incompressible, axisymmetric with constant physical properties, having negligible viscous dissipation and no internal heat generation. Moreover, it is assumed that the axial heat diffusion is negligible as compared to the radial diffusion.

The governing equations under the above assumptions with the usual Prandtl's boundary layer assumptions Schlichting and Gersten (2000), in polar coordinate system for a Casson fluid in the entrance region are as follows:

$$\text{Continuity equation : } \frac{\partial(rv)}{\partial r} + \frac{\partial(ru)}{\partial z} = 0 \quad (3.2.1)$$

$$r - \text{momentum equation : } \frac{w^2}{r} = \frac{1}{\rho} \frac{\partial p}{\partial r} \quad (3.2.2)$$

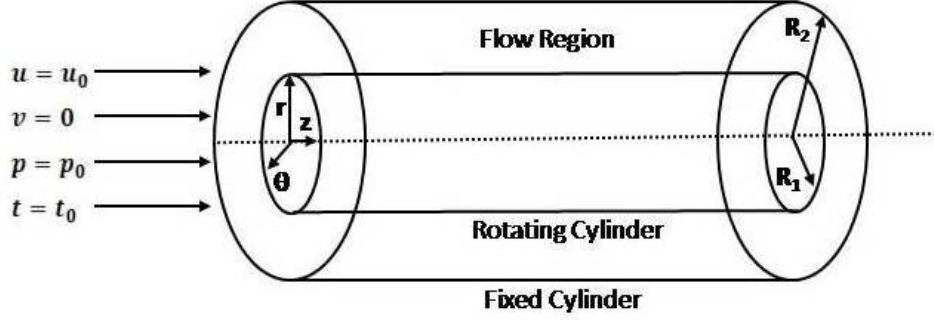


Figure 3.1 Geometry of the Problem

$$\theta - \text{momentum equation : } v \frac{\partial w}{\partial r} + u \frac{\partial w}{\partial z} + \frac{vw}{r} =$$

$$\frac{1}{\rho r^2} \frac{\partial}{\partial r} \left(r^2 \left(\tau_0 + K_c^2 r \frac{\partial}{\partial r} \left(\frac{w}{r} \right) + 2K_c \sqrt{\tau_0 r} \frac{\partial}{\partial r} \left(\frac{w}{r} \right) \right) \right) \quad (3.2.3)$$

$$z - \text{momentum equation : } v \frac{\partial u}{\partial r} + u \frac{\partial u}{\partial z} = -\frac{1}{\rho} \frac{\partial p}{\partial z} +$$

$$\frac{1}{\rho r} \frac{\partial}{\partial r} \left(r \left(\tau_0 + K_c^2 \frac{\partial u}{\partial r} + 2K_c \sqrt{\tau_0} \frac{\partial u}{\partial r} \right) \right) \quad (3.2.4)$$

$$\text{Energy equation : } v \frac{\partial t}{\partial r} + u \frac{\partial t}{\partial z} = \alpha \left[\frac{\partial^2 t}{\partial r^2} + \frac{1}{r} \frac{\partial t}{\partial r} \right] \quad (3.2.5)$$

Here u , v , w are the velocity components in z , r , θ directions respectively, t is the fluid temperature at any point, ρ is the density of the fluid, α is the thermal diffusivity, τ_0 is the yield stress, K_c^2 is a constant for a particular fluid and called the Casson viscosity and p is the pressure.

The boundary conditions of the problem are given by

$$\begin{aligned}
& \text{for } z \geq 0 \text{ and } r = R_1, v = u = 0 \text{ and } w = \omega R_1 \\
& \text{for } z \geq 0 \text{ and } r = R_2, v = u = w = 0 \\
& \text{for } z = 0 \text{ and } R_1 < r < R_2, u = u_0 \\
& \text{at } z = 0, p = p_0
\end{aligned} \tag{3.2.6}$$

Again, the integral form of the continuity Equation (3.2.1) can be given by

$$2 \int_{R_1}^{R_2} r u dr = (R_2^2 - R_1^2) u_0 \tag{3.2.7}$$

It is worth to introduce the following dimensionless variables and parameters

$$R = \frac{r}{R_2}, U = \frac{u}{u_0}, V = \frac{\rho v R_2}{K_c^2}, W = \frac{w}{\omega R_1}, N = \frac{R_1}{R_2}, P = \frac{p - p_0}{\rho u_0^2}, Z = \frac{2z(1 - N)}{R_2 Re}$$

$$Y_c = \frac{\tau_0 R_2}{u_0 K_c^2}, T_a = \frac{2\omega^2 \rho^2 R_1^2 (R_2 - R_1)^3}{\mu_r^2 (R_1 + R_2)}, \text{ here } \mu_r = K_c^2 \left(\frac{\omega R_1}{R_2} \right)$$

$$T = \frac{t - t_0}{t_w - t_0}, Re = \frac{2R_2(1 - N)\rho u_0}{K_c^2}, Pr = \frac{\mu C_p}{K} \left(\frac{\omega R_2}{u_0} \right)^{\frac{1}{2}}$$

Here Y_c is the Casson number, Re is the Reynolds number, T_a is the Taylor number, μ_r is known as reference viscosity, Pr is the Prandtl's number, C_p is the specific heat at constant pressure, K is the thermal conductivity, t_0 is the fluid temperature at annulus entry, t_w is the isothermal wall temperature and N is known as aspect ratio of the annulus.

The dimensionless form of the above Equations (3.2.1) to (3.2.5) and (3.2.7)

are given by

$$\frac{\partial V}{\partial R} + \frac{V}{R} + \frac{\partial U}{\partial Z} = 0 \quad (3.2.8)$$

$$\frac{W^2}{R} = \frac{Re^2(1-N)}{2(1+N)T_a} \frac{\partial P}{\partial R} \quad (3.2.9)$$

$$\begin{aligned} V \frac{\partial W}{\partial R} + U \frac{\partial W}{\partial Z} + \frac{VW}{R} &= \frac{4Y_c^{\frac{1}{2}}}{R} \left(\frac{\partial W}{\partial R} - \frac{W}{R} \right)^{\frac{1}{2}} + Y_c^{\frac{1}{2}} \left(\frac{\partial W}{\partial R} - \frac{W}{R} \right)^{-\frac{1}{2}} * \\ &\left(\frac{\partial^2 W}{\partial R^2} - \frac{1}{R} \frac{\partial W}{\partial R} + \frac{W}{R^2} \right) + \left(\frac{\partial^2 W}{\partial R^2} + \frac{1}{R} \frac{\partial W}{\partial R} - \frac{W}{R^2} \right) + \frac{2Y_c}{R} \end{aligned} \quad (3.2.10)$$

$$\begin{aligned} V \frac{\partial U}{\partial R} + U \frac{\partial U}{\partial Z} &= -\frac{\partial P}{\partial Z} + \frac{1}{R} \frac{\partial U}{\partial R} + \frac{2Y_c^{\frac{1}{2}}}{R} \left(\frac{\partial U}{\partial R} \right)^{\frac{1}{2}} + Y_c^{\frac{1}{2}} \left(\frac{\partial U}{\partial R} \right)^{-\frac{1}{2}} \frac{\partial^2 U}{\partial R^2} \\ &+ \frac{\partial^2 U}{\partial R^2} + \frac{Y_c}{R} \end{aligned} \quad (3.2.11)$$

$$V \frac{\partial T}{\partial R} + U \frac{\partial T}{\partial Z} = \frac{1}{Pr} \left[\frac{\partial^2 T}{\partial R^2} + \frac{1}{R} \frac{\partial T}{\partial R} \right] \quad (3.2.12)$$

and

$$2 \int_N^1 RU dR = (1 - N^2) \quad (3.2.13)$$

The boundary conditions (3.2.6) associated with the hydrodynamic part of the problem in the dimensionless form are given by

$$\begin{aligned} &\text{for } Z \geq 0 \text{ and } R = N, V = U = 0 \text{ and } W = 1 \\ &\text{for } Z \geq 0 \text{ and } R = 1, V = U = W = 0 \\ &\text{for } Z = 0 \text{ and } N < R < 1, U = 1 \\ &\text{at } Z = 0, P = 0 \end{aligned} \quad (3.2.14)$$

Considering the outer cylinder to be adiabatic and the inner cylinder to be isothermal, the following boundary conditions are used for analyzing the thermal part.

$$\begin{aligned}
 &\text{for } Z \geq 0, T = 1 \text{ at } R = N \\
 &\text{for } Z \geq 0, \frac{\partial T}{\partial R} = 0 \text{ at } R = 1 \\
 &\text{for } Z = 0 \text{ and } N < R < 1, T = 0
 \end{aligned} \tag{3.2.15}$$

3.3 SOLUTION OF THE PROBLEM

Considering the mesh network of Figure (3.2), the following difference representations are made. Here ΔR and ΔZ represent the grid size along the radial and axial directions respectively.

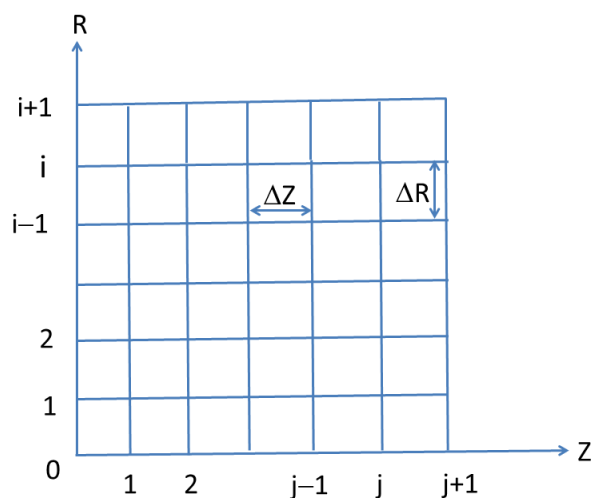


Figure 3.2 Grid Formation for Finite-Difference Representations

$$V_{i+1,j+1} = V_{i,j+1} \left(\frac{N + i\Delta R}{N + (i+1)\Delta R} \right) - \frac{\Delta R}{4\Delta Z} \left(\frac{2N + (2i+1)\Delta R}{N + (i+1)\Delta R} \right) * \tag{3.3.1}$$

$$(U_{i+1,j+1} + U_{i,j+1} - U_{i+1,j} - U_{i,j})$$

$$\frac{W_{i,j+1}^2}{N+i\Delta R} = \frac{(1-N)Re^2}{2T_a(1+N)} \frac{P_{i,j+1} - P_{i-1,j+1}}{\Delta R} \quad (3.3.2)$$

$$\begin{aligned} & V_{i,j} \left[\frac{W_{i+1,j+1} + W_{i+1,j} - W_{i-1,j} - W_{i-1,j+1}}{4\Delta R} \right] + U_{i,j} \left[\frac{W_{i,j+1} - W_{i,j}}{\Delta Z} \right] + \\ & \frac{V_{i,j}W_{i,j}}{N+i\Delta R} = \frac{4(Y_c)^{1/2}}{N+i\Delta R} \left[\frac{W_{i+1,j+1} + W_{i+1,j} - W_{i-1,j} - W_{i-1,j+1}}{4\Delta R} - \frac{W_{i,j}}{N+i\Delta R} \right]^{\frac{1}{2}} \\ & + (Y_c)^{1/2} \left[\frac{W_{i+1,j+1} + W_{i+1,j} - W_{i-1,j} - W_{i-1,j+1}}{4\Delta R} - \frac{W_{i,j}}{N+i\Delta R} \right]^{-\frac{1}{2}} * \\ & \left(\frac{W_{i+1,j+1} + W_{i+1,j} - 2W_{i,j+1} - 2W_{i,j} + W_{i-1,j} + W_{i-1,j+1}}{2(\Delta R)^2} - \right. \\ & \left. \frac{W_{i+1,j+1} + W_{i+1,j} - W_{i-1,j} - W_{i-1,j+1}}{(N+i\Delta R)4\Delta R} + \frac{W_{i,j}}{(N+i\Delta R)^2} \right) + \\ & \left(\frac{W_{i+1,j+1} + W_{i+1,j} - 2W_{i,j+1} - 2W_{i,j} + W_{i-1,j} + W_{i-1,j+1}}{2(\Delta R)^2} + \right. \\ & \left. \frac{W_{i+1,j+1} + W_{i+1,j} - W_{i-1,j} - W_{i-1,j+1}}{(N+i\Delta R)4\Delta R} - \frac{W_{i,j}}{(N+i\Delta R)^2} \right) + \frac{2Y_c}{N+i\Delta R} \quad (3.3.3) \end{aligned}$$

$$\begin{aligned} & P_{i,j+1} + U_{i-1,j+1} \left[\frac{\Delta Z}{2\Delta R(N+i\Delta R)} - \frac{\Delta Z}{2\Delta R} V_{i,j} - \frac{\Delta Z}{(\Delta R)^2} - \frac{(Y_c)^{1/2}\Delta Z}{(\Delta R)^2} * \right. \\ & \left. \left(\frac{U_{i+1,j+1} - U_{i-1,j+1}}{2(\Delta R)} \right)^{-1/2} \right] + U_{i,j+1} \left[U_{i,j} + \frac{2\Delta Z}{(\Delta R)^2} + \frac{2(Y_c)^{1/2}\Delta Z}{(\Delta R)^2} * \right. \\ & \left. \left(\frac{U_{i+1,j+1} - U_{i-1,j+1}}{2(\Delta R)} \right)^{-1/2} \right] + U_{i+1,j+1} \left[-\frac{\Delta Z}{2\Delta R(N+i\Delta R)} + \frac{\Delta Z}{2\Delta R} V_{i,j} - \frac{\Delta Z}{(\Delta R)^2} \right. \\ & \left. - \frac{(Y_c)^{1/2}\Delta Z}{(\Delta R)^2} \left(\frac{U_{i+1,j+1} - U_{i-1,j+1}}{2(\Delta R)} \right)^{-1/2} \right] - \frac{2(Y_c)^{1/2}\Delta Z}{N+i\Delta R} \left(\frac{U_{i+1,j+1} - U_{i-1,j+1}}{2(\Delta R)} \right)^{1/2} \\ & = P_{i,j} + U_{i,j}^2 + \frac{Y_c(\Delta Z)}{N+i\Delta R} \quad (3.3.4) \end{aligned}$$

Where $i=0$ at $R=N$ and $i=m$ at $R=1$. Here m is the number of radial increments in the mesh.

The application of trapezoidal rule to Equation (3.2.13), with the boundary condition (3.2.14) gives

$$\Delta R \sum_{i=1}^{m-1} U_{i,j}(N + i\Delta R) = \left(\frac{1 - N^2}{2} \right) \quad (3.3.5)$$

First, the set of difference Equations (3.3.1) to (3.3.6) have been solved by the finite difference iterative method. Starting with $j=0$ column (annulus entrance) and applying Equation (3.3.3), we have a system of non-linear algebraic equations and this system has been solved by Newton-Raphson method to obtain the values of the velocity component W at the second column $j=1$. Then applying Equations (3.3.2) and (3.3.4) for $1 \leq i \leq m - 1$ and Equation (3.3.5), we get a system of non-linear equations. Again solving this system by Newton-Raphson method to obtain the values of the velocity component U and the pressure P at the second column $j=1$. Lastly, the values of the velocity component V at the second column $j=1$ are obtained from Equation (3.3.1) by Gauss-Jordan method using the known values of U . Repeating this procedure, we can advance, column by column, along the axial direction of the annulus until the flow becomes axially and tangentially fully developed.

With the values of V and U known, the energy Equation (3.2.12) can be considered as a linear equation in T with variable coefficients. By using the implicit finite difference technique, the energy equation can be represented as

$$\begin{aligned} & T_{i+1,j+1} \left(\frac{V_{i,j+1} + V_{i,j}}{8\Delta R} - \frac{1}{2Pr(\Delta R)^2} - \frac{1}{4(N + i\Delta R)Pr\Delta R} \right) + \\ & T_{i-1,j+1} \left(\frac{1}{4(N + i\Delta R)Pr\Delta R} - \frac{V_{i,j+1} + V_{i,j}}{8\Delta R} - \frac{1}{2Pr(\Delta R)^2} \right) = \\ & T_{i,j} \left(\frac{U_{i,j+1} + U_{i,j}}{2\Delta Z} - \frac{1}{Pr(\Delta R)^2} \right) - T_{i,j+1} \left(\frac{U_{i,j+1} + U_{i,j}}{2\Delta Z} + \frac{1}{Pr(\Delta R)^2} \right) + \\ & T_{i+1,j} \left(\frac{1}{2Pr(\Delta R)^2} + \frac{1}{4(N + i\Delta R)Pr\Delta R} - \frac{V_{i,j+1} + V_{i,j}}{8\Delta R} \right) + \\ & T_{i-1,j} \left(\frac{V_{i,j+1} + V_{i,j}}{8\Delta R} - \frac{1}{2Pr(\Delta R)^2} - \frac{1}{4(N + i\Delta R)Pr\Delta R} \right) \end{aligned} \quad (3.3.6)$$

The above equation has solved by using the boundary condition (3.2.15) to obtain the temperature distribution in the annular entrance region. The system of linear equations associated with each column has been solved by Gauss-Jordan elimination method.

3.4 RESULTS AND DISCUSSION

Numerical solutions have been obtained for all different values of Casson Number Y_c , aspect ratio N and various parameters as shown in Table (3.4.1). The Prandtl's number has been chosen as 15. Here, the velocity profiles, pressure variation and temperature distribution along the radial direction R during the rotation of the inner wall of the annuli have been shown in figures (3.3) to (3.22).

Table 3.4.1 List of Various Parameters Used

Various Values of Parameters					
Aspect Ratio N	Radial Position R	Position Z	Axial Position Z	$Rt=Re^2/Ta$	Casson Number Y_c
0.3	0.1		0.01	1	0, 10, 20, 30
0.5	0.1		0.02	10	0, 10, 20, 30
0.8	0.05		0.03	20	0, 10, 20, 30

Figures (3.3) to (3.5) show the development of the tangential velocity profile component W for $N=0.3, 0.5, 0.8$ and for different values of Casson numbers Y_c with Prandtl's number 15. The computation has been done for various values of the parameter Rt to study the effect of rotation of inner cylinder. The values corresponding to $Rt=1, 10$ and 20 are depicted in the figures. The values of tangential velocity decrease from the inner wall to outer wall of the annulus. It is found that with the increase of aspect ratio N , the tangential velocity profile increases. Further, as observed for the other yield-stress fluid, viz. Bingham fluid, here also it is found that with the increase of Casson number, the tangential velocity profile increases. The effect of the parameter Rt is negligible for the tangential velocity.

Figures (3.6) to (3.8) show the development of the axial velocity profile component U for $N=0.3, 0.5, 0.8$ at axial positions of $Z = 0.01, 0.02, 0.03$ and for different values of the Casson numbers Y_c . It is found that, by increasing the aspect ratio N , the axial velocity component U increases at all values of Casson numbers Y_c . Also, it is observed that the velocity profile takes the parabolic form with Casson number Y_c being zero (Newtonian fluid).

The radial velocity profile component V for $N=0.3, 0.5$ and 0.8 , for different values of the Casson numbers Y_c at different axial positions Z are shown in Figures (3.9) to (3.11). Again, the parameter Rt values are taken as 1, 10 and 20 for computational purpose. The values of radial velocity are negative in the region near the outer wall since it is in the opposite direction to the radial coordinate R and it has positive values near the inner wall because it has the same direction of the radial coordinate. The values of the radial velocity decreases with increase of Casson number Y_c . This phenomena is due to the rotation of the inner cylinder of the annuli. It is noted here that the radial velocity components purely depends on the axial coordinate.

Figures (3.12) to (3.14) show the variation of the pressure P along the radial coordinate R for $N=0.3, 0.5$ and 0.8 and for different value of Casson numbers Y_c . It is found that the value of P increases from a minimum at the inner wall to a maximum at the outer wall. Also, it is realized that increase in the value of Casson numbers Y_c , reduces the pressure values P . Further, it is observed that the pressure does not vary so much with respect to the radial coordinate in the region near the outer wall.

Figures (3.15) to (3.22) show the distribution of temperature T for $N=0.3, 0.8$ at axial positions of $Z=0.01, 0.02, 0.03, 0.04$ and for different values of Casson number $Y_c=0, 10, 20, 30$. Here the Prandtl's number is fixed as 15. It is observed from the results obtained, that the temperature decreases with increase of Casson Number for a fixed annular width. When the aspect ratio N increases, it is found that the temperature increases for a fixed Casson Number. Also, it is found that with the increase of axial position the temperature also increasing for a fixed aspect ratio N , Casson Number Y_c .

The present results are compared with other recent work done by Kandasamy et al. (2007a) for a particular case of stationary cylinders and the results in our analysis are matching with the results of it.

3.5 CONCLUSION

From this study, the following conclusions can be drawn:

1. Tangential velocity decreases from the rotating inner wall to the stationary outer wall of the annulus.
2. For a fixed Casson number Y_c , the axial velocity component U increases if we decrease the annular gap.
3. The pressure is found to be minimum at the inner wall and gradually increasing to a maximum at the outer wall for all values of Casson numbers Y_c and pressure variation is not much with respect to the radial coordinate near the outer wall.
4. As observed in the case of Bingham study here also the temperature decreases from the rotating inner wall to the stationary outer wall of the annulus.
5. The temperature is decreasing when we increase the Casson number Y_c and the same phenomena is observed for the increment of aspect ratio N .

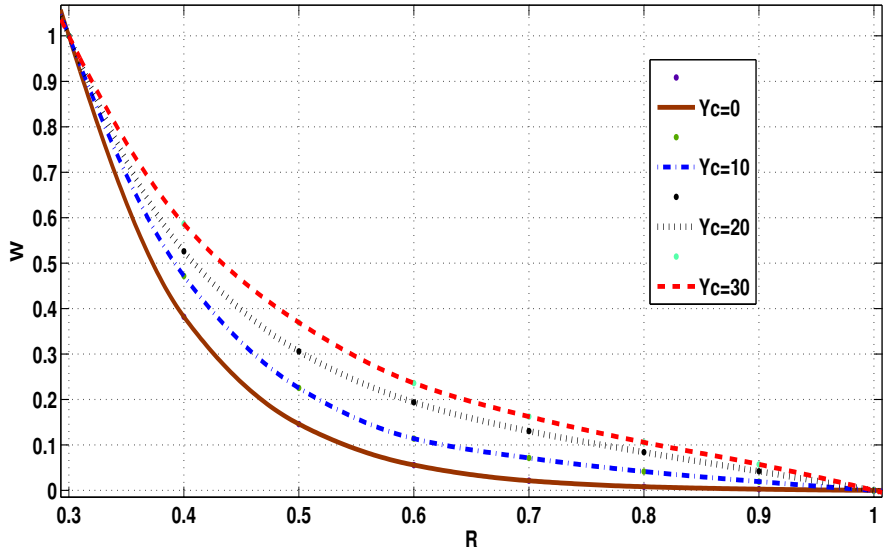


Figure 3.3 Tangential Velocity Profile for $N=0.3$, $R = 0.1$ at $Z = 0.01$

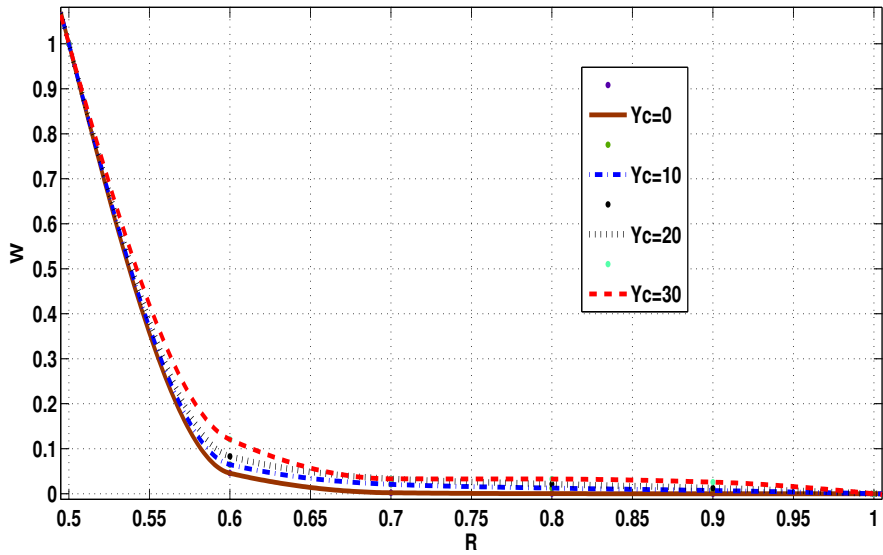


Figure 3.4 Tangential Velocity Profile for $N=0.5$, $R = 0.1$ at $Z = 0.02$

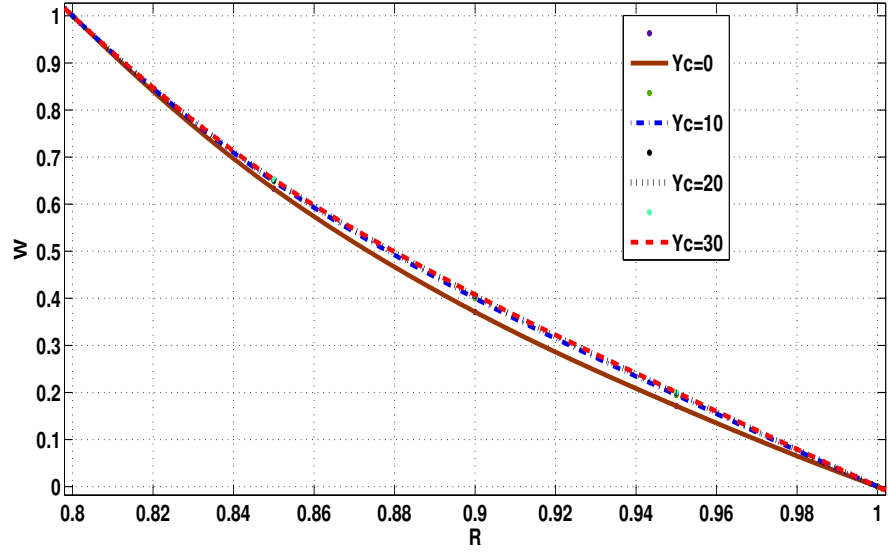


Figure 3.5 Tangential Velocity Profile for $N=0.8$, $R = 0.05$ at $Z = 0.03$

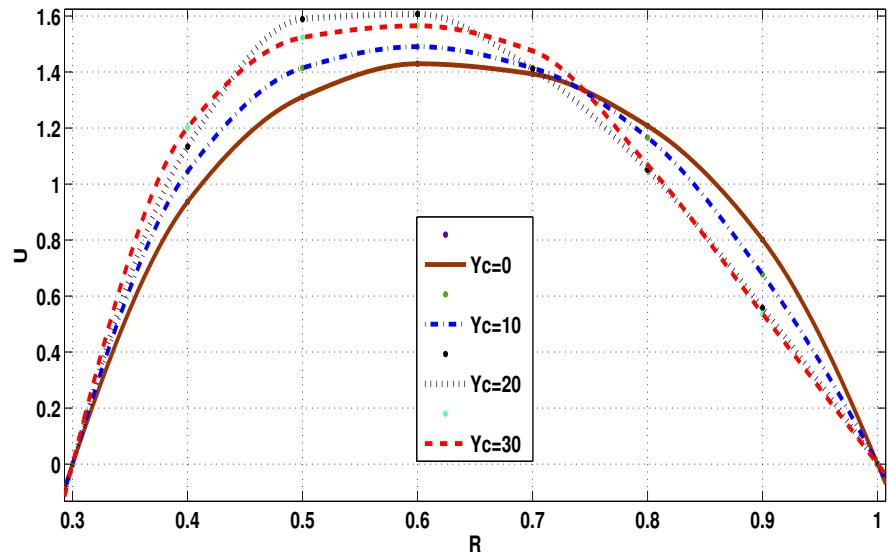


Figure 3.6 Axial Velocity Profile for $N=0.3$, $R = 0.1$ at $Z = 0.01$

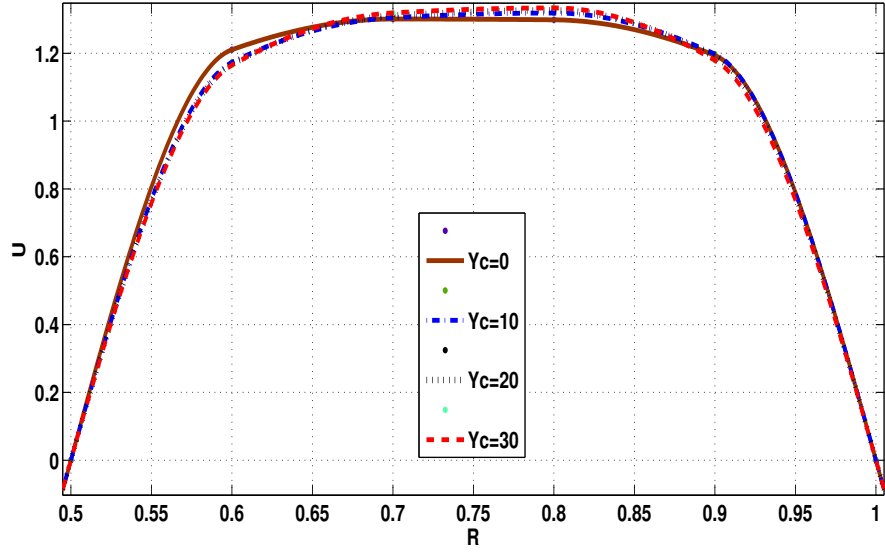


Figure 3.7 Axial Velocity Profile for $N=0.5$, $R = 0.1$ at $Z = 0.02$

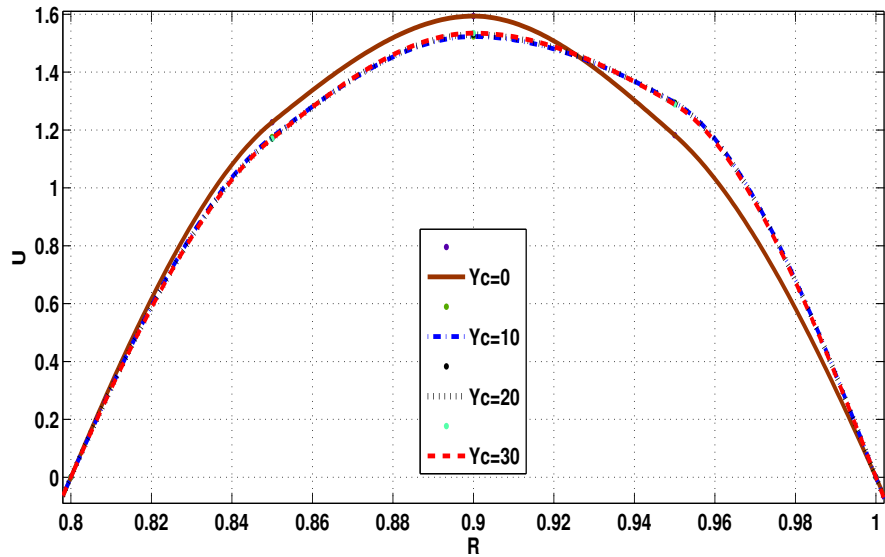


Figure 3.8 Axial Velocity Profile for $N=0.8$, $R = 0.05$ at $Z = 0.03$

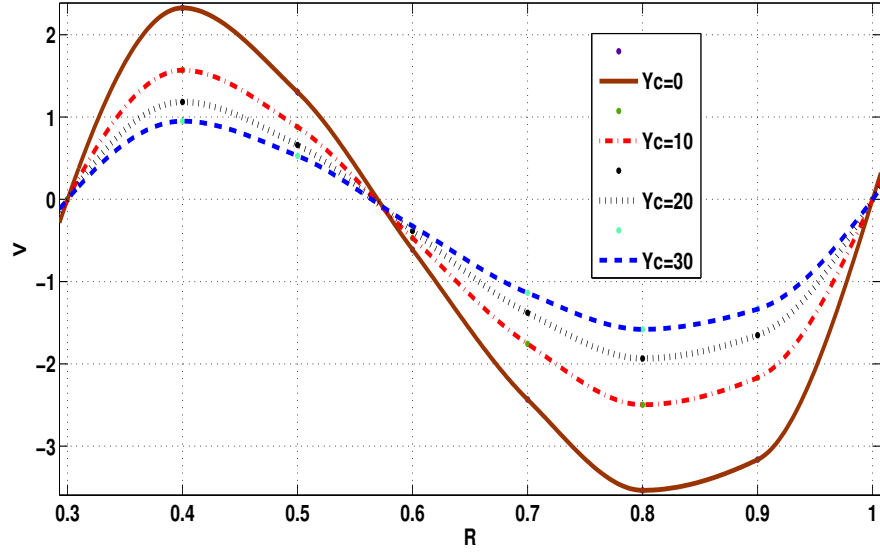


Figure 3.9 Radial Velocity Profile for $N=0.3$, $R = 0.1$ at $Z = 0.01$

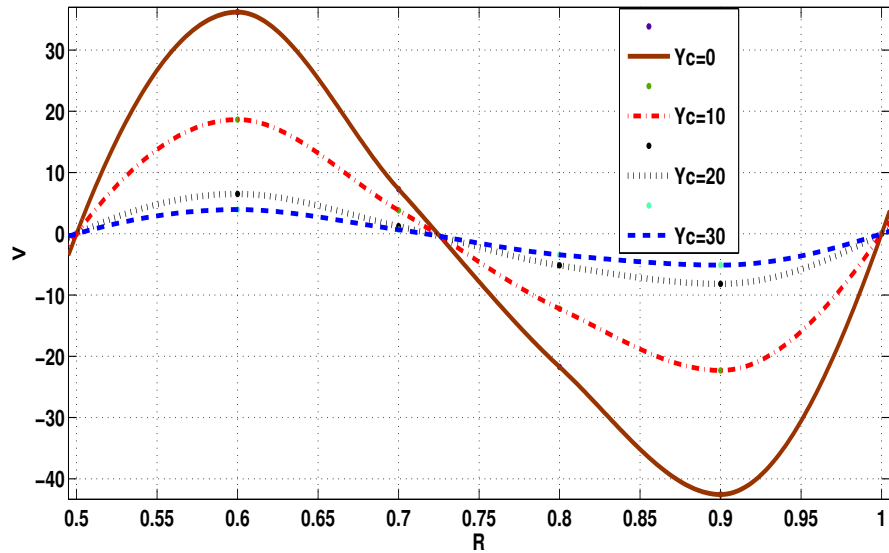


Figure 3.10 Radial Velocity Profile for $N=0.5$, $R = 0.1$ at $Z = 0.02$

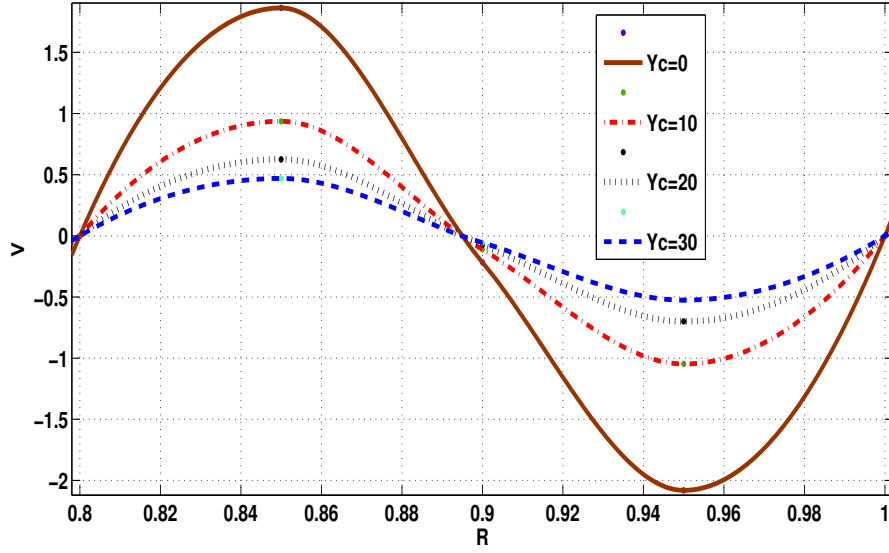


Figure 3.11 Radial Velocity Profile for $N=0.8$, $R = 0.05$ at $Z = 0.03$

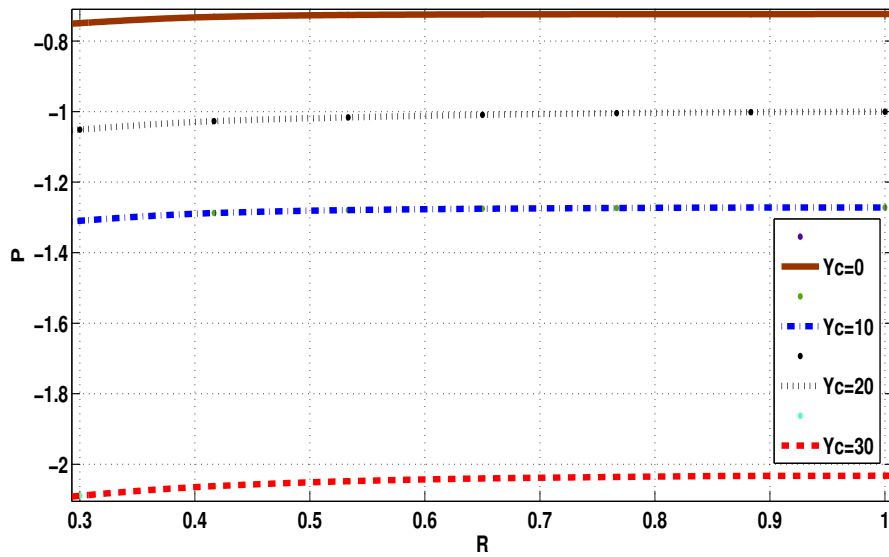


Figure 3.12 Pressure Variation for $N=0.3$, $R = 0.1$ at $Z = 0.01$

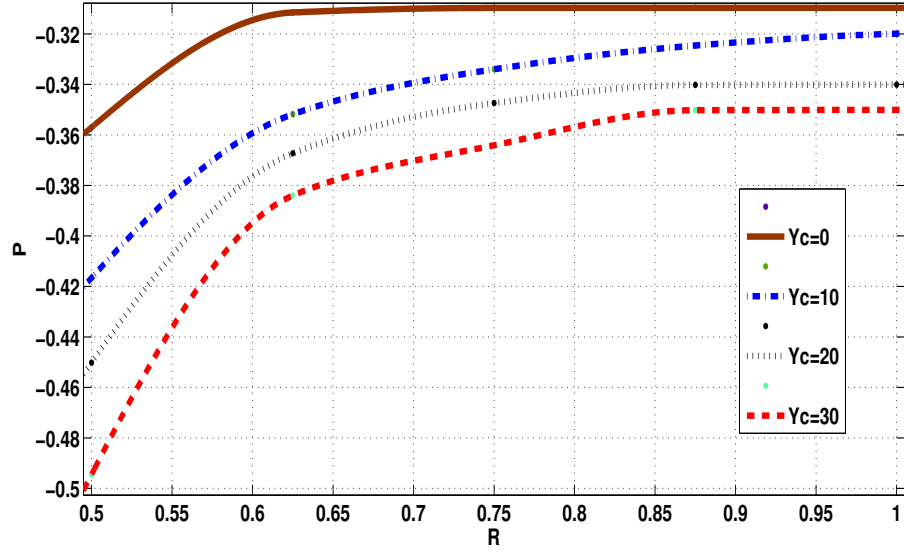


Figure 3.13 Pressure Variation for $N=0.5$, $R = 0.1$ at $Z = 0.02$

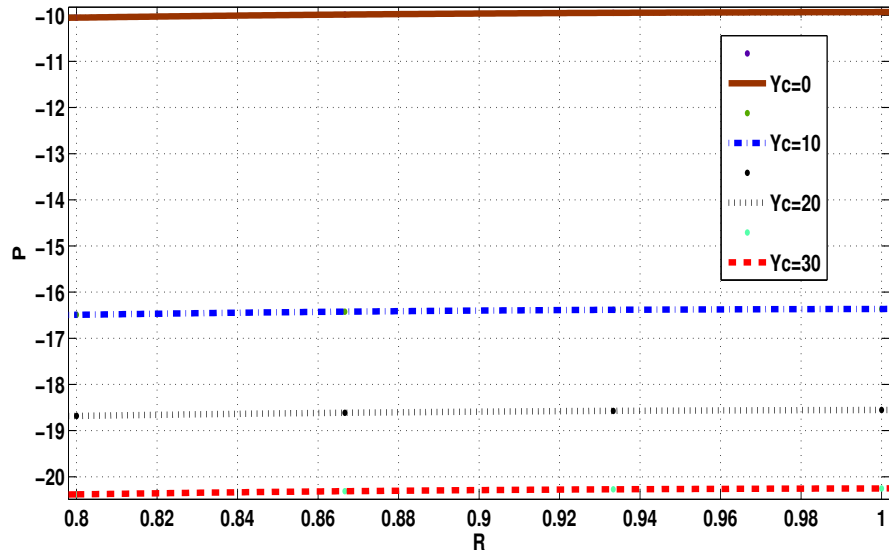


Figure 3.14 Pressure Variation for $N=0.8$, $R = 0.05$ at $Z = 0.03$

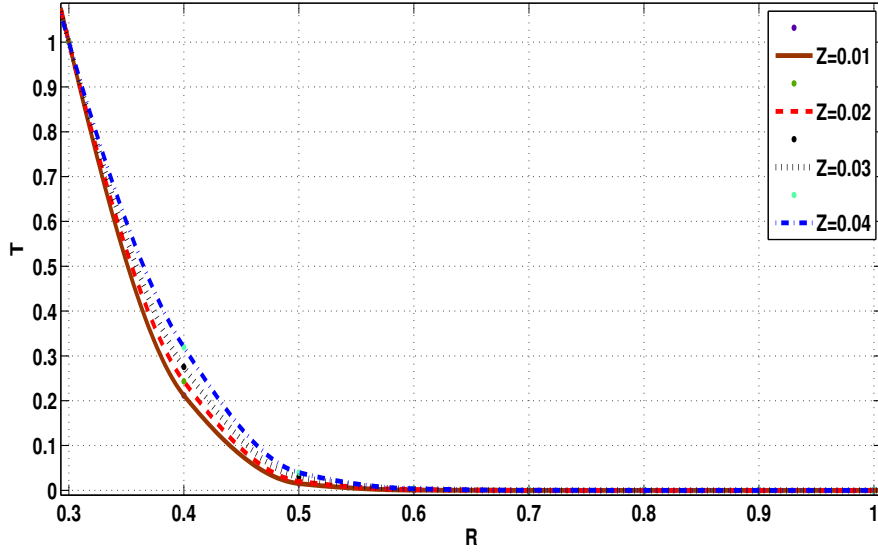


Figure 3.15 Temperature Distribution for $N=0.3$, $Pr=15$ and $Y_c=0$

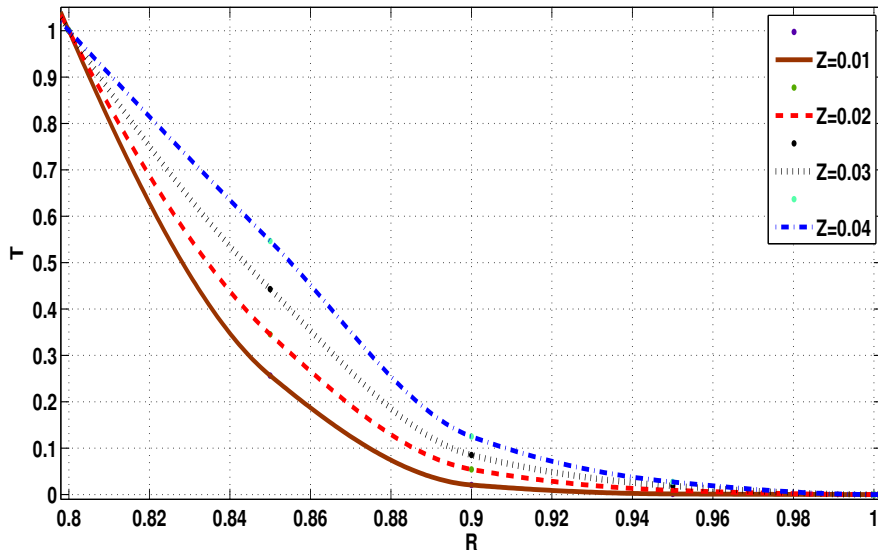


Figure 3.16 Temperature Distribution for $N=0.8$, $Pr=15$ and $Y_c=0$

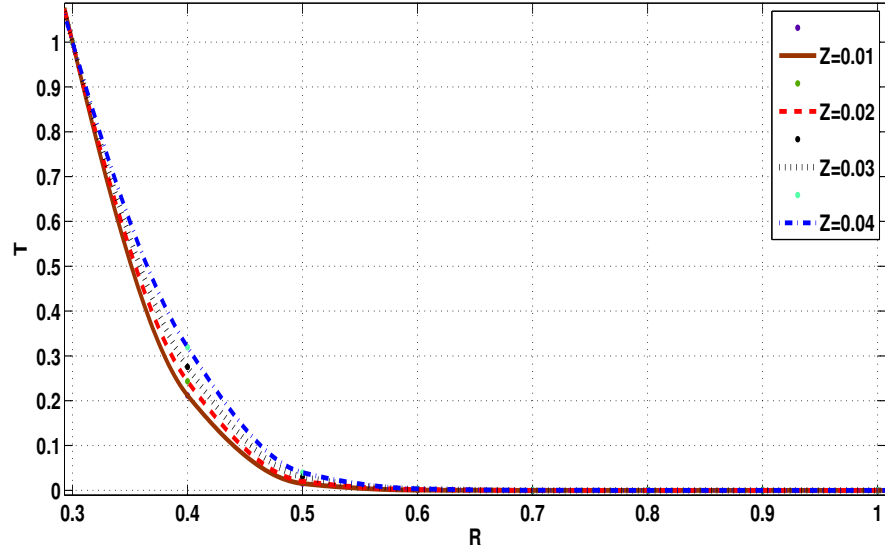


Figure 3.17 Temperature Distribution for $N=0.3$, $Pr=15$ and $Y_c=10$

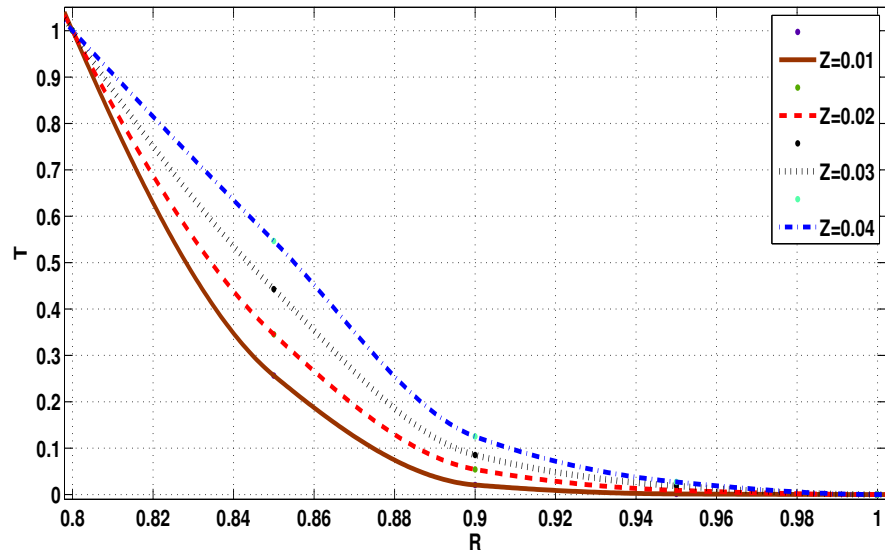


Figure 3.18 Temperature Distribution for $N=0.8$, $Pr=15$ and $Y_c=10$

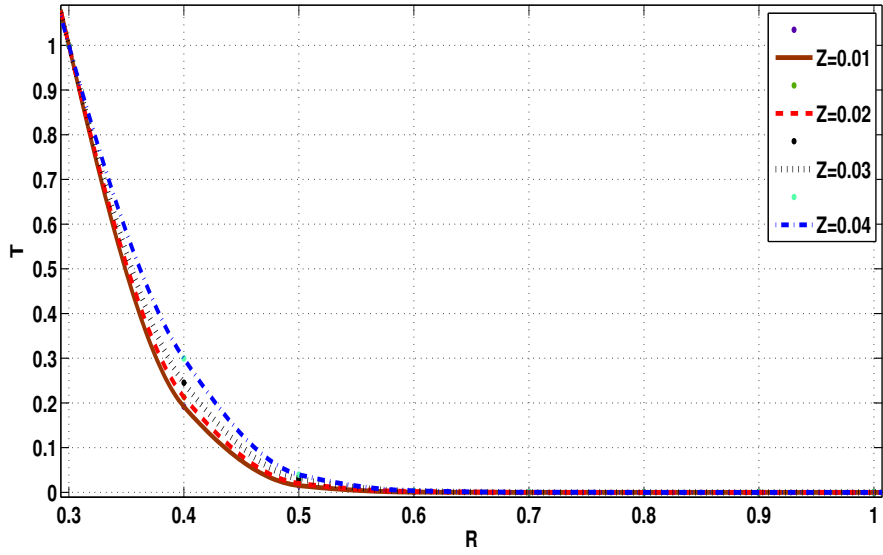


Figure 3.19 Temperature Distribution for $N=0.3$, $Pr=15$ and $Y_c=20$

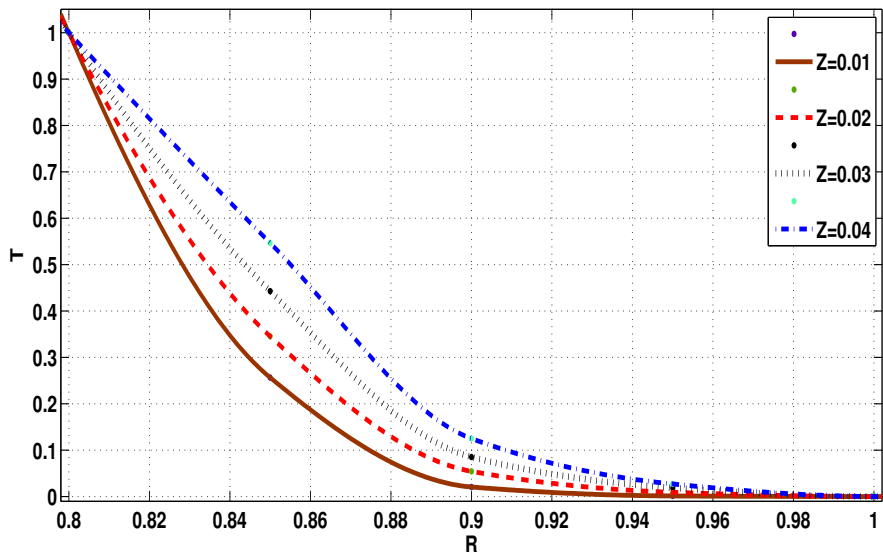


Figure 3.20 Temperature Distribution for $N=0.8$, $Pr=15$ and $Y_c=20$

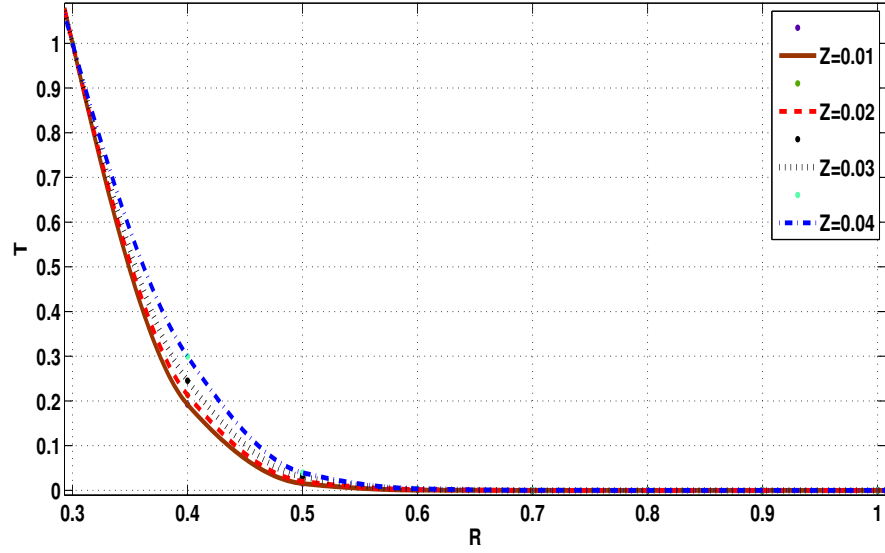


Figure 3.21 Temperature Distribution for $N=0.3$, $Pr=15$ and $Y_c=30$

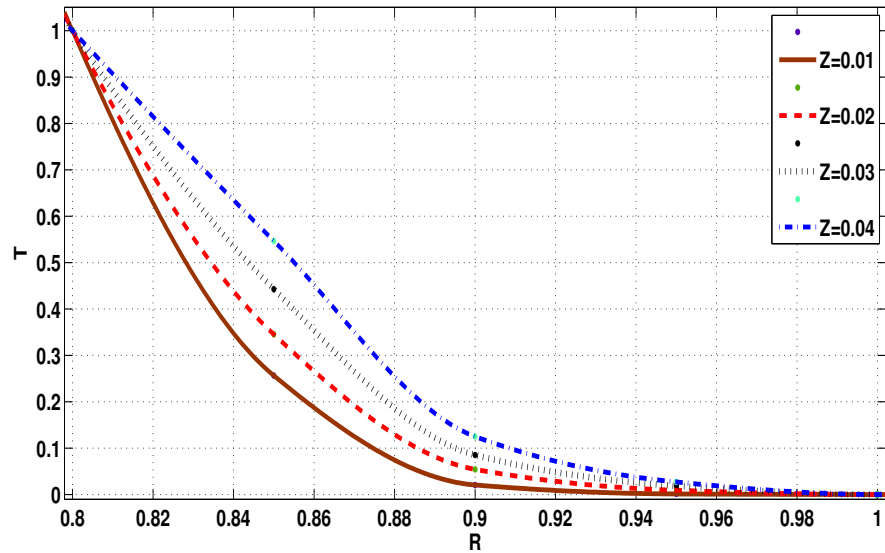


Figure 3.22 Temperature Distribution for $N=0.8$, $Pr=15$ and $Y_c=30$

Chapter 4

ENTRANCE REGION FLOW HEAT TRANSFER IN CONCENTRIC ANNULI WITH ROTATING INNER WALL FOR HERSCHEL-BULKLEY FLUIDS

4.1 INTRODUCTION

Herschel-Bulkley fluids are materials possessing a yield value and in flow, they exhibit the characteristics of shear thinning or shear thickening materials. Shear thinning materials are those which decreases in viscosity as the rate of shear increases and shear thickening materials are the one which increases in viscosity as the rate of shear increases. Herschel-Bukley fluid is the empirical combination of Bingham plastic material and Power law fluids. We are interested in investigating the laminar flow of non-Newtonian fluids in the entrance region of annular channel. In particular, we are analyzing these problems with the assumption that the inner cylinder is rotating and the outer cylinder is at rest. The entrance region flow in channels constitutes a problem of fundamental interest in engineering applications. The behaviour of the fluid in the entrance region may play a significant part in the total length of the channel and the pressure drop may be markedly greater than for the case where the flow is regarded as fully developed throughout the channel. The development of boundary layer is visualized when the fluid enters an annulus and the fully developed velocity profile is observed in the region starting from

the point down-stream where the boundary layers meet asymptotically with the outer edge of the plug flow zone.

A finite difference analysis of the entrance region flow heat transfer of Herschel-Bulkley fluids in concentric annuli with rotating inner wall has been carried out and presented in this chapter. The analysis is made for simultaneously developing hydrodynamic and thermal boundary layer in concentric annuli with the inner cylinder assumed to be rotating with a constant angular velocity and the outer cylinder being stationary. A finite difference analysis is used to obtain the velocity profiles, pressure variation and temperature distribution along the radial direction. With the Prandtl's boundary layer assumptions, the continuity, momentum and energy equations are solved iteratively using a finite difference method. Computational results are obtained for various non-Newtonian flow parameters, geometrical considerations and analyzed extensively for the influence of these parameters on the flow.

4.2 MATHEMATICAL FORMULATION OF THE PROBLEM

The geometry of the problem is as shown in Figure (2.1). The flow is steady, laminar, incompressible, axisymmetric with constant physical properties, having negligible viscous dissipation and no internal heat generation. Moreover, it is assumed that the axial heat diffusion is negligible as compared to the radial diffusion. The governing equations in polar coordinate system (r, θ, z) for a Herschel-Bulkley fluid in the entrance region are:

$$\text{Continuity equation : } \frac{\partial(rv)}{\partial r} + \frac{\partial(ru)}{\partial z} = 0 \quad (4.2.1)$$

$$r - \text{momentum equation : } \frac{w^2}{r} = \frac{1}{\rho} \frac{\partial p}{\partial r} \quad (4.2.2)$$

$$\theta - \text{momentum equation} : v \frac{\partial w}{\partial r} + u \frac{\partial w}{\partial z} + \frac{vw}{r} = \frac{1}{\rho r^2} \frac{\partial}{\partial r} \left(r^2 \left(\tau_0 + k \left[r \frac{\partial}{\partial r} \left(\frac{w}{r} \right) \right]^n \right) \right) \quad (4.2.3)$$

$$z - \text{momentum equation} : v \frac{\partial u}{\partial r} + u \frac{\partial u}{\partial z} = -\frac{1}{\rho} \frac{\partial p}{\partial z} + \frac{1}{\rho r} \frac{\partial}{\partial r} \left(r \left[\tau_0 + k \left(\frac{\partial u}{\partial r} \right)^n \right] \right) \quad (4.2.4)$$

$$\text{Energy equation} : v \frac{\partial t}{\partial r} + u \frac{\partial t}{\partial z} = \alpha \left[\frac{\partial^2 t}{\partial r^2} + \frac{1}{r} \frac{\partial t}{\partial r} \right] \quad (4.2.5)$$

Here k is the consistency index and n is the flow index.

The boundary conditions associated with the hydrodynamic part of the problem are already given in Equation (2.2.6) as well as in Equation (3.2.6).

The continuity Equation (4.2.1) can be expressed in the following integral form as

$$2 \int_{R_1}^{R_2} r u dr = (R_2^2 - R_1^2) u_0 \quad (4.2.6)$$

The following dimensionless variables and parameters are introduced.

$$R = \frac{r}{R_2}, U = \frac{u}{u_0}, V = \frac{\rho v R_2}{\mu_r}, W = \frac{w}{\omega R_1}, N = \frac{R_1}{R_2}, P = \frac{p - p_0}{\rho u_0^2}, Z = \frac{2z(1 - N)}{R_2 Re}$$

$$Y_h = \frac{\tau_0}{k} \left(\frac{R_2}{u_0} \right)^n, T_a = \frac{2\omega^2 \rho^2 R_1^2 (R_2 - R_1)^3}{\mu_r^2 (R_1 + R_2)}, \text{ here } \mu_r = k \left(\frac{\omega R_1}{R_2} \right)^n$$

$$Re = \frac{\rho 2(R_2 - R_1) u_0}{\mu_r}, T = \frac{t - t_0}{t_w - t_0}, Pr = \frac{\mu C_p}{K} \left(\frac{\omega R_2}{u_0} \right)^{1-n}$$

Here Y_h is the Hershel-Bulkley number, Re is the Reynolds number, T_a is the Taylor number and μ_r is know as reference viscosity.

Equations (4.2.1) to (4.2.5) and (4.2.7) in the dimensionless form are given by

$$\frac{\partial V}{\partial R} + \frac{V}{R} + \frac{\partial U}{\partial Z} = 0 \quad (4.2.7)$$

$$\frac{W^2}{R} = \frac{Re^2(1-N)}{2(1+N)T_a} \frac{\partial P}{\partial R} \quad (4.2.8)$$

$$\begin{aligned} V \frac{\partial W}{\partial R} + U \frac{\partial W}{\partial Z} + \frac{VW}{R} &= \frac{2}{R} \left(\frac{\partial W}{\partial R} - \frac{W}{R} \right)^n + n \left(\frac{\partial W}{\partial R} - \frac{W}{R} \right)^{n-1} * \\ \left(\frac{\partial^2 W}{\partial R^2} - \frac{1}{R} \frac{\partial W}{\partial R} + \frac{W}{R^2} \right) &+ \frac{2Y_h}{R} \end{aligned} \quad (4.2.9)$$

$$V \frac{\partial U}{\partial R} + U \frac{\partial U}{\partial Z} = -\frac{\partial P}{\partial Z} + \frac{1}{R} \left(\frac{\partial U}{\partial R} \right)^n + n \left(\frac{\partial U}{\partial R} \right)^{n-1} \frac{\partial^2 U}{\partial R^2} + \frac{Y_h}{R} \quad (4.2.10)$$

$$V \frac{\partial T}{\partial R} + U \frac{\partial T}{\partial Z} = \frac{1}{Pr} \left[\frac{\partial^2 T}{\partial R^2} + \frac{1}{R} \frac{\partial T}{\partial R} \right] \quad (4.2.11)$$

and

$$2 \int_N^1 RU dR = (1 - N^2) \quad (4.2.12)$$

The boundary conditions (2.2.6) associated with the hydrodynamic part of the problem in the dimensionless form are given in Equation (2.2.14) and for the thermal part, considering the outer cylinder to be adiabatic and the inner cylinder to be isothermal, the boundary conditions are given in Equation (2.2.15).

4.3 SOLUTION OF THE PROBLEM

Based on the grid formation shown in Figure (2.2), the finite difference form of the governing equations are given below:

$$V_{i+1,j+1} = V_{i,j+1} \left(\frac{N + i\Delta R}{N + (i+1)\Delta R} \right) - \frac{\Delta R}{4\Delta Z} \left(\frac{2N + (2i+1)\Delta R}{N + (i+1)\Delta R} \right) * \\ (U_{i+1,j+1} + U_{i,j+1} - U_{i+1,j} - U_{i,j}) \quad (4.3.1)$$

$$\frac{W_{i,j+1}^2}{N + i\Delta R} = \frac{(1-N)Re^2}{2T_a(1+N)} \frac{P_{i,j+1} - P_{i-1,j+1}}{\Delta R} \quad (4.3.2)$$

$$V_{i,j} \left[\frac{W_{i+1,j+1} + W_{i+1,j} - W_{i-1,j} - W_{i-1,j+1}}{4\Delta R} \right] + U_{i,j} \left[\frac{W_{i,j+1} - W_{i,j}}{\Delta Z} \right] + \\ \frac{V_{i,j}W_{i,j}}{N + i\Delta R} = \frac{2}{N + i\Delta R} \left[\frac{W_{i+1,j+1} + W_{i+1,j} - W_{i-1,j} - W_{i-1,j+1}}{4\Delta R} - \frac{W_{i,j}}{N + i\Delta R} \right]^n \\ + n * \left[\frac{W_{i+1,j+1} + W_{i+1,j} - W_{i-1,j} - W_{i-1,j+1}}{4\Delta R} - \frac{W_{i,j}}{N + i\Delta R} \right]^{n-1} * \\ \left(\frac{W_{i+1,j+1} + W_{i+1,j} - 2W_{i,j+1} - 2W_{i,j} + W_{i-1,j} + W_{i-1,j+1}}{2(\Delta R)^2} \right. \\ \left. - \frac{W_{i+1,j+1} + W_{i+1,j} - W_{i-1,j} - W_{i-1,j+1}}{(N + i\Delta R)4\Delta R} + \frac{W_{i,j}}{(N + i\Delta R)^2} \right) + \frac{2Y_h}{N + i\Delta R} \quad (4.3.3)$$

$$U_{i-1,j+1} \left[-\frac{\Delta Z}{2\Delta R} V_{i,j} - \frac{n\Delta Z}{2^{n-1}(\Delta R)^{n+1}} (U_{i+1,j+1} - U_{i-1,j+1})^{n-1} \right] \\ P_{i,j+1} + U_{i,j+1} \left[U_{i,j} + \frac{n\Delta Z}{2^{n-2}(\Delta R)^{n+1}} (U_{i+1,j+1} - U_{i-1,j+1})^{n-1} \right] + \\ U_{i+1,j+1} \left[\frac{\Delta Z}{2\Delta R} V_{i,j} - \frac{n\Delta Z}{2^{n-1}(\Delta R)^{n+1}} (U_{i+1,j+1} - U_{i-1,j+1})^{n-1} \right] - \\ - \frac{\Delta Z}{N + i\Delta R} \left(\frac{U_{i+1,j+1} - U_{i-1,j+1}}{2\Delta R} \right)^n = P_{i,j} + U_{i,j}^2 + \frac{Y_h(\Delta Z)}{N + i\Delta R} \quad (4.3.4)$$

Where $i=0$ at $R=N$ and $i=m$ at $R=1$. Here m is the number of radial increments in the mesh.

Again, the application of trapezoidal rule to Equation (4.2.13) gives

$$\frac{\Delta R}{2}(NU_{0,j} + U_{m,j}) + \Delta R \sum_{i=1}^{m-1} U_{i,j}(N + i\Delta R) = \left(\frac{1 - N^2}{2} \right)$$

The boundary condition (2.2.14) gives $U_{0,j} = U_{m,j} = 0$ and the above equation reduces to

$$\Delta R \sum_{i=1}^{m-1} U_{i,j}(N + i\Delta R) = \left(\frac{1 - N^2}{2} \right) \quad (4.3.5)$$

The computational procedure is again as stated in the chapter 3. The set of difference Equations (4.3.1) to (4.3.6) have been solved by the iterative procedure. Starting at the $j=0$ column (annulus entrance) and applying Equation (4.3.3) for $1 \leq i \leq m - 1$, we get a system of non-linear algebraic equations. This system has been solved by using Newton-Raphson method to obtain the values of the tangential velocity component W at the second column $j=1$. Then applying Equations (4.3.2) and (4.3.4) for $1 \leq i \leq m - 1$ and Equation (4.3.5), we get a system of non-linear equations. Again solving this system by Newton-Raphson method, we obtain the values of the axial velocity component U and the pressure P at the second column $j=1$. Finally, the values of the radial velocity component V at the second column $j=1$ are obtained from Equation (4.3.1) by Gauss-Jordan method using the known values of U . Repeating this procedure, we can advance, column by column, along the axial direction of the annulus until the flow becomes axially and tangentially fully developed.

With the values of V and U known, the energy Equation (4.2.12) can be considered as a linear equation in T with variable coefficients. By using the implicit finite difference technique, the energy equation can be represented as

$$\begin{aligned}
& T_{i+1,j+1} \left(\frac{V_{i,j+1} + V_{i,j}}{8\Delta R} - \frac{1}{2Pr(\Delta R)^2} - \frac{1}{4(N + i\Delta R)Pr\Delta R} \right) + \\
& T_{i-1,j+1} \left(\frac{1}{4(N + i\Delta R)Pr\Delta R} - \frac{V_{i,j+1} + V_{i,j}}{8\Delta R} - \frac{1}{2Pr(\Delta R)^2} \right) = \\
& T_{i,j} \left(\frac{U_{i,j+1} + U_{i,j}}{2\Delta Z} - \frac{1}{Pr(\Delta R)^2} \right) - T_{i,j+1} \left(\frac{U_{i,j+1} + U_{i,j}}{2\Delta Z} + \frac{1}{Pr(\Delta R)^2} \right) + \\
& T_{i+1,j} \left(\frac{1}{2Pr(\Delta R)^2} + \frac{1}{4(N + i\Delta R)Pr\Delta R} - \frac{V_{i,j+1} + V_{i,j}}{8\Delta R} \right) + \\
& T_{i-1,j} \left(\frac{V_{i,j+1} + V_{i,j}}{8\Delta R} - \frac{1}{2Pr(\Delta R)^2} - \frac{1}{4(N + i\Delta R)Pr\Delta R} \right) \tag{4.3.6}
\end{aligned}$$

Equation (4.3.6), with the boundary conditions (2.2.15) have been used to obtain the temperature distribution in the annular entrance region. The system of linear equations associated with each column has been solved by Gauss-Jordan elimination method.

4.4 RESULTS AND DISCUSSION

Numerical calculations have been performed for all admissible values of Herschel-Bulkley number Y_h , aspect ratio N and various parameters as shown in Table (4.4.1). The Prandtl's number has been chosen as 7. The velocity profiles and pressure variation along radial direction R have been computed for different values of N and Y_h are shown in Figures (4.3) to (4.22). The temperature distributions during the rotation of the inner wall of the annuli have been shown in Figures (4.23) to (4.28).

Table 4.4.1 List of Various Parameters Used

Various Values of Parameters					
Aspect Ratio N	Radial Position R	Axial Position Z	$Rt = Re^2/T_a$	Flow Index n	Herschel-Bulkley number Y_h
0.3	0.1	0.02	10	0.5, 1, 1.5	0, 10, 20, 30
0.8	0.05	0.03	20	0.5, 1, 1.5	0, 10, 20, 30

Figures (4.3) to (4.8) show the development of the tangential velocity profile component W for $N=0.3$ and 0.8 , for values of n as 0.5 , 1 , and 1.5 and for different values of Herschel-Bulkley numbers. The values of tangential velocity decrease from the inner wall to outer wall of the annulus. It is found that with the increase of aspect ratio N , the tangential velocity profile increases. That is, the tangential velocity is more when the gap of the annuli is small. Also, it is observed that the value of W increases with the increasing value of flow index n . Further, it is found that with the increase of Herschel-Bulkley number, the tangential velocity profile increases. This means, the tangential velocity tends to increase for the thick viscous fluids when the inner cylinder is rotating. The effect of the parameter Rt is negligible for the tangential velocity.

Figures (4.9) to (4.14) show the development of the axial velocity profile component U for $N=0.3$, 0.8 and the value of n chosen as 0.5 , 1 , and 1.5 , for different values of the Herschel-Bulkley numbers. It is found that increasing the flow index n , the axial velocity component increases at all values of Herschel-Bulkley numbers and the velocity profile develops faster as n increases. It indicates that the axial velocity is more for shear thinning fluids ($n > 1$) and for shear thickening fluids ($n < 1$) the axial velocity component is less. Also it is observed that the velocity profile takes the parabolic form as n tends to 1 with Herschel-Bulkley number being zero (Newtonian fluid).

The radial velocity profile component V for $N=0.3$ and 0.8 when $n=1$, at different sections of the axial direction Z are shown in Figures (4.15) and (4.16). The values of radial velocity are negative in the region near the outer wall since it is in the opposite direction to the radial coordinate R and it has positive values near the inner wall because it has the same direction of the radial coordinate. This phenomena is due to the rotation of the inner cylinder of the annuli. It is noted here that the radial velocity components purely depends on the axial coordinate.

Figures (4.17) to (4.22) show the variation of the pressure P along the radial coordinate R for $N=0.3$ and 0.8 and the value of $n=0.5$, 1 , and 1.5 . It is found that the value of P increases from a minimum at the inner wall to

a maximum at the outer wall for all values of the parameter n . Further it is realized that increase in the value of Herschel-Bulkley numbers Y_h , the pressure P values also increases. This is because of the fact that the pressure will tend to be lower for thick viscous fluids. Moreover, it is observed that the pressure does not vary so much with respect to the radial coordinate in the region near the outer wall.

The temperature distribution along radial direction have been plotted for different axial positions with $N = 0.3, 0.8, n = 0.5, 1, 1.5$ and $Y_h = 0, 10$. Here the temperature distributions during the rotation of the inner wall of the annuli have been shown in Figures (4.23) to (4.28). It is observed from the results obtained, that the temperature decreases with increase of Herschel-Bulkley Number for a fixed annular width. When the aspect ratio N increases, it is found that the temperature increases for a fixed Herschel-Bulkley Number Y_h . Moreover, with the increase of flow index 'n' the temperature decreases for a fixed aspect ratio N and Herschel-Bulkley Number. Also, it is found that with the increase of axial position the temperature also increasing for a fixed aspect ratio N and Herschel-Bulkley Number Y_h .

The present results are compared with available results in literature for various particular cases and are found to be in agreement. When the Herschel-Bulkley Number $Y_h = 0$ and $n = 1$, our results match with the results corresponded to Newtonian fluid of Coney and El-Shaarawi (1974a). Also when the Herschel-Bulkley number $Y_h = 0$, our results match with the results corresponded to power-law fluids given by Sayed-Ahmed and Sharaf-El-Din (2006). In the case of non-rotating cylinders, the results in our analysis are matching with that of the results of Kandasamy et al. (2007b). Also, in the case of non-thermal part these results matches with the results of Kandasamy and Nadiminti (2015).

4.5 CONCLUSION

The velocity distribution, pressure variation and temperature variations along radial direction R have been presented geometrically. From this study, the following can be concluded.

1. Tangential velocity decrease from the inner wall to outer wall of the annulus and the tangential velocity is high for thick viscous fluids.
2. Increasing the flow index n , the axial velocity component U increases at all values of Herschel-Bulkley numbers Y_h and the velocity profile develops faster as 'n' increases.
3. Radial velocity is found to be depends only on the axial coordinate.
4. Pressure increases from a minimum at the inner wall to a maximum at the outer wall for all values of the flow index 'n' and pressure does not vary so much with respect to the radial coordinate in the region near the outer wall.
5. The temperature decreases from the rotating inner wall to the stationary outer wall of the annulus.
6. When increasing the Herschel-Bulkley Number, it is observed that the temperature decreases.
7. With the increase of flow index 'n', the temperature decreases.
8. When aspect ratio N increases, it is found that the temperature increases.
9. With the increase of axial position Z , the temperature also increases.

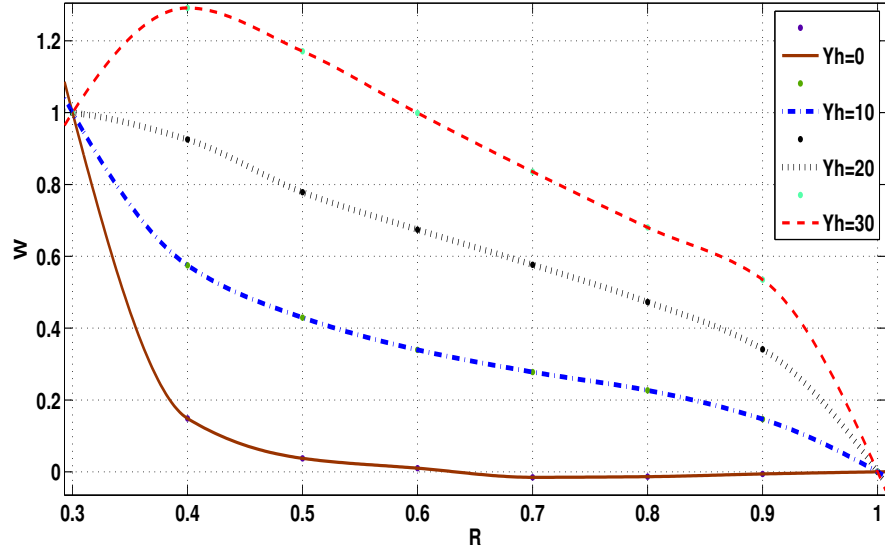


Figure 4.1 Tangential Velocity Profile for $N=0.3$, $n=0.5$, $R = 0.1$, $Z = 0.02$

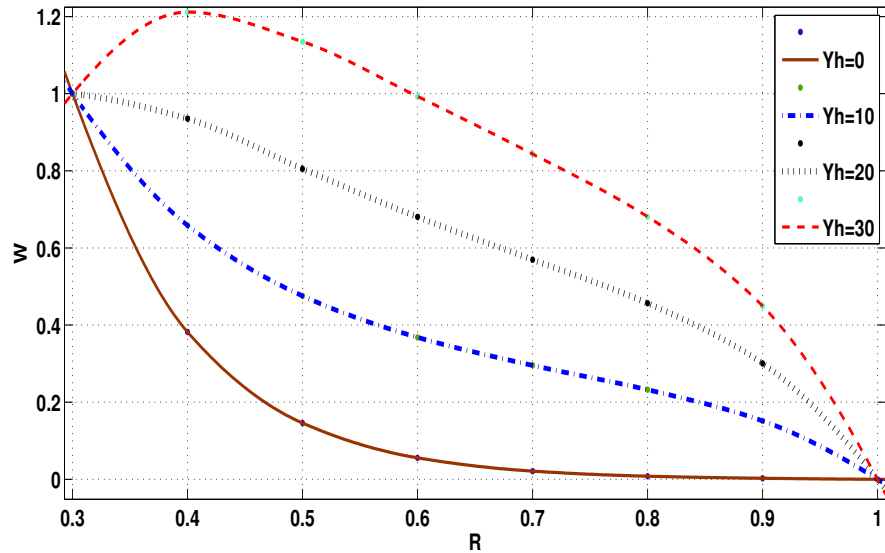


Figure 4.2 Tangential Velocity Profile for $N=0.3$, $n=1$, $R = 0.1$ at $Z = 0.02$

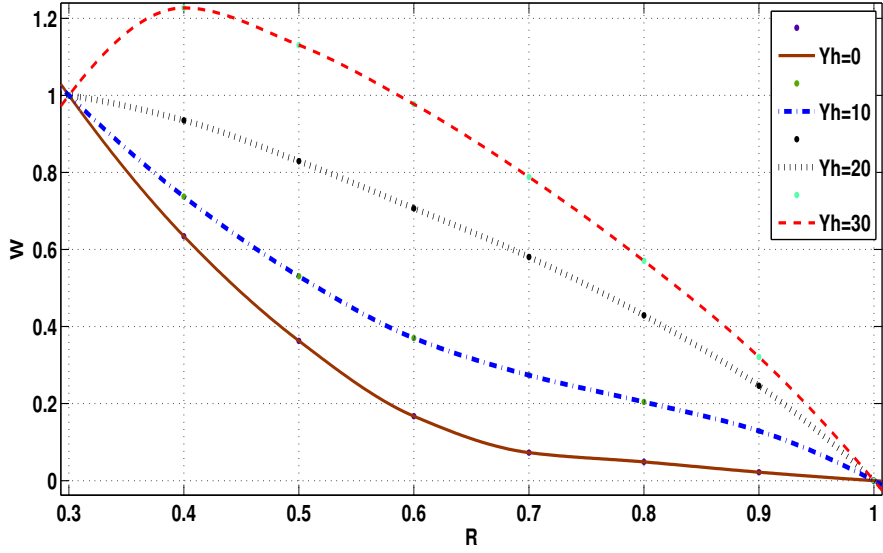


Figure 4.3 Tangential Velocity Profile for $N=0.3$, $n=1.5$, $R = 0.1$, $Z = 0.02$

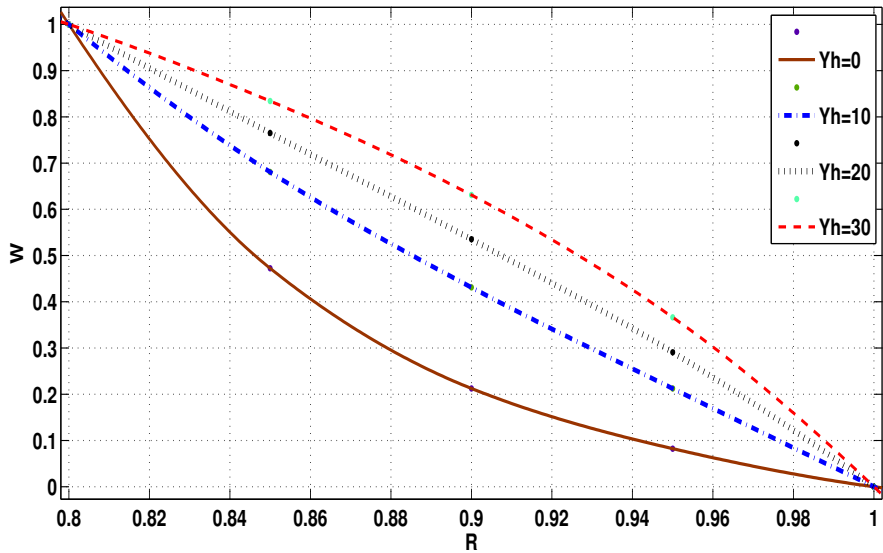


Figure 4.4 Tangential Velocity Profile for $N=0.8$, $n=0.5$, $R = 0.05$, $Z = 0.03$

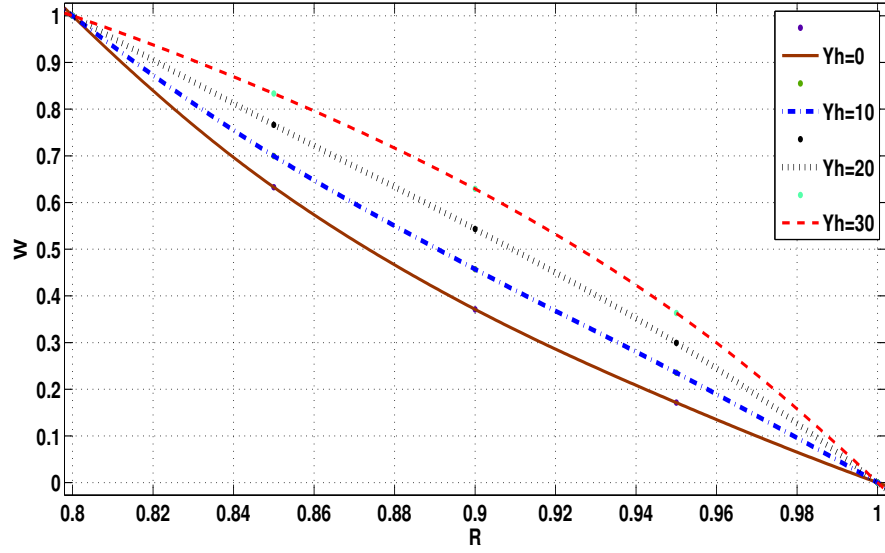


Figure 4.5 Tangential Velocity Profile for $N=0.8$, $n=1$, $R = 0.05$ at $Z = 0.03$

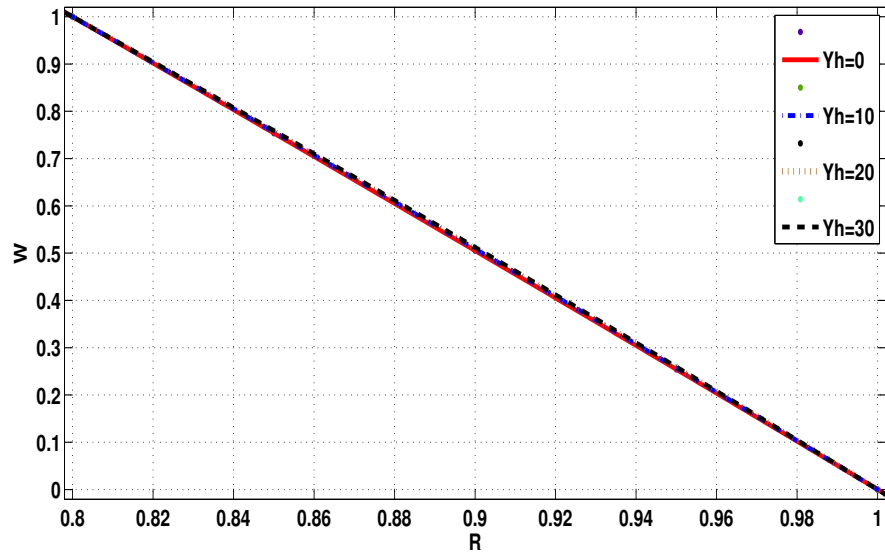


Figure 4.6 Tangential Velocity Profile for $N=0.8$, $n=1.5$, $R = 0.05$, $Z = 0.03$

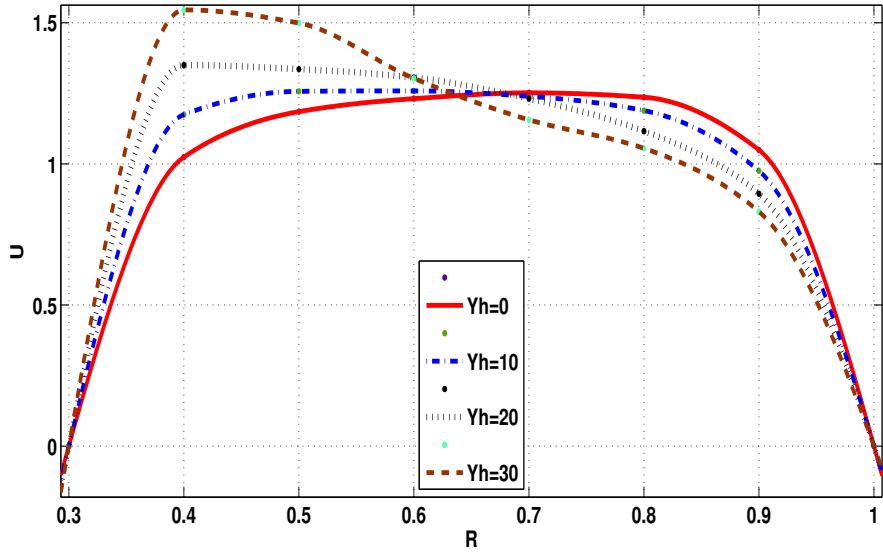


Figure 4.7 Axial Velocity Profile for $N=0.3$, $n=0.5$, $R=0.1$ at $Z=0.02$

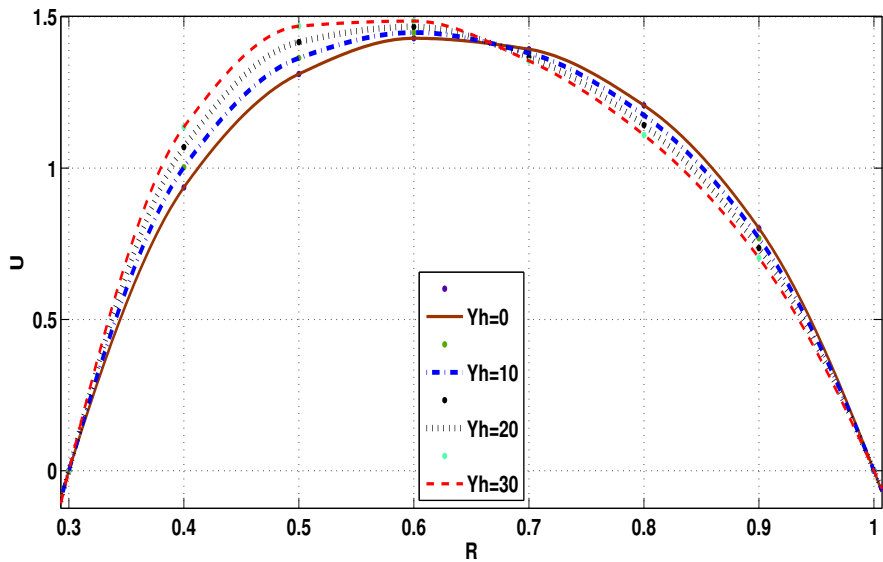


Figure 4.8 Axial Velocity Profile for $N=0.3$, $n=1$, $R=0.1$ at $Z=0.02$

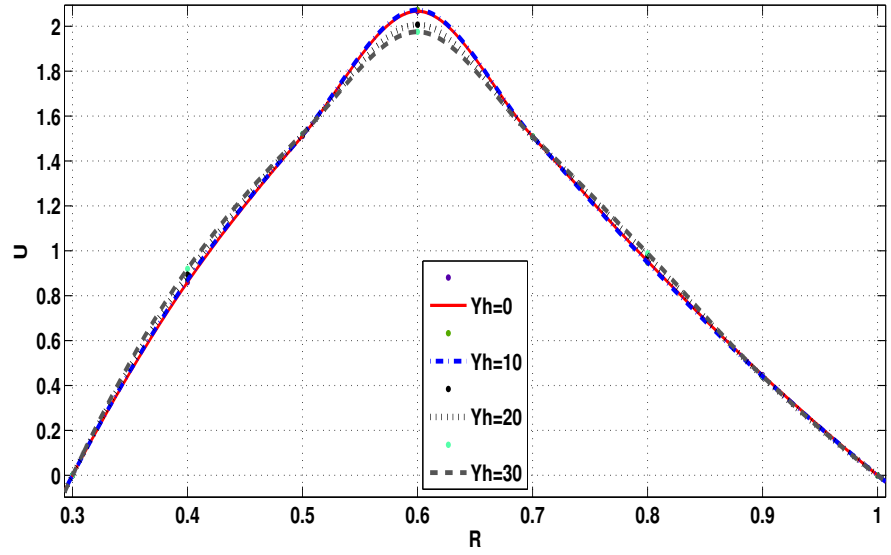


Figure 4.9 Axial Velocity Profile for $N=0.3$, $n=1.5$, $R = 0.1$ at $Z = 0.02$

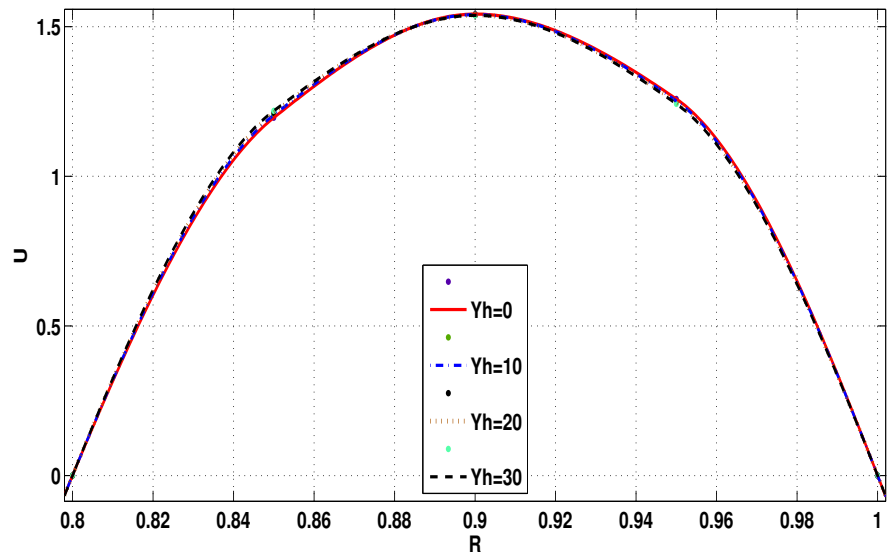


Figure 4.10 Axial Velocity Profile for $N=0.8$, $n=0.5$, $R = 0.05$ at $Z = 0.03$

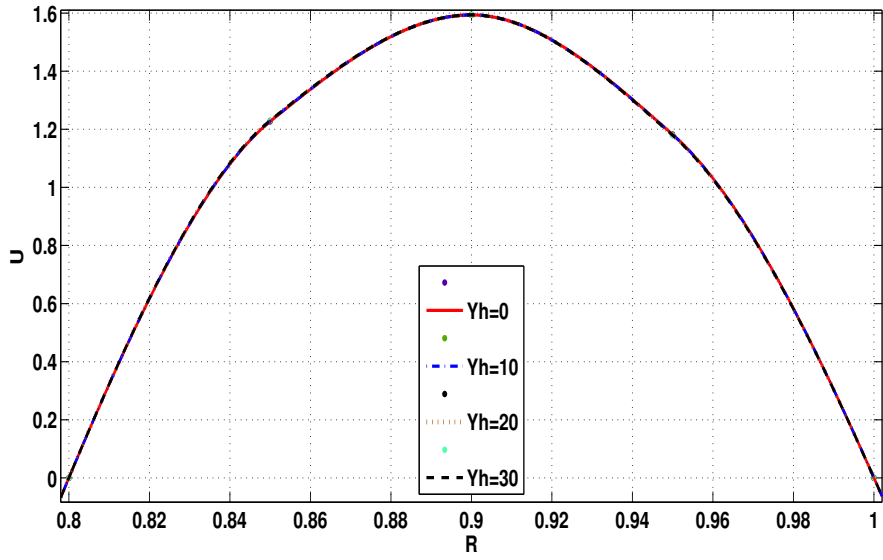


Figure 4.11 Axial Velocity Profile for $N=0.8$, $n=1$, $R = 0.05$ at $Z = 0.03$

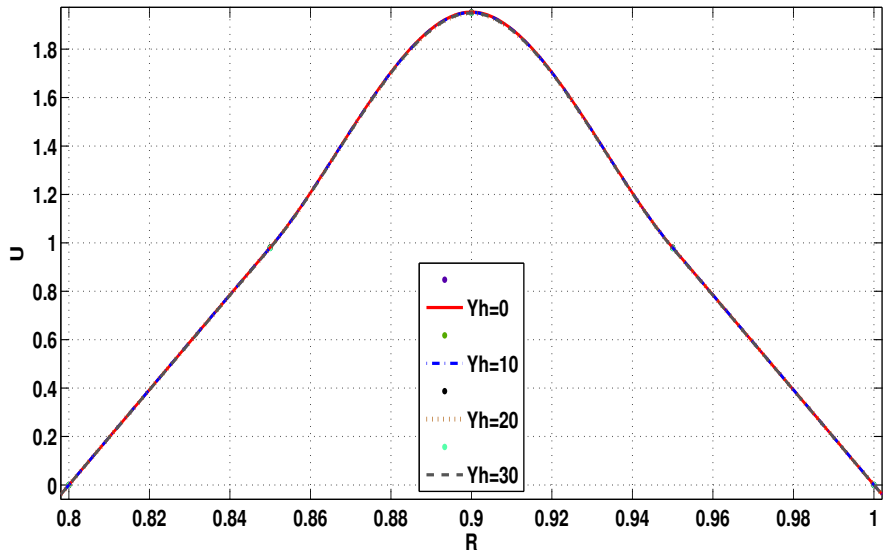


Figure 4.12 Axial Velocity Profile for $N=0.8$, $n=1.5$, $R = 0.05$ at $Z = 0.03$

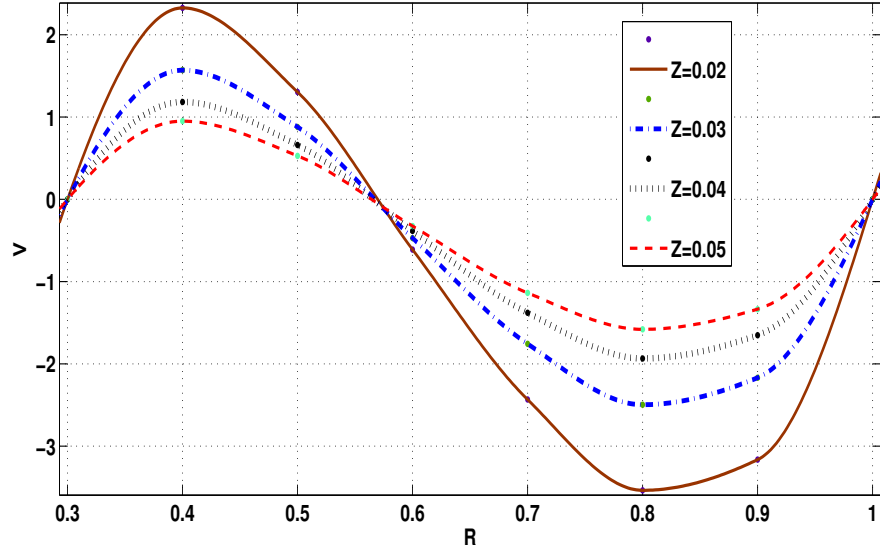


Figure 4.13 Radial Velocity Profile for $N=0.3$, $n=1$, $R = 0.1$ at $Z = 0.02$

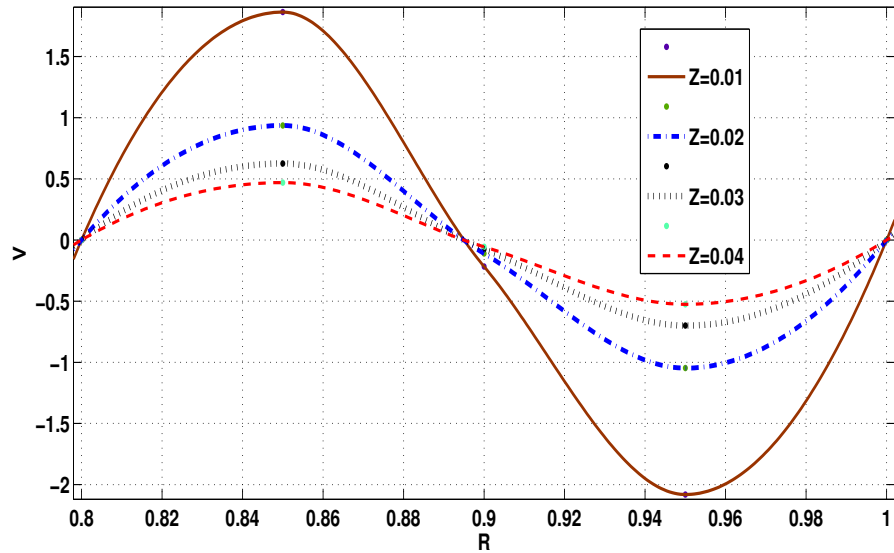


Figure 4.14 Radial Velocity Profile for $N=0.8$, $n=1$, $R = 0.05$ at $Z = 0.03$

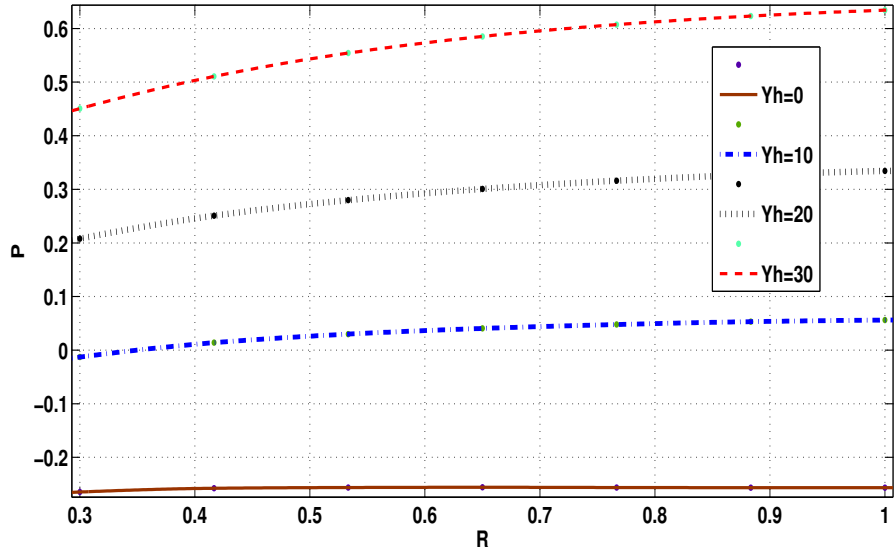


Figure 4.15 Pressure Variation for $N=0.3$, $n=0.5$, $R = 0.1$ at $Z = 0.02$

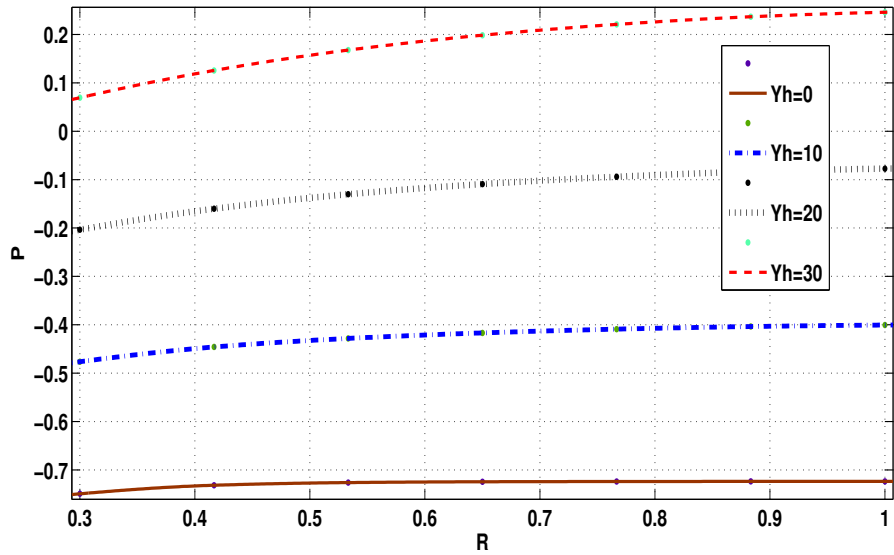


Figure 4.16 Pressure Variation for $N=0.3$, $n=1$, $R = 0.1$ at $Z = 0.02$

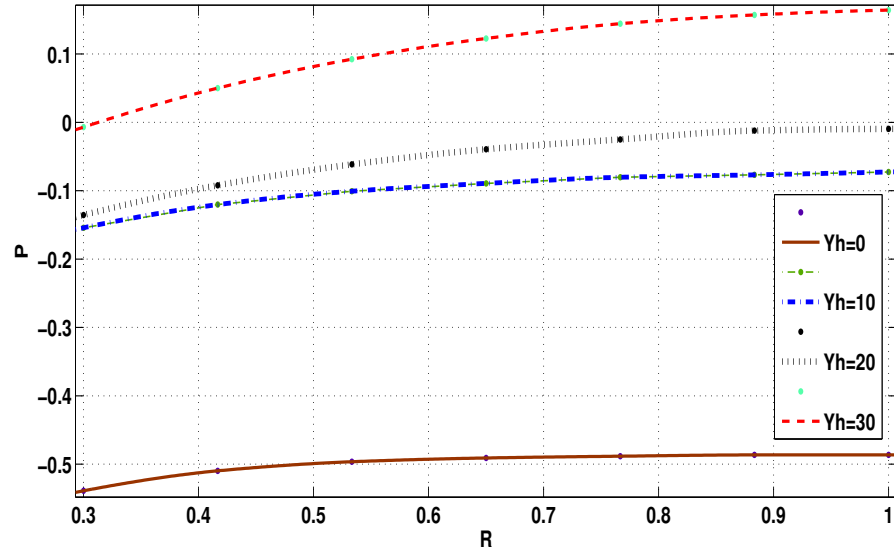


Figure 4.17 Pressure Variation for $N=0.3$, $n=1.5$, $R = 0.1$ at $Z = 0.02$

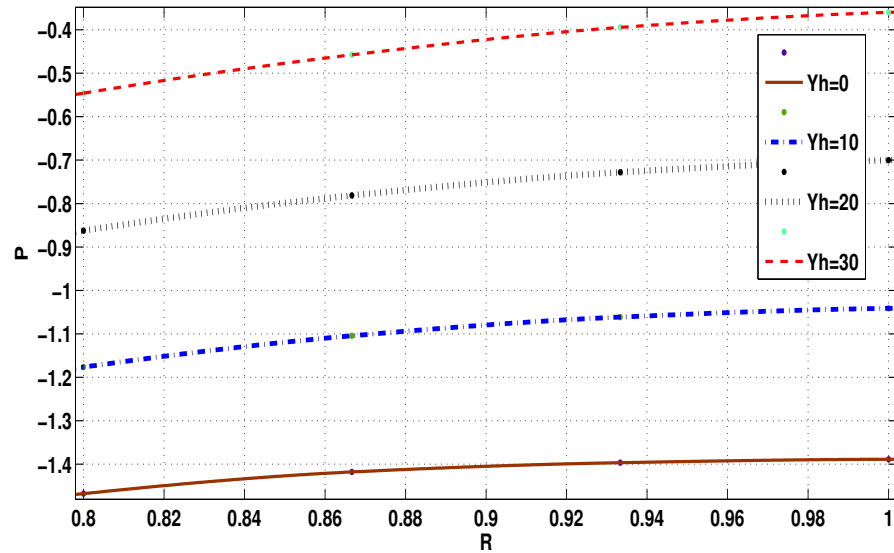


Figure 4.18 Pressure Variation for $N=0.8$, $n=0.5$, $R = 0.05$ at $Z = 0.03$

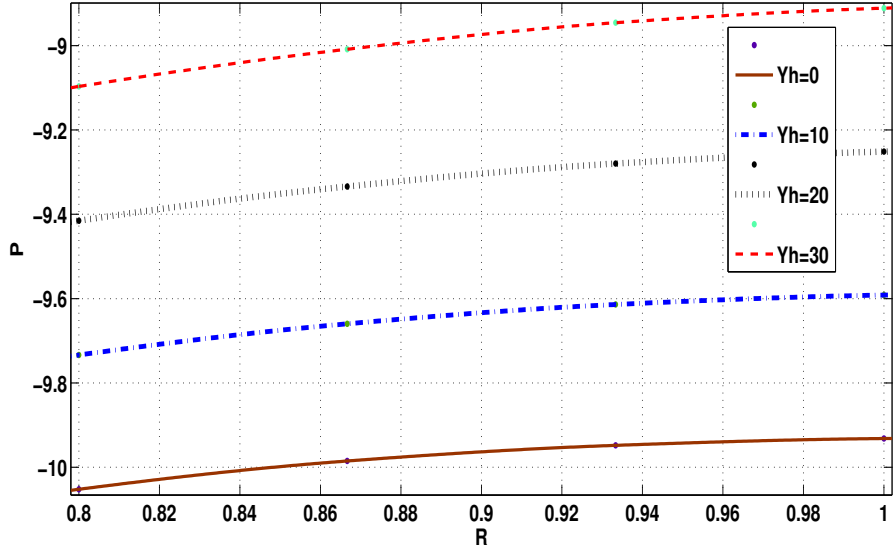


Figure 4.19 Pressure Variation for $N=0.8$, $n=1$, $R = 0.05$ at $Z = 0.03$

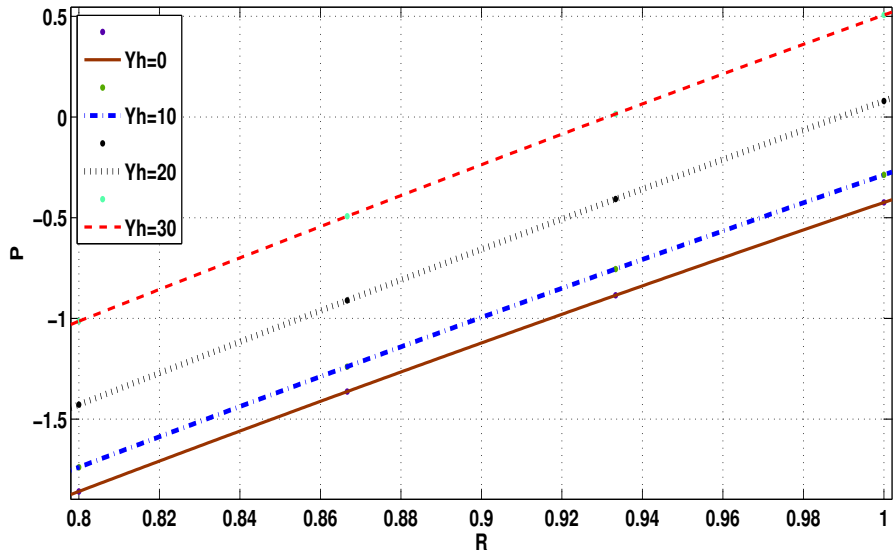


Figure 4.20 Pressure Variation for $N=0.8$, $n=1.5$, $R = 0.05$ at $Z = 0.03$

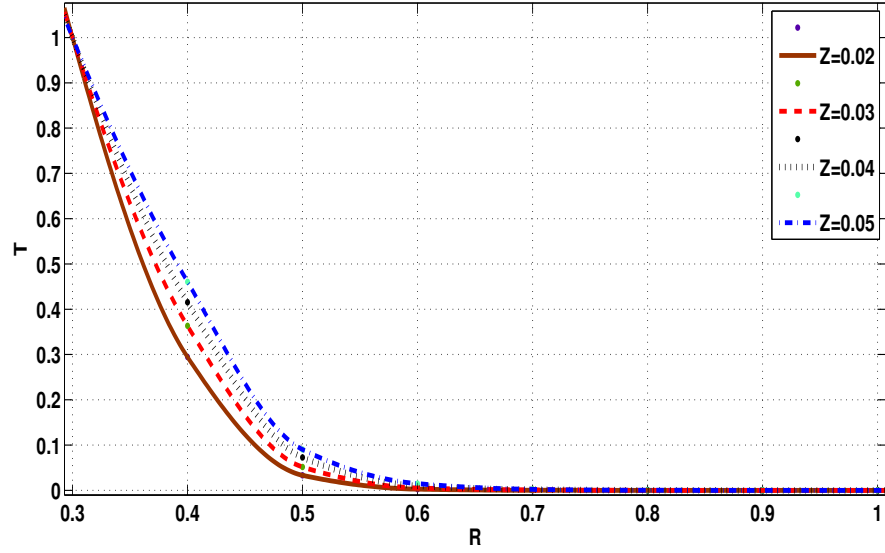


Figure 4.21 Temperature Distribution for $N=0.3$, $n=0.5$, $Pr=7$ and $Y_h=0$

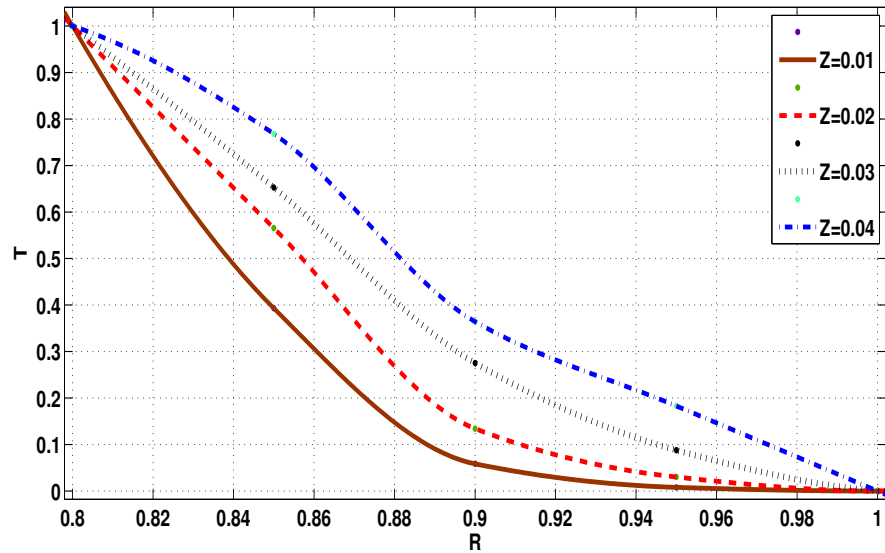


Figure 4.22 Temperature Distribution for $N=0.8$, $n=0.5$, $Pr=7$ and $Y_h=10$

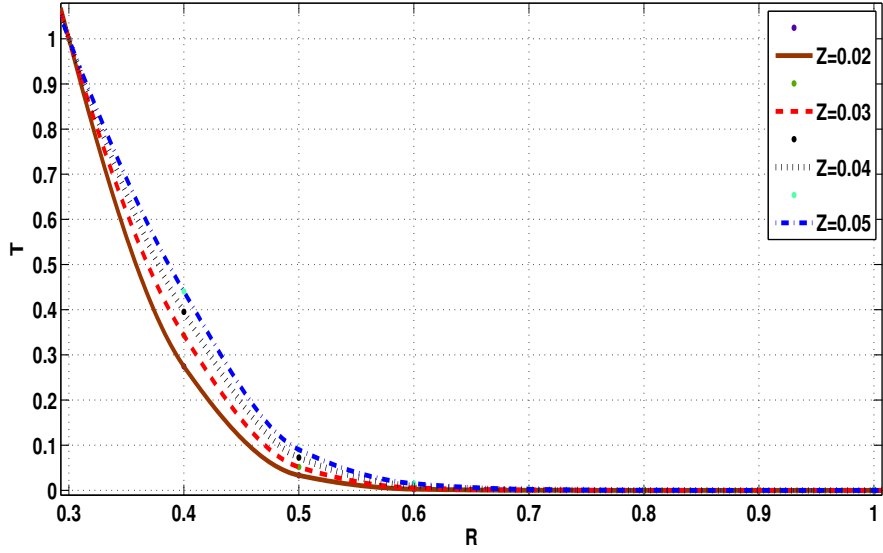


Figure 4.23 Temperature Distribution for $N=0.3$, $n=1$, $Pr=7$ and $Y_h=0$

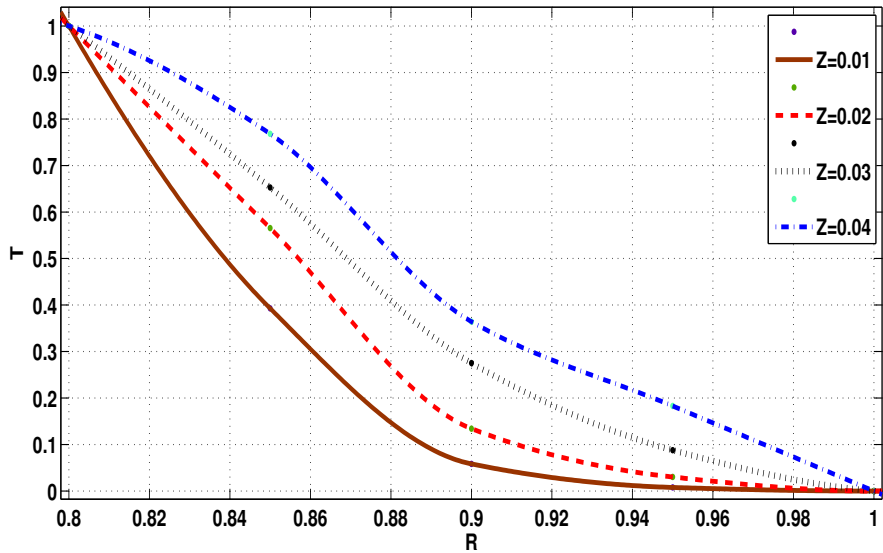


Figure 4.24 Temperature Distribution for $N=0.8$, $n=1$, $Pr=7$ and $Y_h=10$

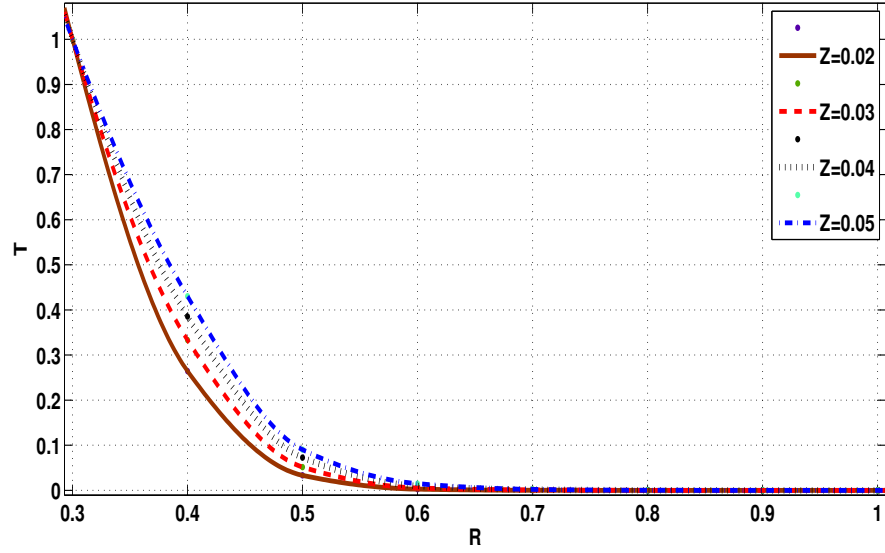


Figure 4.25 Temperature Distribution for $N=0.3$, $n=1.5$, $Pr=7$ and $Y_h=0$

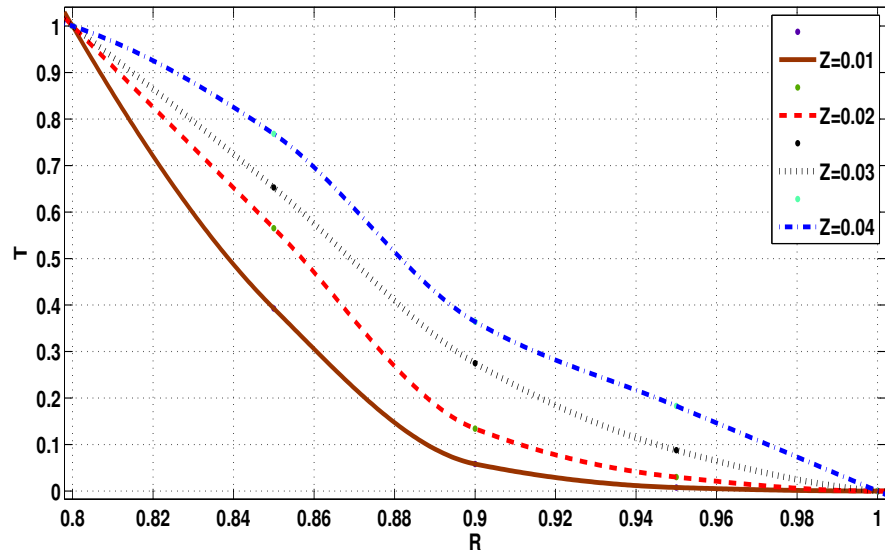


Figure 4.26 Temperature Distribution for $N=0.8$, $n=1.5$, $Pr=7$ and $Y_h=10$

Chapter 5

CONCLUSION AND FUTURE SCOPE

5.1 CONCLUSION

Numerical results for the entrance region flow heat transfer in concentric annuli with rotating inner wall for the viscoplastic fluids have been presented. The effects of the non-Newtonian flow characteristics and geometrical parameters on the velocity profiles, pressure variation and temperature distribution are studied. Numerical calculations have been performed for all admissible values of yield numbers, flow index n and aspect ratio N . The velocity profiles, pressure variation and temperature distribution along radial direction R have been presented geometrically. From this study, the following can be concluded.

VELOCITY PROFILES

- * For all the viscoplastic fluids analyzed, it is observed that the values of tangential velocity W decrease from the inner wall to outer wall of the annulus and it is observed that with the increase of aspect ratio N , the tangential velocity profile increases. That is, the tangential velocity is more when the gap of the annuli is small.
- * By increasing the aspect ratio N , the axial velocity component U increases.

- * The values of radial velocity V are negative in the region near the outer wall since it is in the opposite direction to the radial coordinate R and it has positive values near the inner wall because it has the same direction of the radial coordinate.
- * For Newtonian fluid the shape of the axial velocity profile is parabolic. It is very much evident in our investigation, as the parameters B , Y_c , and Y_h with flow index n being one, tending to zero refer Newtonian fluid.

PRESSURE VARIATION

- * It is found that the value of the pressure P increases from a minimum at the inner wall to a maximum at the outer wall.
- * Moreover, it is observed that the pressure P does not vary so much with respect to the radial coordinate in the region near the outer wall.

TEMPERATURE DISTRIBUTION

- * The temperature decreases T from the rotating inner wall to the stationary outer wall of the annulus.
- * It is observed from the results obtained, that the temperature T decreases, when the aspect ratio N increases.
- * Also, it is found that with the increase of axial position Z , the temperature T also increases for a fixed aspect ratio N .

5.2 FUTURE SCOPE

The effects of the rotation of the annular cylinders in a concentric way as well as in the opposite direction can be studied further. Then the flow of such time-independent non-Newtonian fluids in eccentric annuli can be analyzed.

REFERENCES

- Ahmed, M. S. and Attia, H. A. (1998). “Magnetohydrodynamic flow and heat transfer of a non-newtonian fluid in an eccentric annulus”. *Can. J. Phys*, 76:391–401.
- Alexandrou, A. N., McGilvray, T. M., and Burgos, G. (2001). “Steady Herschel-Bulkley fluid flow in three dimensional expansions”. *J. Non-Newtonian Fluid Mechanics*, 100(1-3):77–96.
- Batra, R. L. and Das, B. (1992). “Flow of a Casson fluid between two rotating cylinders”. *Fluid Dynamic Research*, 9(1–3):133–141.
- Batra, R. L. and Jena, B. (1990). “Entrance region flow of blood in concentric annulus”. *International Journal of Engineering Science*, 28(5):407–419.
- Batra, R. L. and Kandasamy, A. (1990). “Entrance flow of Herschel-Bulkley fluids in a duct”. *Fluid Dynamics Research*, 6(1):43–50.
- Batra, R. L. and Kandasamy, A. (1992). “Entrance region flow of a Casson fluid in a straight channel”. *Polym.–Plast. Technol. Eng.*, 31(5–6):527–540.
- Batra, R. L. and Sudarsan, V. R. (1992). “Laminar flow heat transfer in the entrance region of concentric annuli for power-law fluids”. *CMAMP*, 95(1):1–16.
- Bird, R. B., Dai, G. C., and Yarusso, B. J. (1983). “The rheology and flow of visco-plastic materials”. *Reviews in Chemical Engineering*, 1(1):1–70.
- Cheng, T. and Deville, M. (1996). “Pulsatile flow of non-newtonian fluids through arterial stenoses”. *Journal of Biomechanics*, 29(7):899–908.
- Coney, J. and El-Shaarawi, M. (1974a). “A contribution to the numerical solution of developing laminar flow in the entrance region of concentric

- annuli with rotating inner walls”. *Journal of Fluids Engineering*, 96(4):333–340.
- Coney, J. and El-Shaarawi, M. (1974b). “Laminar heat transfer in the entrance region of concentric annuli with rotating inner walls”. *Journal of Heat Transfer*, 96(4):560–562.
- Coney, J. and El-Shaarawi, M. (1975). “Finite difference analysis for laminar flow heat transfer in concentric annuli with simultaneously developing hydrodynamic and thermal boundary layers”. *International Journal for numerical methods in engineering*, 9(1):17–38.
- Das, B. (1992). “Entrance region flow of the Hershel-Bulkley fluid in a circular tube”. *Fluid Dynamic Research*, 10(1):39–53.
- Dash, R., Mehta, K., and Jayaraman, G. (1996). “Casson fluid flow in a pipe filled with a homogeneous porous medium”. *International Journal of Engineering Science*, 34(10):1145–1156.
- Fung, Y. C. (1981). “Mechanical properties of living tissues”. *Biomechanics Springer-Verlag*, pages 68–71.
- Gupta, R. C. (1987). “Laminar two-dimensional entrance region flow of power-law fluids”. *Acta Mechanica*, 67:129–137.
- Gupta, R. C. (1990). “Laminar two-dimensional entrance region flow of Power-law fluids - ii.”. *Acta Mechanica*, 84:209–215.
- Hammad, K. J., Vradis, G. C., and Otugen, M. V. (2001). “Laminar flow of a herschel-bulkley fluid over an axisymmetric sudden expansion”. *Journal of fluids engineering*, 123(3):588–594.
- Hussain, Q. and Sharif, M. (2000). “Numerical modeling of helical flow of viscoplastic fluids in eccentric annuli”. *AIChE journal*, 46(10):1937–1946.
- Kandasamy, A. (1996). “Entrance region flow heat transfer in concentric annuli for bingham fluid”. *Proc. Third asian pacific conference on computational mechanics*, 4:1697–1702.

- Kandasamy, A., Karthik, K., and Phanidar, P. (2007a). “Entrance region flow heat transfer in concentric annuli for casson fluid”. *Proceedings of Thermal Issues in Emerging Technologies (ThETA), Cairo, Egypt*.
- Kandasamy, A., Karthik, K., and Phanidar, P. (2007b). “Entrance region flow heat transfer in concentric annuli for herschel-bulkley fluids”. *Computational fluid dynamics journal*, 16(2):103–114.
- Kandasamy, A. and Nadiminti, S. R. (2015). “Entrance region flow in concentric annuli with rotating inner wall for herschel-bulkley fluids”. *International Journal of Applied and Computational Mathematics*, 1(2):235–249.
- Liu, J. and Shah, V. (1975). “Numerical solution of a casson fluid in the entrance of annular tubes”. *Applied Scientific Research*, 31(3):213–222.
- Maia, M. C. A. and Gasparetto, C. A. (2003). “A numerical solution for the entrance region of non-Newtonian flow in annuli”. *Brazilian Journal of Chemical Engineering*, 20(2):1–18.
- Manglik, R. and Fang, P. (2002). “Thermal processing of viscous non-newtonian fluids in annular ducts: effects of power-law rheology, duct eccentricity, and thermal boundary conditions”. *International Journal of Heat and Mass Transfer*, 45(4):803–814.
- Mishra, I., Kumar, S., and Mishra, P. (1985). “Entrance region flow of Bingham plastic fluids in concentric annulus”. *Indian Journal of Technology*, 23(3):81–87.
- Misra, J. C. and Ghosh, S. K. (2000). “Flow of a Casson fluid in a narrow tube with a side branch”. *International Journal of Engineering Science*, 38:2045–2077.
- Nadiminti, S. R. and Kandasamy, A. (2016a). “Entrance region flow heat transfer in concentric annuli with rotating inner wall for bingham fluid”. *Periodica Polytechnica Mechanical Engineering*, 60(3):167–179.
- Nadiminti, S. R. and Kandasamy, A. (2016b). “Entrance region flow in concentric annuli with rotating inner wall for bingham fluid”. *Journal of Computational and Applied Mechanics*, 11(2):137–157.

- Narang, B. S. (1983). “Exact solution for entrance region flow between parallel plates”. *International journal of heat and fluid flow*, 4 (3):177–181.
- Nouar, C., Lebouché, M., Devienne, R., and Riou, C. (1995). “Numerical analysis of the thermal convection for herschel-bulkley fluids”. *International journal of heat and fluid flow*, 16(3):223–232.
- Nowak, Z. and Gajdeczko, B. (1983). “Laminar entrance region flow of the Bingham fluid”. *Acta Mechanica*, 49:191–201.
- Pai, R. G. and Kandasamy, A. (2014). “Entrance region flow of herschel-bulkley fluid in an annular cylinder”. *Applied Mathematics*, 5(13):1964–1976.
- Pham, E. M. (1994). “Entry and exit flows of casson fluids”. *The Canadian Journal of Chemical Engineering*, 72(6):1080–1084.
- Poole, R. and Chhabra, R. (2010). “Development length requirements for fully developed laminar pipe flow of yield stress fluids”. *J. Fluids Eng.*, 132(3):034501–034504.
- Rachid, C. (2002). “Laminar flow of power-law fluids in the entrance region of a pipe”. *Chemical Engineering Science*, 57(21):4435–4443.
- Round, G. and Yu, S. (1993). “Entrance laminar flows of viscoplastic fluids in concentric annuli”. *The Canadian Journal of Chemical Engineering*, 71(4):642–645.
- Sankar, D. S. and Hemalatha, K. (2007). “A non-Newtonian fluid flow model for blood flow through a catheterized artery-steady flow”. *Applied Mathematical Modeling*, 31:1847–1864.
- Sayed-Ahmed, M. E. and Sharaf-El-Din, H. (2006). “Entrance region flow of a Power-law fluid in concentric annuli with rotating inner wall”. *International Communication in Heat and Mass Transfer*, 33(5):654–665.
- Schlichting, H. and Gersten, K. (2000). *Boundary Layer Theory*. Springer.
- Skelland, A. H. P. (1967). *Non-Newtonian Flow and Heat transfer*. John Wiley and sons.

- Soares, E. J., Naccache, M. F., and Mendes, P. R. S. (1999). “Heat transfer to viscoplastic liquids flowing laminarily in the entrance region of tubes”. *International journal of heat and fluid flow*, 20:60–67.
- Soares, J., Monica Naccache, F., and Paulo Souza Mendes, R. (2003). “Heat transfer to viscoplastic materials flowing axially through concentric annuli”. *International Journal of Heat and Fluid Flow*, 24:762–773.
- Swati, M., Prativa, R. D., and Krishnendu, B. (2013). “Casson fluid flow over an unsteady stretching surface”. *Ain Shams Engineering Journal*, 4:933–938.
- Tandon, P. N., Srivastava, L. M., and Kushwaha, K. (1994). “Developing blood flow in the entrance region of an artery”. *International Journal of Bio-Medical Computing*, 36(4):257–265.
- Viana, M. J. G., Nascimento, U. d. C. S., Quaresma, J. N. N., and Macêdo, E. N. (2001). “Integral transform method for laminar heat transfer convection of herschel-bulkley fluids within concentric annular ducts”. *Brazilian Journal of Chemical Engineering*, 18(4):337–358.
- Wilkinson, W. L. (1960). *“Non-Newtonian fluids”*. Pergamon Press.
- William, S. (2010). *“Introduction to Fluid Mechanics”*. Taylor and Francis group.
- Yuan, S. W. (1970). *“Foundations of Fluid Mechanics”*. Prentice–Hall International Inc.

PUBLICATIONS

International Journals:

1. A. Kandasamy and Srinivasa Rao Nadiminti, (2015), “Entrance region flow in concentric annuli with rotating inner wall for Herschel-Bulkley fluids ”. *International Journal of Applied and Computational Mathematics*, 1(2), 235-249. (Springer)
2. Srinivasa Rao Nadiminti and A. Kandasamy, (2016), “Entrance region flow heat transfer in concentric annuli with rotating inner wall for Bingham fluid ”. *Periodica Polytechnica Mechanical Eng.*, 60(3), 167-179.
3. Srinivasa Rao Nadiminti and A. Kandasamy, (2016), “Entrance region flow in concentric annuli with rotating inner wall for Bingham fluid ”. *Journal of Computational and Applied Mechanics*, 11(2), 137-157.
4. Srinivasa Rao Nadiminti and A. Kandasamy, (2017), “Entrance region flow heat transfer in concentric annuli with rotating inner wall for Herschel-Bulkley fluids ”. *MATEC Web of Conferences*, 95, 12011.
5. Srinivasa Rao Nadiminti and A. Kandasamy, (2017), “Numerical solution of entrance region flow heat transfer of Casson fluid in concentric annuli with rotating inner wall ”. (Under Review)

International Conferences:

1. Srinivasa Rao Nadiminti and A. Kandasamy, (2016), “Numerical solution of entrance region flow of Casson fluid in concentric annuli with rotating inner wall ”. *International Conference on Mathematical Computer Engineering*, VIT University, Chennai, India.

BIODATA

Name : Srinivasa Rao Nadiminti
Email : srinudm@gmail.com
Date of Birth : 05 August 1984.
Contact No : +91-9740249480/8328232455
Permanent address : N. Srinivasa Rao,
S/o N. Simhachalam Naidu,
Kambara valasa Village,
Veeraghattam Mandal,
Srikakulam Dist - 532 460,
Andhra Pradesh - India.

Educational Qualifications :

Degree	Year	Institution / University
B.Sc. Mathematics	2004	M.R College, Vizianagaram.
M.Ed. Mathematics	2006	Andhra University, Visakhapatnam.
M.Sc. Mathematics	2009	Pondicherry University, Puducherry.
M.Phil. Applied Mathematics	2012	Pondicherry University, Puducherry.